



Publicly Accessible Penn Dissertations

Summer 8-14-2009

Single Molecule Studies of Myosin-Ib

Joseph M. Laakso

University of Pennsylvania, jlaakso@mail.med.upenn.edu

Follow this and additional works at: <http://repository.upenn.edu/edissertations>

 Part of the [Biophysics Commons](#)

Recommended Citation

Laakso, Joseph M., "Single Molecule Studies of Myosin-Ib" (2009). *Publicly Accessible Penn Dissertations*. 18.
<http://repository.upenn.edu/edissertations/18>

This paper is posted at Scholarly Commons. <http://repository.upenn.edu/edissertations/18>
For more information, please contact libraryrepository@pobox.upenn.edu.

Single Molecule Studies of Myosin-Ib

Abstract

Myosin-Is are the single-headed, membrane-associated members of the myosin superfamily that are found in many eukaryotic cells. These actin-based motors have been shown to play important roles in powering membrane dynamics, defining cytoskeletal structure, and regulating mechanical signal-transduction. However, many molecular details of myosin-I function are not known. My goal has been to determine the mechanical and kinetic properties of a myosin-I isoform (myo1b) as it undergoes its force-generating power stroke under physiological tension and when external mechanical loads are applied to it. We therefore characterized the force dependence of myo1b splice isoforms using an optical trap and a novel isometric force clamp. Myo1b is alternatively spliced within the regulatory domain of the molecule, yielding motors that have “lever-arms” with different lengths. We found the actin-attachment kinetics of all myo1b splice isoforms to be highly force sensitive, with forces of < 2 pN decreasing the rate of actin detachment > 75 fold. However, we found that the magnitude of the tension sensitivities depend on the splice isoform. Therefore, we propose that the tension sensing properties of myo1b are transcriptionally regulated. Finally, we found the tension sensitivity of myo1b to be regulated by calcium, such that micromolar calcium concentrations effectively uncouple the myosin active site from lever arm rotation. Taken together, this work supports a model in which myosin-Is play roles in generating and sustaining membrane tension, and that the mechanochemical properties of this protein are regulated by alternative splicing and calcium.

Degree Type

Dissertation

Degree Name

Doctor of Philosophy (PhD)

Graduate Group

Biochemistry & Molecular Biophysics

First Advisor

E. Michael Ostap

Keywords

Single Molecule, Myosin, Unconventional Myosin

Subject Categories

Biophysics

Publicly accessible Penn Dissertations

University of Pennsylvania

Year 2009

Single Molecule Studies of Myosin-Ib

Joseph M. Laakso

University of Pennsylvania, jlaakso@mail.med.upenn.edu

This paper is posted at ScholarlyCommons.

<http://repository.upenn.edu/edissertations/18>

SINGLE MOLECULE STUDIES OF MYOSIN-IB

Joseph M. Laakso

A DISSERTATION

In

Biochemistry and Molecular Biophysics

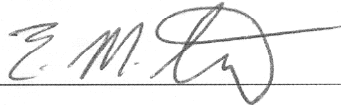
Presented to the Faculties of the University of Pennsylvania

In

Partial Fulfillment of the Requirements for the

Degree of Doctor of Philosophy

2009



E. Michael Ostap, Professor of Physiology

Supervisor of Dissertation



Kathryn M. Ferguson, Associate Professor of Physiology

Graduate Group Chairperson

Dissertation Committee

Yale E. Goldman, Professor of Physiology

H. Lee Sweeney, Professor of Physiology

Henry Shuman, Research Associate Professor of Physiology

John W. Weisel, Professor of Cell and Developmental Biology

Kim A. Sharp, Associate Professor of Biochemistry and Biophysics

Phong Tran, Assistant Professor of Cell and Developmental Biology

Single Molecule Studies of Myosin-IB

©

2009

Joseph M. Laakso

Acknowledgements

The University of Pennsylvania has been a fantastic environment to pursue graduate training in biochemistry and biophysics, and the work presented in this thesis is the product of collaborations and interactions with a great many people at the University. First and foremost, I must thank my thesis advisor, Dr. Mike Ostap, for his consistent support and encouragement over the years. Also Dr. Henry Shuman, who along with Mike, has provided patient instruction in the fundamentals of the biochemical and biophysical sciences to prepare me for the next steps in my career. The opportunity to conduct cutting edge research, and discover how proteins work in such exquisite detail, is a magnificent experience made all the more valuable by working with such talented and gracious scientists, and I remain very grateful for the opportunity. Also my thesis committee, who have supported my development from a time when the only data I could collect were the interactions between the two molecules I was least interested in.

I will greatly miss my labmates in the Ostap laboratory, I can think of no other group of people whose cheerful approach to labwork in general can keep one motivated through the most difficult portions of graduate school. Dave Hokanson, my student mentor and labmate, was a guide who thoughtfully provided me with advice throughout the confusing early semesters in graduate school. Tianming Lin, besides keeping me constantly supplied with proteins and reagents, gave me early instruction on protein preparation and motility assays. Nanyun Tang instructed me in tissue culture when I first joined the lab as a rotation student. Jennine Dawicki-

McKenna has been a constant source of conversation and laughter, making the time spent doing data analysis go by much faster. Our discussions of cell biology and your project have been very helpful as I approach the transition to that field.

Elizabeth Feeser has given me advice on my own transition to a postdoc, thank you for answering my questions even when you were interviewing at Penn. John Lewis, and Serapion Pырpassopoulos, as fellow optical-trap specialists, have been sources of knowledge and ideas for one such as myself with a limited physics background.

It also helps to have intelligent people working on the same instrument going through the same problems to let me know that I'm not going crazy! I must particularly thank John Lewis for doing so much great work on the Maximum Likelihood Estimation programs I used for so much of our data analysis.

Beyond the Ostap Lab, as I began my training on the optical trap, Scott Owens and Yasuharu Takagi were extremely helpful in getting me started on such a complicated and delicate instrument. The Pennsylvania Muscle Institute, as a whole, has been a great source of collaborations and expertise. Dr. Yale Goldman in particular has provided helpful support and discussions far beyond his role as thesis chair. Also, thanks go out to my undergraduate research advisors at SUNY Geneseo, Dr. Lihua Jin and H. Cristina Geiger, for giving me an opportunity to do research in an academic setting and begin my career as a scientist.

Outside of science, there are a number of people who have had a direct role in my education and interest in pursuing a graduate career in the sciences. My parents have been ideal role models, and as supportive as parents could possibly be.

Words on a page simply cannot describe my appreciation for their kindness and direction over the years. Besides providing me with the means to become whatever I wished to become, they set an example through their own approach to both their careers and life outside of work that I hold in the highest regard. Thank you for everything you have done for me and all you still continue to do. My extended family as well, for keeping me grounded and appreciative of all life has to offer.

My swim coaches, John Ogden and Dan Demeter, were the first people to truly test me and force me to find out what I could accomplish through hard work. The lessons learned from spending hours staring at a black line at the bottom of a pool are the lessons that can be applied to the hours spent staring at dancing voltage traces on a computer monitor. Also to my good friends, Brent Bernkrant, Joe Murin, Seth Newell, Doug Metcalf, Mike Harradine, and Kevin West (who, coincidentally, will be defending his Ph.D thesis within 24 hours of my own scheduled defense); I continue to look forward to times spent together over a cold beer, telling the same old stories we tell every year.

Finally, my deepest thanks and love go out to my girlfriend Katie Swavy, who for the past four years has been as patient, understanding, and supportive as I could have ever hoped for in a significant other. She has been the best thing about living in Philadelphia, and has the unique ability to put me in a good mood simply by laughing, even if she happens to be laughing at me! I look forward to starting the next chapter of our life together in Maryland.

Thank you all.

ABSTRACT

SINGLE MOLECULE STUDIES OF MYOSIN-IB

Joseph M. Laakso

Supervisor: Dr. E. Michael Ostap

Myosin-Is are the single-headed, membrane-associated members of the myosin superfamily that are found in many eukaryotic cells. These actin-based motors have been shown to play important roles in powering membrane dynamics, defining cytoskeletal structure, and regulating mechanical signal-transduction. However, many molecular details of myosin-I function are not known. My goal has been to determine the mechanical and kinetic properties of a myosin-I isoform (myo1b) as it undergoes its force-generating power stroke under physiological tension and when external mechanical loads are applied to it. We therefore characterized the force dependence of myo1b splice isoforms using an optical trap and a novel isometric force clamp. Myo1b is alternatively spliced within the regulatory domain of the molecule, yielding motors that have “lever-arms” with different lengths. We found the actin-attachment kinetics of all myo1b splice

isoforms to be highly force sensitive, with forces of < 2 pN decreasing the rate of actin detachment > 75 fold. However, we found that the magnitude of the tension sensitivities depend on the splice isoform. Therefore, we propose that the tension sensing properties of myo1b are transcriptionally regulated. Finally, we found the tension sensitivity of myo1b to be regulated by calcium, such that micromolar calcium concentrations effectively uncouple the myosin active site from lever arm rotation. Taken together, this work supports a model in which myosin-Is play roles in generating and sustaining membrane tension, and that the mechanochemical properties of this protein are regulated by alternative splicing and calcium.

Table of Contents

List of Tables	xiii
List of Illustrations	xiv
1. Introduction	1
1.1 Objectives of thesis and experimental approach	1
1.2 Specific aims	2
1.3 The cytoskeleton.....	5
1.4 Cytoskeletal motors.....	9
1.5 The myosin superfamily of molecular motors.....	10
1.6 Myosins in the context of the actin cytoskeleton	11
1.7 Myosin II	15
1.7.1 Myosin II in skeletal muscle.....	15
1.7.2 Domain architecture of Myosin-II.....	17
1.7.3 High-resolution structure of the myosin II motor domain.....	19
1.7.4 Biochemical cycle of myosin	21
1.7.5 The swinging lever arm model	24
1.8 Myosin I.....	31
1.8.1 Isolation and characterization of myosin-I.....	31
1.8.2 General features of myosin-Is	33
1.8.3 Myosin-I tails.....	34

1.8.4 The myosin-I lever arm	37
1.8.5 Potential functions of myosin-Is.....	39
1.9 Myosin-Ib	42
1.10 Towards a molecular explanation of the Fenn effect.	48
1.10.1 Experimental observation of the Fenn effect in muscle.	48
1.10.2 ADP release as it relates to muscle shortening.....	50
1.10.3 Biochemical evidence for a nucleotide sensitive/insensitive transition	51
1.10.4 Direct measurements of myosin strain dependence	53
1.10.4.1 Single molecule measurements of strain-dependent ADP release	53
1.10.4.2 Strain-sensitive reversal of the power stroke.....	59
1.11 Optical Trapping Techniques	60
1.12 Thesis Overview	65
2. Methods	67
2.1 Protein and reagent preparations	67
2.1.1 Buffer recipes	67
2.1.2 Coomassie Plus protein concentration determination.	68
2.1.3 Myosin constructs.....	69
2.1.4 G-actin preparation	71
2.1.5 Rhodamine-phalloidin labeled f-actin (RPFA) preparation	72
2.1.6 N-ethyl maleimide(NEM) modified myosin-II	72
2.1.7 NEM-myosin-II coated beads.....	73
2.2 Apparatus.....	74

2.2.1	Optical Trap.....	74
2.2.2	Calibration of the Optical Trap.....	76
2.2.3	Isometric force feedback	79
2.2.4	Stage position feedback.....	81
2.2.5	Calibration of the isometric force feedback loop	82
2.2.6	Calibration of the stage feedback loop	82
2.3	Experimental protocol	84
2.3.1	Motility chamber preparation.....	84
2.3.2	Data Collection.....	85
2.3.3	Steady state ATPase	88
2.3.4	Transient Pi release.....	89
2.4	Data Analysis.....	90
2.4.1	Selection of events.....	90
2.4.2	Ensemble Averaging	93
2.4.3	Maximum likelihood estimation.....	95
2.4.4	Stiffness measurements	95
3.	Results	98
3.1	Myosin-Ib can act as a molecular tension sensor	98
3.1.1	Detection of single molecule interactions	98
3.1.2	Kinetics of Myo1b substeps	100
3.1.3	Myo1b is a high duty-ratio motor under load.....	103

3.1.4 ADP release is the predominant strain-sensitive transition in the myo1b biochemical cycle	108
3.1.5 The myo1b force sensitive state is not reversible by phosphate rebinding	110
3.2 Force sensitivity can be tuned by alternative splicing of the myo1b LCBD	114
3.2.1 Step and substep sizes of myo1b splice isoforms.....	115
3.2.3 Force sensitivity of myo1b splice isoforms.....	119
3.3 Calcium regulation of myo1b mechanochemistry.....	124
3.3.1 Free calcium reduces myo1b step size	125
3.3.2 Effect of calcium on myo1b force sensitivity.....	127
3.4 Stiffness of myo1b constructs	129
3.4.1 The stiffness of the actomyo1b crossbridge is linearly related to the lever arm length.....	130
3.4.2 The average stiffness of myo1b in the presence of calcium.....	131
3.4.3 Double reversal events during forced oscillations.....	132
4. Discussion.....	134
4.1 Summary of results.....	134
4.2 Data collected at low resisting loads	135
4.2.1 Validation of single molecule data	135
4.2.2 The myo1b working stroke is composed of two substeps.....	136
4.3 Myosin-Ib is a high duty-ratio motor under load	138
4.3.1 Myosin-Ib is extremely sensitive to low physiological forces	138

4.3.2 ADP release is the force sensitive transition	140
4.3.3 The force sensitive state is not reversible by excess phosphate	142
4.3.4 Alternative splicing tunes the force sensitivity of myo1b	143
4.4 The origin of the large distance parameter	146
4.4.1 Motions of the lever arm under load	146
4.4.2 Loop-1 of myo1b	149
4.4.3 Magnesium release as a gate for ADP release.....	150
4.5 Crossbridge stiffness and the lever arm of myo1b.	152
4.5.1 The actomyo1b crossbridge does not behave as an elastic cantilever..	152
4.6 Calcium regulation of force sensitivity	155
4.6.1 Calcium reduces the force sensitivity of myo1b	155
4.6.2 How does calcium binding affect the force sensitivity	157
4.7 The observation of high-gain “reversals”	158
4.8 Cellular implications	161
4.9 Conclusions	164
References	166

List of Tables

Table 1.1 Rate and equilibrium constants for myo1b at 37 degrees C.....	45
Table 3.1 Kinetic parameters and force sensitivity of myo1b constructs.....	122

List of Illustrations

1. 1	Types of cytoskeletal filaments	7
1. 2	Types of cytoskeletal motors	10
1. 3	Actin networks at the leading edge of the cell	12
1. 4	Organization of skeletal muscle	16
1. 5	Schematic of myosin-II subdomains	18
1. 6	High resolution structure of myosin-II	20
1. 7	The Lymn-Taylor biochemical cycle	23
1. 8	Electron micrographs of fixed muscle	25
1. 9	Movement of the lever arm upon ADP release	27
1. 10	A rotation of the converter drives lever arm movement	30
1. 11	Coordination of biochemistry, structure, and actin affinity in the myosin ATPase cycle	32
1. 12	Proposed molecular functions for vertebrate myosin-Is	34
1. 13	Calmodulin-like light chains adopt multiple conformations when bound to IQ motifs	38
1. 14	Tissue expression patterns of myo1b	44
1. 15	Myo1b kinetic scheme	46
1. 16	The myo1b working stroke occurs in two steps	47
1. 17	The Fenn effect	49
1. 18	Model for a strain sensitive biochemical transition	52
1. 19	Model for strain-dependent Myo1in-V processivity	55
1. 20	Force affects the lifetime of the first substep for Myosin-V	57
1. 21	Attachment kinetics of myosin-II under high dynamic load	60
1. 22	Ray optics diagram of an optical trap	62
2. 1	Myo1b constructs	69
2. 2	Dual-beam optical trap	75
2. 3	Power spectrum analysis for detector calibration and trap stiffness measurement	78
2. 4	Motion of the isometric force clamp during an actomyosin attachment	80
2. 5	Stage position control	83
2. 6	Calibration of the isometric force clamp	84
2. 7	Selection of actomyo1b interactions	92
2. 8	Observation of "reversal" events	94
2. 9	Myo1b crossbridge stiffness measurement	97
3. 1	Single molecule actomyo1b attachments	99
3. 2	Ensemble averaging of single events at low resisting load	101
3. 3	Distribution of attachment lifetimes at various ATP concentration	102
3. 4	Model for detachment	103
3. 5	Actomyo1b attachment lifetimes in the presence of force	104
3. 6	Force dependence of actomyo1b attachment durations	105
3. 7	Myo1b is a high duty ratio motor under load	106

3. 8	Effect of force on substep lifetimes.....	109
3. 9	Ensemble averages of attachment durations under load.....	111
3. 10	Free phosphate has little effect on myo1b tension sensitivity.....	112
3. 11	Phosphate does not alter attachment kinetics under load.....	113
3. 12	Attachment lifetimes for myo1b splice isoforms.....	116
3. 13	Step and substep sizes of myo1b constructs.....	117
3. 14	Step sizes vs. IQ motifs.....	118
3. 15	Observation of a force transition for myo1b.....	119
3. 16	Demonstration of stage feedback during actomyo1b interactions.....	120
3. 17	Sample interactions for myo1b lever arm constructs.....	121
3. 18	Force dependence of myo1b constructs.....	123
3. 19	Distance parameter vs. substep size.....	124
3. 20	Effect of calcium on myo1b step size.....	126
3. 21	Effect of calcium on force sensitivity.....	128
3. 22	Myo1b phase loop analysis.....	129
3. 23	Stiffness of individual actomyo1b interactions.....	131
3. 24	Stiffness versus IQ motifs.....	132
3. 25	Double reversal event.....	133
4. 1	ADP release is the force sensitive transition.....	141
4. 2	Free energy interpretation of the large distance parameter.....	148
4. 3	Coordination of ADP and magnesium in the nucleotide binding pocket.....	151
4. 4	The myo1b lever arm is not an elastic cantilever.....	154
4. 5	Possible model for reversal events.....	159
4. 6	Model for molecular function of myosin-I.....	163

1. Introduction

1.1 Objectives of thesis and experimental approach

Myosins encompass a functionally and biochemically diverse superfamily of proteins comprised of at least 24 different classes (Foth, Goedecke & Soldati 2006, Richards, Cavalier-Smith 2005), including the extensively studied muscle myosin, otherwise known as conventional myosin II. While certain elements of myosin structure and function are common to all members of the superfamily, such as ATP hydrolysis and actin binding, many of the cellular functions and regulatory mechanisms of members of the myosin superfamily remain to be studied in detail. Essential to our understanding of myosin function is in depth knowledge of the mechanical and biochemical differences between individual myosins.

Single molecule techniques are a set of increasingly useful tools to probe the mechanics of motor proteins. These techniques can be employed to make measurements at the nanometer (nm) distance and pico-Newton (pN) force scales necessary to directly observe molecular motor forces and displacements (Knight, Mashanov & Molloy 2005). The development of infrared-laser based optical trapping systems has led to the ability to trap and manipulate particles which, coupled to various “handles”, serve as reporters for the motions of and forces produced by single molecules (Ashkin 1997).

The experiments described in this thesis will use single molecule techniques to examine the biochemical and biophysical properties of a myosin molecular motor, myosin-Ib (myo1b). Our experimental system gives us a unique opportunity to probe myo1b with various forces and chemical tests. Regulation by alternative splicing of myo1b is also tested by performing similar experiments with the different naturally occurring splice isoforms of myo1b. Solution biochemistry data is used to confirm measurements of myosin kinetics at the single molecule level, as well as draw broader conclusions about the functional properties of myo1b. These data, taken together, not only identify and characterize the sensitive regulatory properties of unconventional myosins, but also add to our general understanding of motor proteins and how they respond to forces.

1.2 Specific aims

The first aim of this thesis is to characterize the response of myo1b to external force resisting the power stroke. Structural and biochemical evidence suggest that myosin-I produces force and displacement along the actin filament via a two-step mechanism that is correlated with the release of ATP hydrolysis products. We and others have proposed that one of these substeps is a force sensitive transition that may become rate limiting under load. Functionally, this will have a direct effect on the lifetime of acto-myo1b attachments. Using a feedback-enhanced optical trapping system developed by Takagi, Goldman and Shuman (Takagi et al.

2006a), we can measure the forces and displacements produced by single myosin molecules during an acto-myosin interaction. By ensemble averaging individual interactions, we can confirm the two-step mechanism for myo1b and correlate the steps with release of ATP hydrolysis products. We can then measure the lifetimes of acto-myo1b interactions under a variety of resistive loads via force feedback to determine the sensitivity of substeps to external load. This work will probe the mechanochemistry of myo1b in great detail and add to our understanding of how motor proteins can respond to changes in force.

The second specific aim is to examine the regulation of myo1b mechanical properties. Myo1b is alternatively spliced to generate three naturally occurring proteins having regulatory domains consisting of 4, 5, or 6 IQ motifs that bind calmodulin (CaM) in a calcium sensitive manner. We predict that these splice isoforms will have step sizes that vary linearly with the number of IQ motifs. We can then determine if increasing lever arm length affects the force sensitivity of myo1b. Specifically, one can predict that increasing lever arm length will increase force sensitivity by changing the distance over which the force must act to exit the force sensitive transition state. We can further probe regulation of force sensitivity by conducting force dependence experiments in the presence of free calcium. The biochemical properties of myo1b are known to be regulated by calcium, however if calcium binding to light chains along the regulatory domain causes a change in the crossbridge compliance, force sensitivity of myo1b could be abolished. This would suggest that tension sensing properties of myo1b could be regulated by free cellular

calcium concentration. By repeating the step size and force dependence measurements for myo1b splice isoforms, as well as testing the effect of free calcium on force dependence, we can gain deeper insight into both the structural basis for tuning of force sensitivity, as well as how that force sensitivity is regulated by intracellular signaling molecules. Answers from these experiments will open new questions into the cellular functions of myo1b.

The third specific aim is to measure the stiffness of the acto-myo1b crossbridge. In our experiments, we can oscillate the stage during acto-myo1b interactions by known amounts using an additional feedback loop connected to a piezo stage controller. By simultaneously measuring the force produced by the myosin as it resists stretching due to the stage oscillation, we can measure the myo1b force-extension properties. These measurements will then be made for the myo1b splice isoforms from aim 2, which will allow us to determine if the myo1b lever arm behaves as a rigid rod with uniform stiffness, or rather has compliant elements of varying stiffness. Making these measurements in the presence of free calcium will also allow us to determine if the effect of calcium on force sensitivity is due to increasing compliance of the myo1b lever arm.

Collectively, achieving these specific aims will address the mechanical properties of myo1b and how they are regulated. The characterization of myo1b as a possible tension sensor, as well as how that tension sensitivity is regulated, will change how we view potential myosin-I functions inside of cells, and probe how biochemical properties of motors are altered by force.

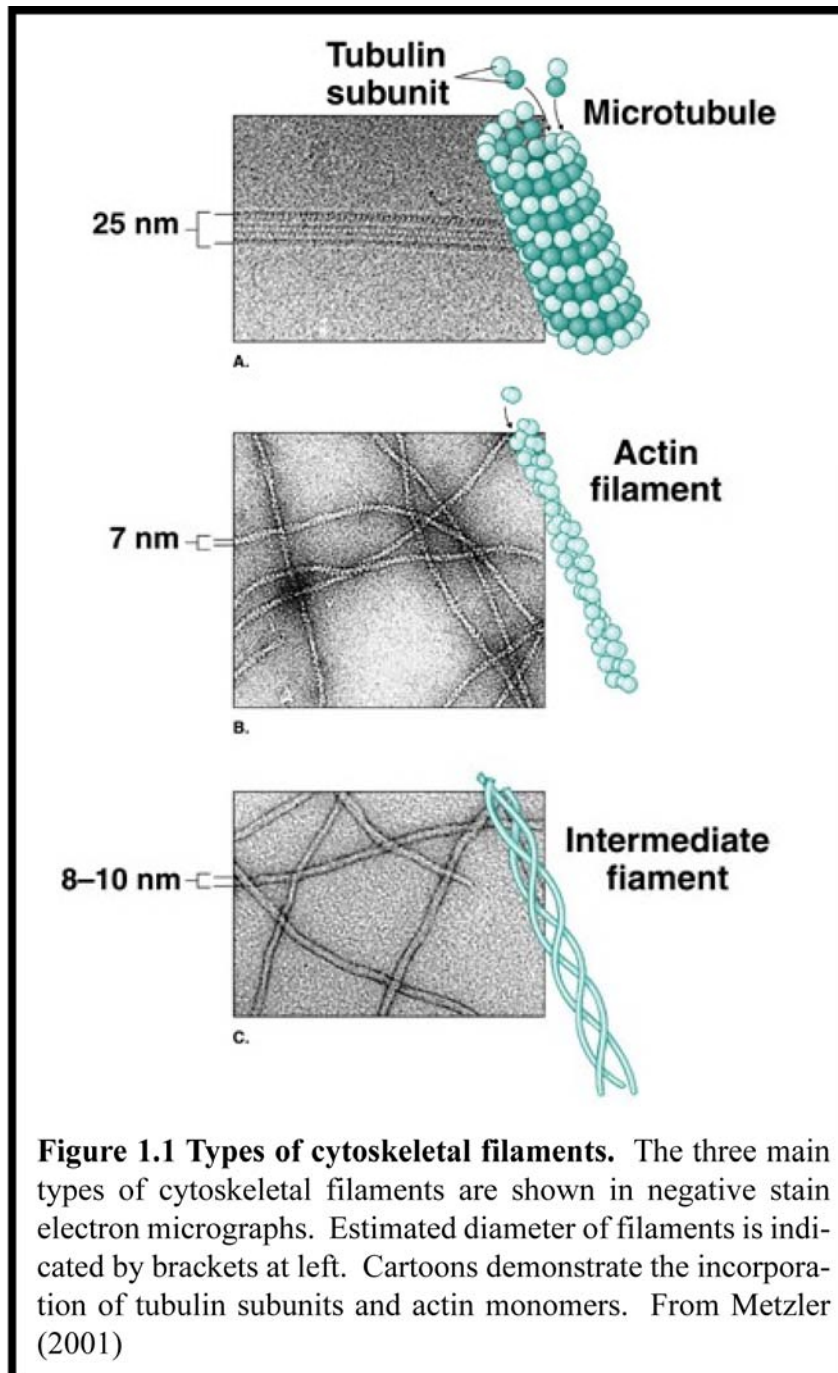
1.3 The cytoskeleton

The eukaryotic cytoskeleton collectively refers to a network of protein filaments and associated proteins that serve a variety of cellular functions including structural support, intracellular transport, motility and division. Central to these functions are three sets of proteins that can dynamically polymerize to form filaments. Through polymerization, cytoskeletal proteins can produce force and power motility, form tracks which can provide a framework for moving cellular cargoes, develop structures and organelles such as the thin filament in muscle and the eukaryotic centriole, and compartmentalize the cell through molecular crowding. Each type of filament has its own unique regulatory properties and associated proteins.

Actin filaments (f-actin) are formed by the addition of globular monomers (g-actin) with Mg·ATP, into a helical filament (STRAUB, FEUER 1950). When incorporated into a filament, an actin monomer can hydrolyze its bound ATP, resulting in an ADP-actin form that is less stable and more likely to depolymerize. G-actin monomers are always incorporated in a specific orientation, resulting in a polarized filament with two ends (termed barbed and pointed) that differ in their relative rates of monomer incorporation (Wegner 1976). The polarity of the actin filament results in a g-actin concentration dependent phenomenon called “treadmilling” in which ATP-actin monomers are added to the barbed end, while

ADP-actin dissociates from the pointed end. In the cell however, actin filaments may be stabilized or destabilized by a variety of regulatory factors (reviewed in (Pantaloni, Le Clainche & Carlier 2001)).

Microtubules (MTs) are composed of GTP-bound alpha and beta tubulin dimers with each alpha tubulin connected to the beta tubulin of the following dimer to form a polarized protofilament. Protofilaments are arranged next to each other in the same orientation to form an imperfect helix which, like actin, has a polarity with a specified + and – end. Another similarity to actin is that the hydrolysis of bound nucleotide destabilizes the filament and prevents binding of monomers to the end of the filament. Thus, microtubules can undergo a treadmilling process similar to actin (Margolis, Wilson 1978), yet again we find that the dynamics of microtubule assembly and disassembly are highly regulated inside the cell. MTs are organized with minus ends terminating in a microtubule organizing center (Frankel 1976) (MTOC) which serves to stabilize the minus ends and promote MT growth radially from the MTOC. Microtubule dynamics are summarized by a process called dynamic instability (Mitchison, Kirschner 1984), in which rapidly growing MTs are protected by a “GTP cap” where the kinetics of GTP-bound monomer addition are faster than the rate of GTP hydrolysis. If the free concentration of monomer is reduced, or the kinetics of monomer addition are otherwise slowed, then the GTP cap is lost and GDP-tubulin rapidly depolymerizes in a process called “catastrophe”. By reintroducing a GTP cap through addition of monomers, steady growth of MTs



can be rescued. MTs have their own repertoire of binding partners with diverse functions termed microtubule associated proteins, or MAPs.

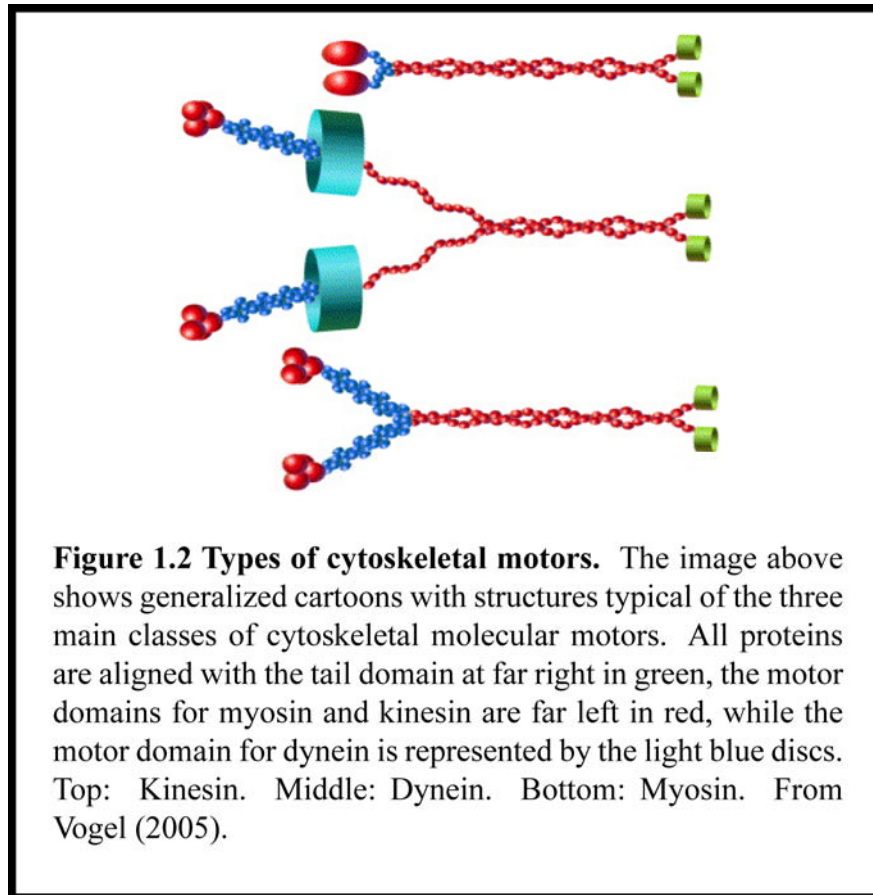
Intermediate filaments (IFs) are a diverse superfamily of proteins including at least 65 different genes sorted into 5 different classes. (Helfand, Chang & Goldman 2004). IFs are distinct from other cytoskeletal filaments in a number of ways, for instance they form filaments that are not polarized, they do not bind or hydrolyze nucleotides, and the expression of IFs is cell and tissue specific, resulting in unique IF profiles for certain cell types. Although IFs do not serve as tracks for molecular motors, emerging evidence suggests that IF localization and motility are mediated by molecular motors such as dynein (Helfand et al. 2002), and kinesin (Gyoeva, Gelfand 1991).

These three types of proteins comprise the main structural elements of the eukaryotic cytoskeleton. Through their dynamic assembly, they can influence a wide variety of processes and functions as well as produce force and higher-order structure. Fundamental to the function of cytoskeletal filaments are their interactions with molecular motors. In addition to proper localization of IFs, motor proteins can link the cytoskeleton to other organelles such as the plasma membrane, or produce force and power directional movement along filaments.

1.4 Cytoskeletal motors

Motor proteins may be broadly defined as any protein that is able to utilize chemical energy, usually in the form of ATP, to produce mechanical work. In the context of the cytoskeleton, three main classes of motor proteins hydrolyze ATP to produce force and directional displacement along microtubules or F-actin. Kinesins and dyneins utilize microtubule based tracks, while myosins use f-actin. These three protein families commonly share three functional domains summarized in figure 1.2. A motor domain, which is responsible for binding to the cytoskeletal track and also catalyze the hydrolysis of ATP. A globular tail domain, which can bind cargoes or serve regulatory functions. And a “neck,” also known as the light chain binding domain (LCBD), connecting the motor to the tail, which may be involved in the binding of accessory proteins or dimerization of motors. (Tyreman, Molloy 2003).

There are well-studied examples from each of these classes of motor proteins that could highlight the diversity in function and regulation of motor proteins that can be studied via single molecule techniques. This thesis will specifically deal with the myosin superfamily of proteins, so the remaining introduction will place an emphasis on the structural and mechanical studies of myosin leading up to the experiments presented herein.



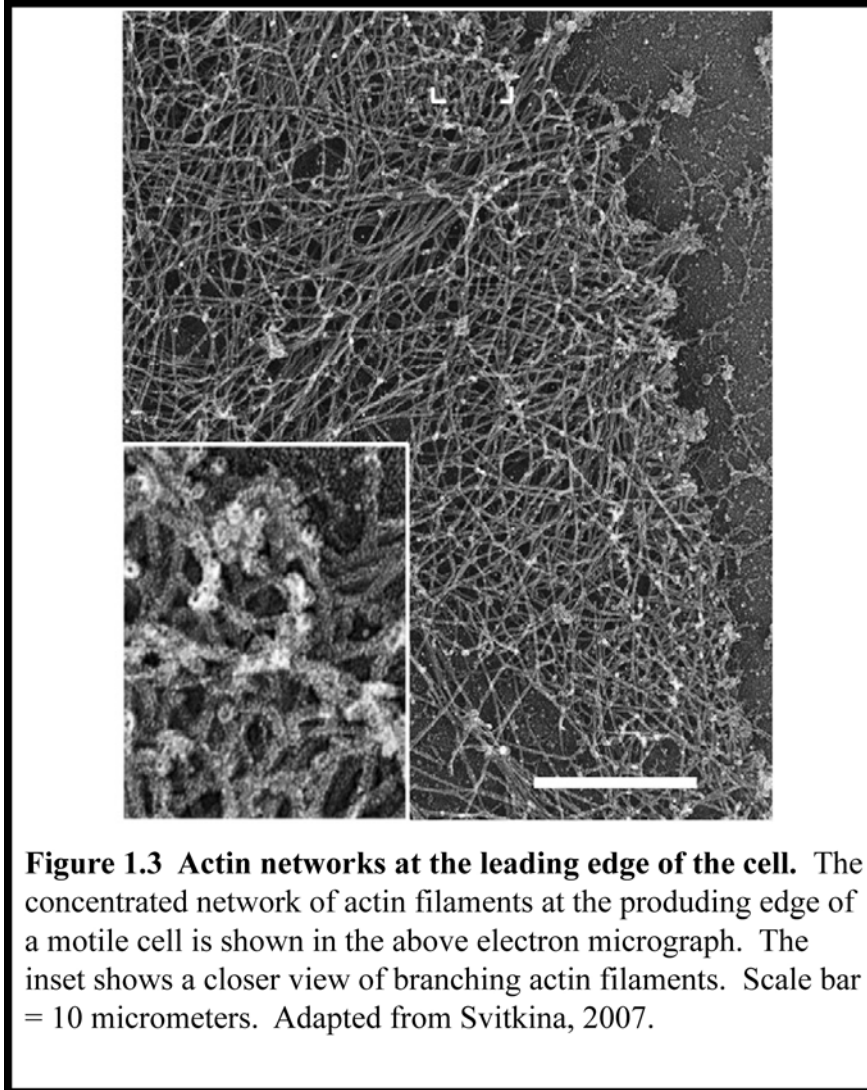
1.5 The myosin superfamily of molecular motors

The myosin superfamily of molecular motors encompasses at least 24 classes of proteins sharing a common highly conserved amino-terminal motor domain which binds actin and hydrolyzes ATP to produce force and do work (Foth, Goedecke & Soldati 2006). The carboxy-terminus of the protein is composed of a tail, which is highly divergent among the different classes of myosin and may contain functional motifs such as Src-homology 3 (SH3), and pleckstrin homology (PH) domains. Additionally, the tail may form a coiled-coil to dimerize myosin heavy chains as is the case for myosin V (Cheney et al. 1993). Connecting the head

and tail is the neck, otherwise known as the regulatory domain or the light chain binding domain, which serves as a “lever arm” to amplify small conformational changes in the motor domain (see 1.6 in this thesis). Along the neck are IQ motifs (consensus sequence IQXXRGXXR) which bind calmodulin (CaM) or calmodulin-like proteins (Cheney, Mooseker 1992).

1.6 Myosins in the context of the actin cytoskeleton

The actin cytoskeleton, coupled to the action of myosin motor proteins, provides the framework and driving force for a number of fundamental cell biological processes. Electron microscopy of cortical actin networks inside the cell shows a dense meshwork of f-actin (figure 1.3) that might be expected to pose a challenge for the long distance transport of cargoes. The creation of this meshwork is due to the action of proteins that promote nucleation of a new filament on the side of a preexisting actin filament according to what is known as the dendritic nucleation model (Mullins, Heuser & Pollard 1998, Svitkina, Borisy 1999, Pollard, Borisy 2003). Briefly, generation of a new branch point in the filament network is accomplished through the activation of a member of the



Wiskott-Aldrich syndrome family of proteins (WASP family) such as N-WASP, that simultaneously binds to a complex of two proteins (the Arp2/3 complex) that are closely related to actin, giving rise to the name actin related protein (Arp). The close structural similarity of the Arp2/3 proteins to actin monomers helps them serve as a nucleation site for a new actin filament, which appears as a branch point on the old filament.

The branched filaments consistently extend at an angle from the preexisting filament at a 70° angle, with the polarization of the new filament in the same orientation as the preexisting filament. Therefore the growth of new filaments in the context of filopodia or lamellopodia at the leading edge of the cell could provide a force to drive processes such as cell motility (Lindberg, Hoglund & Karlsson 1981), or vesiculation of endosomes, reviewed in (Soldati 2003). Perhaps the best described example of force production by an actin network through the polymerization of new filaments is the motility of the pathogen *Listeria monocytogenes* (Tilney, Portnoy 1989). *Listeria* can propel itself through the cytoplasm of its host cell essentially by “surfing” on a wave of actin polymerization due to proteins on one end of the pathogen that activate actin polymerization factors like those which generate the branched actin filaments described above. This activity occurs independently of the action of motor proteins, showing that actin itself can produce a force sufficient to drive the motion of cytoplasmic compartments or vesicles.

Although actin can do work independently of motor proteins, coupling actin polymerization to the action of myosins can expand the range of biological functions attributable to the cytoskeleton in eukaryotic organisms. The extension of lamellipodia into phagocytic cups for the engulfment of an extracellular object involves the coordinated action of myosins and the actin cytoskeleton {{229 Swanson,J.A. 1999; 230 Cox,D. 2002}}. In a similar fashion, the actin cytoskeleton and associated myosin motors have been implicated in macropinocytic events in

acanthamoeba (Ostap et al. 2003)(Swanson et al. 1999, Cox et al. 2002). Organelle transport by myosins is also dependent on having a dynamic actin cytoskeleton that can polymerize into filaments and turn over monomers (Semenova et al. 2008).

Thus, the interactions between the actin cytoskeleton and myosin motors provide a coordinated mechanism through which a cell can support a variety of functions not limited to long distance transport of organelles or vesicles. While the breadth of this field is beyond the scope of this thesis, it is important to consider the range of potential functions for a myosin, and how those functions are regulated. Functions such as tethering of an organelle in the cortical actin network require that myosins remain fixed to an actin filament for a long period of time. Long-distance transport of organelles, on the other hand, requires that myosin motors be able to navigate the dense network of filaments in the cytoplasm. Furthermore, the regulation of myosin force production to prevent improper timing of organelle movements enables the motor to effectively function in the cell.

There are similarities in myosin structure and biochemistry common to members of the superfamily that can provide a background against which we can compare the details of the work presented in this thesis. Perhaps the earliest and most comprehensively studied example of a myosin-actin system is provided by myosin-II, otherwise known as conventional myosin, in the context of skeletal muscle.

1.7 Myosin II

1.7.1 Myosin II in skeletal muscle

Myosin II is best known as the force-generating contractile protein in muscle. Skeletal muscle (figure 1.4) is an organ system composed of a series of long, cylindrical, multinucleated cells called fibers, which are arranged into bundles. Within each fiber are the contractile units of muscle, myofibrils. Myofibrils consist of repeating units connected in series called sarcomeres. The sarcomeres contain the principle force-generating structure of muscle consisting of two types of filaments, the thick and thin filaments. The thick filament was isolated and identified by A. Szent-Gyorgyi and found to be Myosin II (Szent-Gyorgyi 1941, Szent-Gyorgyi, Banga 1941). The thin filament was characterized by F. B. Straub and named actin for its ability to activate the myosin in the thick filament.

The thick and thin filaments are oriented in such a way that the heads of the myosin in the thick filament exist in a bipolar arrangement and free to interact with the actin in the thin filament (HUXLEY 1963). This orientation allows myosins to power sliding of the thin filament relative to the thick filament from both ends of the sarcomere, thus contracting the Z-disks on either side of the myofilaments towards the center of the sarcomere. The degree of overlap between the filaments would therefore be expected to change during muscle stimulation, which turns out to be the case (HUXLEY, NIEDERGERKE 1954) (PAGE, HUXLEY 1963). This model for muscle contraction, based on the interaction of myosin and actin in thick and thin

filaments is called the “sliding filament theory” of muscle contraction, proposed by A.F. Huxley (HUXLEY 1957).

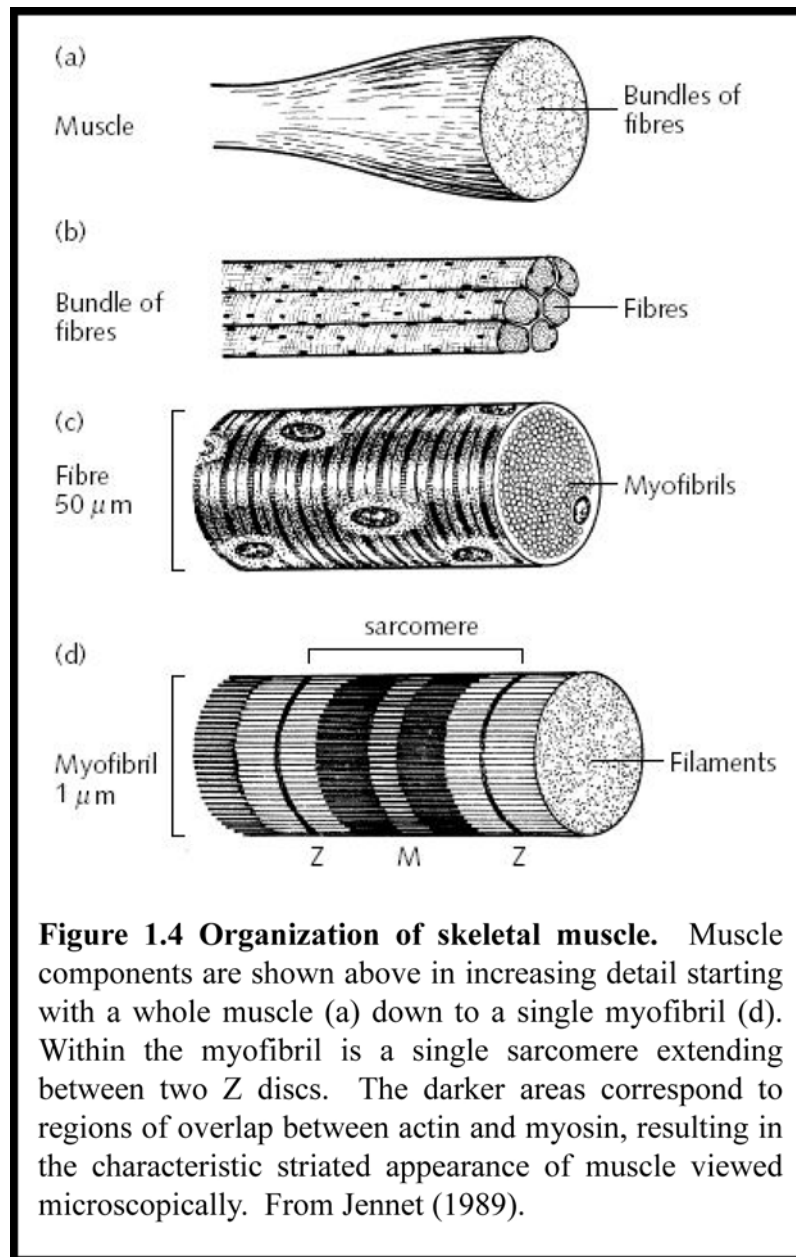
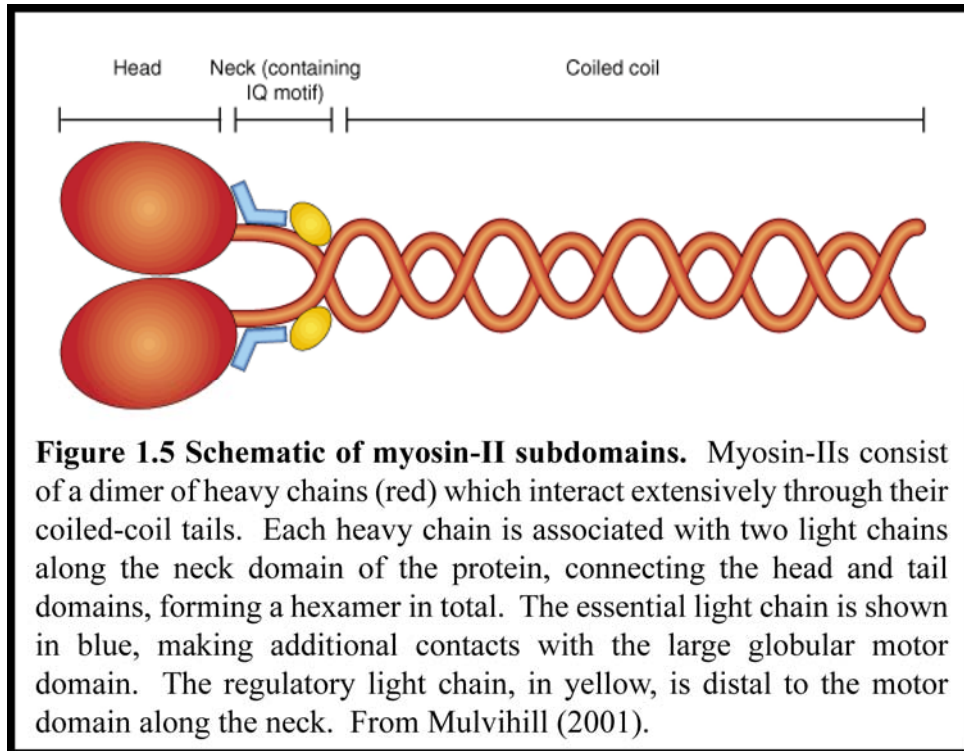


Figure 1.4 Organization of skeletal muscle. Muscle components are shown above in increasing detail starting with a whole muscle (a) down to a single myofibril (d). Within the myofibril is a single sarcomere extending between two Z discs. The darker areas correspond to regions of overlap between actin and myosin, resulting in the characteristic striated appearance of muscle viewed microscopically. From Jennet (1989).

1.7.2 Domain architecture of Myosin-II

Myosin II is a hexameric protein of total molecular weight (MW) ~500 kDa consisting of two dimerized heavy chains of MW ~200 kDa with associated light chains of MW ~19 kDa and ~25 kDa. Limited proteolytic digestion of myosin II produces two fragments which are distinguished by high percentage coiled-coil structure (light meromyosin, LMM) versus the ability to bind actin and hydrolyze ATP (heavy meromyosin, HMM) (GERGELY 1953)(MIHALYI, SZENT-GYORGYI 1953, SZENT-GYORGYI 1953). Work by Susan Lowey et al. showed that HMM could be further digested to produce HMM-subfragment 1, which contained single monomer heads and associated light chains, and HMM-subfragment 2, which contained part of the coiled-coil rod (Lowey et al. 1969). This provided evidence that myosin was a dimer of heavy chains joined through association of their coiled-coil tails. The insoluble nature of the coiled-coil region of LMM suggested early on that it was the component responsible for thick filament formation in muscle.

Isolation and identification of the light chains of myosin II was accomplished by various chemical treatments, including urea, guanidine-HCl, or alkaline pH followed by gel electrophoresis separation (Gershman, Stracher & Dreizen 1969) (Frederiksen, Holtzer 1968) to generate three species of light chain with different molecular weights, one of which was ~19 kDa, and two ~25 kDa. The 25 kDa light chains were determined



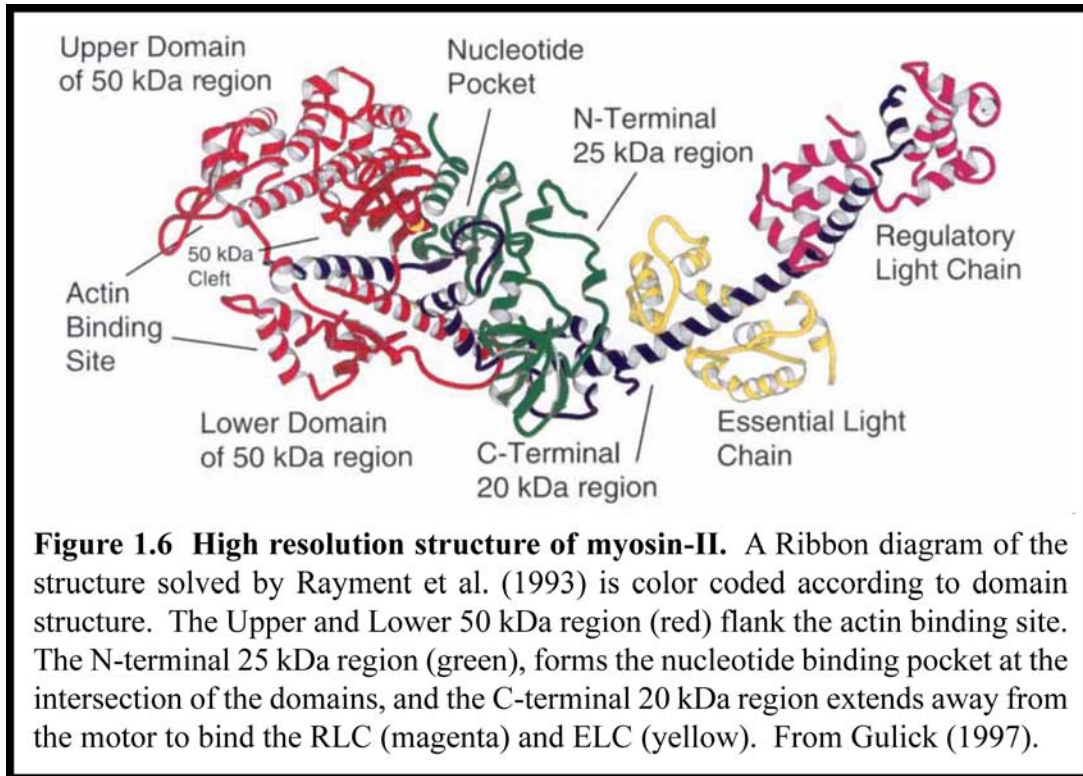
to be required for catalytic function of the myosin ATPase (Dreizen et al. 1967) and are therefore called the essential light chains (ELC). The regulatory light chain (RLC), while nonessential for overall function of the protein, is regulated via phosphorylation by myosin light chain kinase (MLCK), which increases the actin-activated ATPase of the myosin (Small, Sobieszek 1977). Myosin-II light chains are structurally related to the protein calmodulin, which binds to the neck region of other myosin superfamily proteins.

This early work on myosin II structure identified the three important domains that are now known to be common to all cytoskeletal motor proteins. The head in subfragment 1 binds actin and hydrolyzes ATP, while the long coiled-coil tail is responsible for dimerization and higher-order organization of the protein.

Joining the head and tail is the neck region, otherwise known as the regulatory domain, which has associated light chains responsible for both overall function and proper regulation of myosin activity.

1.7.3 High-resolution structure of the myosin II motor domain

The motor domain represents the most highly conserved feature of all members of the myosin superfamily, and the general structural features of the myosin II head are likely similar among all myosins with few exceptions. The first high-resolution structure of myosin II was obtained in 1993 (Rayment et al. 1993b) by methylating lysine residues of subfragment 1 to generate a crystallizable construct with the associated light chains (figure 1.6). Three main fragments originally identified by limited proteolytic digestion of the S1, termed the 50 kDa, 25 kDa, and 20 kDa regions, dominate the overall structure with the 50 kDa region forming the actin binding site and the 20 kDa region extending away from the motor as an extended alpha-helix.



At the intersection of these domains is a 7-stranded beta-sheet with the nucleotide binding pocket located at the end of the central beta strand. The three main elements of the binding pocket consist of three loops; switch I, switch II, and the P-loop. These loops interact with the magnesium ion, catalytic water, and nucleotide and can transmit information about the nucleotide hydrolysis state in the pocket to the rest of the molecule. These conserved elements make myosins a member of a much larger family of proteins called P-loop NTPases, which includes kinesin.

The 50 kDa region is separated by a cleft that spans the length of the entire domain and connects the nucleotide binding pocket with the actin binding site. The actin binding site is composed of residues from both the upper and lower domains,

and the relative motions of the two domains have consequences for the actin affinity of myosin. Importantly, this cleft was recognized early on as a means of communication between the actin-myosin interface and nucleotide binding pocket (Rayment et al. 1993a). When the myosin is bound to an actin filament the cleft is closed to allow proper formation of the actin-binding interface. The cleft must be open, however, to allow space for the gamma-phosphate of ATP in the nucleotide binding pocket. Such communication would be necessary to ensure proper coupling of the biochemical cycle of myosin to force production. (Small, Sobieszek 1977)

1.7.4 Biochemical cycle of myosin

Early solution kinetics studies of the ATP hydrolysis activity of myosin established that (1) binding of ATP to myosin causes dissociation of the actomyosin complex and (2) that under steady-state conditions, actin increases the overall rate of ATP hydrolysis by a single myosin head (Eisenberg, Zobel & Moos 1968). This led to a proposal for a possible scheme for muscle contraction based on cyclic binding and hydrolysis of ATP, actin, and myosin. A series of papers following this work by EW Taylor and RW Lymn elucidated the biochemical mechanism of this cycle using transient kinetic techniques (Lymn, Taylor 1971, Lymn, Taylor 1970, Taylor, Lymn & Moll 1970).

In order to measure the rate of hydrolysis of ATP, Lymn and Taylor developed the chemical quench-flow apparatus. Briefly, by modifying a conventional stopped-flow experiment, they could mix samples containing substrate

and product and acid-quench the reaction after a set time by varying flow rate or tubing length. Phosphate liberation could then be measured by the amount of radioactive phosphate (from labeled ATP) in solution. From this analysis, they determined that the initial rate of phosphate release of 50-75 s⁻¹, termed the “phosphate burst”, corresponded to the steady-state rate of hydrolysis of ATP (Lymn, Taylor 1971, Lymn, Taylor 1970), but was slower than the rate of dissociation of actomyosin by ATP (> 250 s⁻¹) as measured by dissolution of solution turbidity. Rapid gel separation of myosin and radiolabeled hydrolysis products in the absence of actin showed that the rates of ADP and phosphate release were both slow and likely rate limiting under steady-state conditions (Taylor, Lymn & Moll 1970). Repeating the gel separation technique in the presence of actin however, showed that the hydrolysis products dissociate from myosin faster by at least a factor of 10 in the presence of actin (Lymn, Taylor 1971).

Taken together, the work by Lymn and Taylor show that hydrolysis of ATP likely occurs after dissociation of myosin from actin, and the rate of product release is sped up greatly by binding of actin to myosin. This provided detailed biochemical clues to the actomyosin ATPase cycle as it relates to muscle contraction, and the Lymn and Taylor model as summarized in figure 1.7 provides quantitative biochemical counterparts to the main aspects of the Huxley sliding filament theory. Future work would expand the biochemical cycle and further elucidate structural and strong/weak binding states associated with specific biochemical states (figure 1.11).

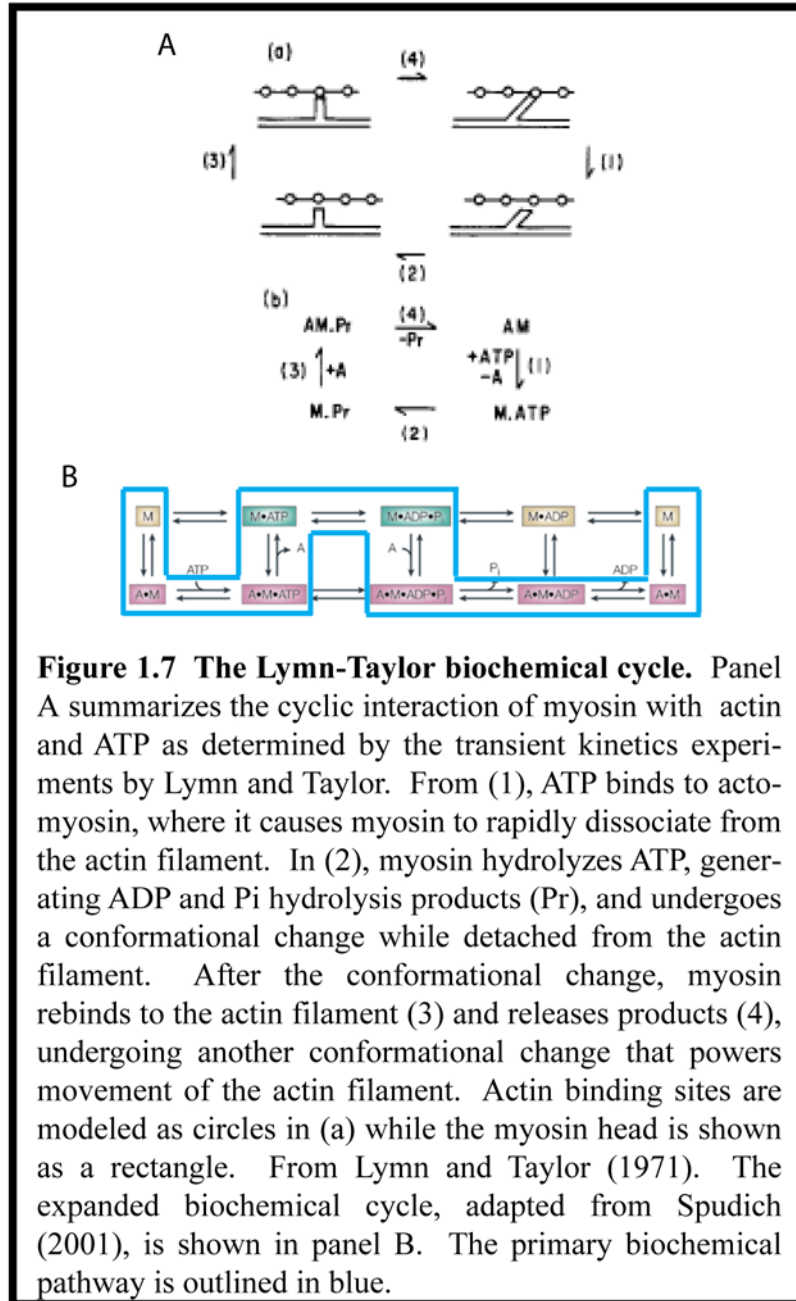


Figure 1.7 The Lymn-Taylor biochemical cycle. Panel A summarizes the cyclic interaction of myosin with actin and ATP as determined by the transient kinetics experiments by Lymn and Taylor. From (1), ATP binds to actomyosin, where it causes myosin to rapidly dissociate from the actin filament. In (2), myosin hydrolyzes ATP, generating ADP and Pi hydrolysis products (Pr), and undergoes a conformational change while detached from the actin filament. After the conformational change, myosin rebinds to the actin filament (3) and releases products (4), undergoing another conformational change that powers movement of the actin filament. Actin binding sites are modeled as circles in (a) while the myosin head is shown as a rectangle. From Lymn and Taylor (1971). The expanded biochemical cycle, adapted from Spudich (2001), is shown in panel B. The primary biochemical pathway is outlined in blue.

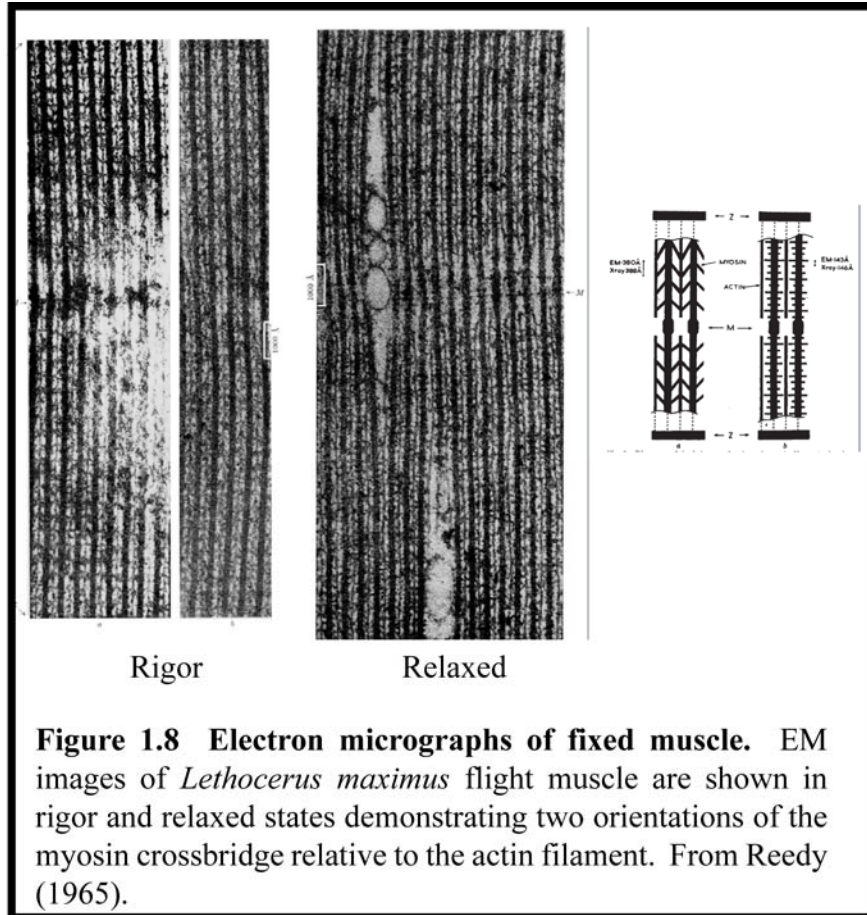
This cycle is a common feature among all members of the myosin superfamily although the individual rate constants may differ (De La Cruz, Ostap 2004). One of the consequences of alterations in particular rate constants in the

actomyosin ATPase cycle is to change the fraction of time the myosin spends attached to the actin filament, otherwise known as the duty ratio. By modifying the duty ratio, a myosin motor can be kinetically tuned to perform different functions inside a cell, highlighting a biochemical method of functional diversity in the myosin superfamily. A theme of this thesis is how force can affect this biochemical cycle in predictable ways, such as modifying the duty ratio, and what these effects might be on the function of an unconventional myosin.

1.7.5 The swinging lever arm model

In order to couple the biochemical cycle of myosin to the relative movement of thick and thin filaments in muscle, or the movement of intracellular cargoes by unconventional myosins, it is necessary to determine how force is converted from the chemical energy stored in ATP to mechanical work. The nature of this mechanical work is produced by a rotation of the myosin lever arm, coupled to release of ATP hydrolysis products, in what is now called the “power stroke”. The crystal structure of the myosin S1 gives an indication of how movements in the motor domain may be coupled to an angular change in the long alpha-helix extending away from the motor domain (the lever), however the snapshot of a rigor conformation alone gives an incomplete picture of the dynamics of the power stroke of myosin.

Early electron micrographs showed that the interaction between thick and thin filaments was accomplished by the presence of a crossbridge now known to be

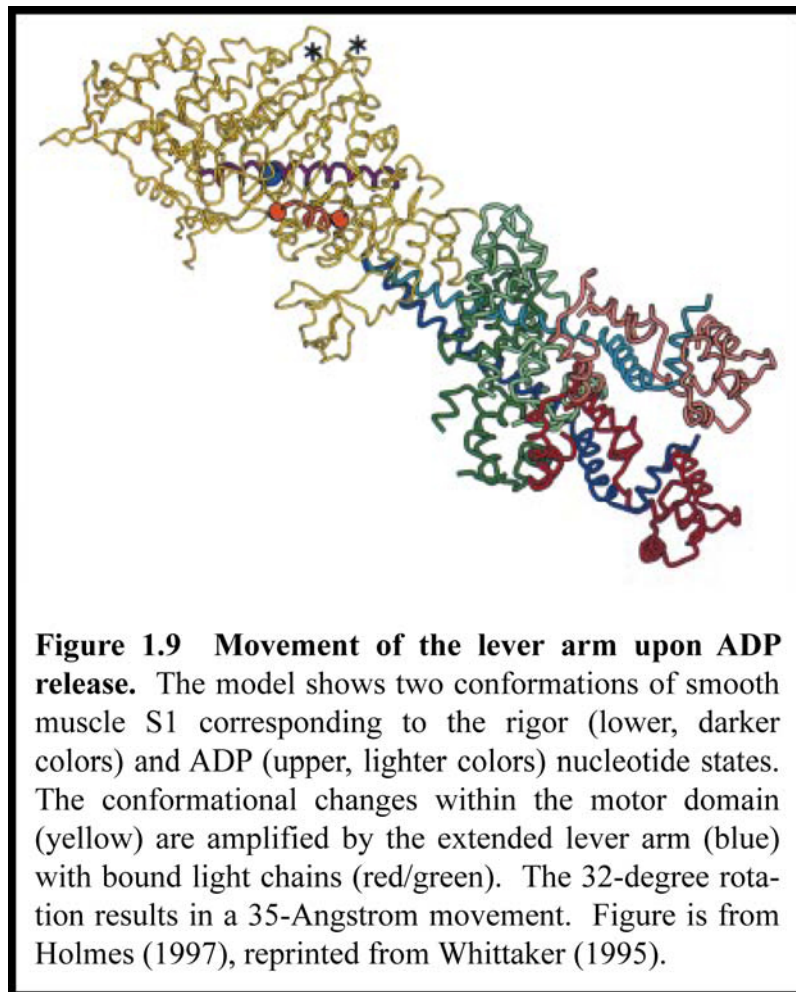


the head domain of myosin II (HUXLEY 1957). The first direct observations of multiple states of crossbridge attachment were made by comparing electron micrographs of insect flight muscle prepared in the presence and absence of ATP to generate the relaxed and rigor conformations of the crossbridge (Reedy, Holmes & Tregear 1965). The rigor preparation showed crossbridges tilted at an angle of 45° relative to the thin filament. Alternatively, muscle fixed in the presence of ATP showed a different orientation, with the myosin heads roughly 90° or perpendicular to the thin filament. This work was further substantiated by low angle x-ray

diffraction patterns, which showed that actin and myosin helical periodicities did not change between resting and contraction, while the changes in 145 Å meridional reflections corresponding to the helical arrangement of crossbridges suggested a significant change between relaxed and rigor muscle (Reedy, Holmes & Tregear 1965, Huxley, Brown & Holmes 1965, Huxley, Brown 1967). This work led to H. E. Huxley's 1969 proposal that a change in the orientation of the crossbridges, coupled somehow to ATP hydrolysis, could account for force production during muscle shortening (Huxley 1969).

Direct experimental evidence soon followed the predictions made by the diffraction patterns. Crossbridges could be partially synchronized by subjecting frog muscle fibers to rapid length changes and measuring the resulting changes in tension in the interval during and immediately after the length changes. In these experiments, a rapid tension change during the length change (T1) is followed by a slower resolution (T2) of tension to the resting state. This work was interpreted to mean that the crossbridge of muscle was composed of two elements in series, an elastic element responsible for the initial generation of tension as well as a visco-elastic element which would eventually share the tension generated by the first element (Huxley, Simmons 1971). The overall response was due to the stretching of the coiled-coil domain of the myosin in response to the rapid length change (T1), which was followed by a rotation of the S1 head of the myosin backwards about a fulcrum point to what we now know is the pre-power stroke state (T2). The overall conclusions (Huxley et al. 1983) of this work were very much in line with the

proposal of the swinging cross-bridge model, and in line with subsequent x-ray diffraction patterns during crossbridge sliding with millisecond time resolution showing the decrease in intensity of the 145 Å meridional reflection (Huxley et al. 1983).



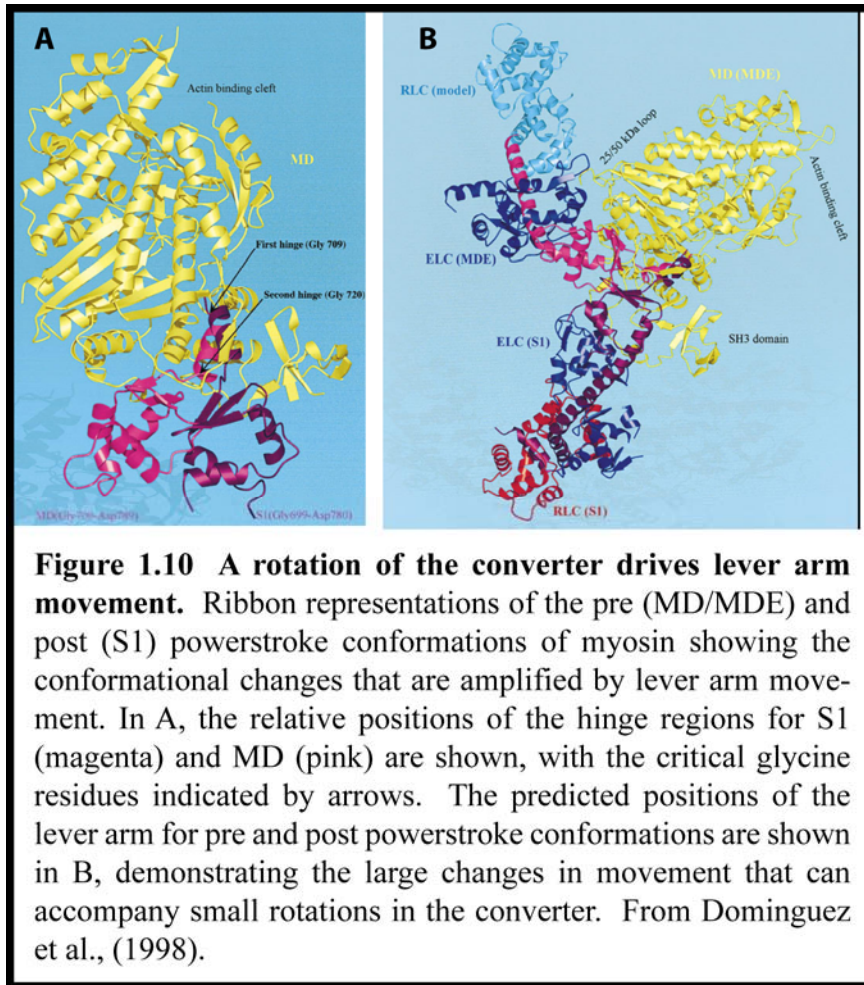
Synchronization of force generation by tilting was correlated with a specific change in biochemical states, specifically the release of phosphate from the myosin head (Hibberd et al. 1985). Hibberd and colleagues utilized a “caged” ATP compound which could be activated by laser-pulse photolysis to synchronously

activate muscle crossbridges and induce a rapid tension decrease corresponding to crossbridge detachment. The amplitude of the restoration of that tension, which occurs due to force generation by active crossbridges, is reduced in the presence of 10mM free phosphate. This is a consequence of Pi rebinding to AM·ADP and generating a weakly bound state. Since the restoration of tension is due to entry into the force generating state, the rate of tension generation can be expressed as the sum of the forward and reverse rate constants for the force generating state. The rate of tension restoration is increased in 10 mM phosphate, suggesting that rebinding of phosphate to AM·ADP also reverses the power stroke that accompanies force generation.

Direct visualization of different cross bridge states coupled to biochemical states would be fundamental to graduation of the swinging crossbridge model to the swinging lever-arm model for the myosin power stroke, and very compelling evidence has been generated from structural studies capturing myosin S1 in different conformations. Cryo-EM reconstructions from two different myosins in the presence and absence of MgADP displayed two different orientations of the lever arm extending away from the motor domain, with little structural change within the motor domain itself (Jontes, Wilson-Kubalek & Milligan 1995, Whittaker et al. 1995). The rotations of the lever arm in these studies accounted for $\sim 23^\circ$ for smooth muscle myosin II (a conventional myosin, figure 1.9) and 32° for brush-border myosin I (an unconventional myosin). These angular rotations resulted in displacements of 35 Å and 50 Å respectively along the axis of the actin filament.

These reconstructions provided evidence that a change in biochemical state in the nucleotide binding pocket could correspond to changes in the lever arm orientation. The comparison between ADP and rigor states also suggested that there could be an additional force generating step after phosphate release.

A limitation of the EM reconstructions, however, was their lack of fine resolution of the motor domain. Although the authors could correctly state that no large-scale readjustments to the motor domain occurred, the location of the pivot point for the lever arm was not resolvable. Crystal structures of vertebrate smooth muscle myosin in a pre-power stroke state were determined in the presence of ADP·AlF₄, an ATP analogue; as well as ADP·BeF_x, a transition state analogue (Dominguez et al. 1998). In comparison with the 1993 Rayment et al. skeletal muscle structure, the structures in the presence of ATP or transition state analogues showed a tilt of the “converter” domain, so named due to it being a communication point with interactions bridging both the nucleotide binding pocket of myosin as well as the lever arm. In both pre-power stroke structures, the converter is tilted roughly 70° relative to the post-power stroke structure in the Rayment 1993 S1 structure due to rotations about two conserved glycine residues in the SH-1 helix (positions 709 and 720, figure 1.10), however the major rotation occurs at Gly720, suggesting it is the pivot point for the power stroke. Mutations in these residues uncouple the biochemical cycle of myosin from the power stroke, rendering it unable to undergo the conformational changes necessary to produce force (Patterson et al. 1997) .



An important prediction of the swinging lever-arm model is that the effective length of the lever arm will affect the force generated by the rotation of the converter domain. The development of actin-gilding motility assays (Kron, Spudich 1986), in which myosin molecules are fixed to the surface of a glass coverslip and allowed to interact with free fluorescently-labeled actin filaments, provides an opportunity to test such a prediction. Uyeda et al. generated myosin constructs with 0 – 3 light chain binding sites to create lever arms of different predicted lengths. In agreement with the swinging lever arm model, the velocity of sliding actin filaments

moving on the surface of the myosin-coated coverslip were linearly related to the length of the lever arm (Uyeda, Abramson & Spudich 1996a). In an analogous experiment, Anson and coworkers generated artificial lever arms with comparable stiffness by substituting alpha-actinin repeats for light chain binding sites and found similar results in motility assays (Anson et al. 1996). Importantly, the kinetic properties of the motor were unchanged by the length of the neck, suggesting that the neck served primarily as a rigid lever arm which amplified the small conformational changes in the motor domain.

Taken together, the swinging lever arm model is supported by a convincing sum of evidence. The coordination of biochemistry, force production, and angular movement of the lever demonstrate in exquisite detail how the cyclic hydrolysis of ATP by myosin, coupled to structural states that differ in actin affinity, can produce force by amplifying a conformational change in the converter region of the motor into a large displacement of the lever arm (figure 1.11). One of the aims of this thesis is to examine the lever arm as it relates to other properties of the myosin, specifically force dependence and stiffness.

1.8 Myosin I

1.8.1 Isolation and characterization of myosin-I

In 1973 Pollard and Korn purified an ATPase from *Acanthamoeba* Castellani which shared many common features with the known myosins from

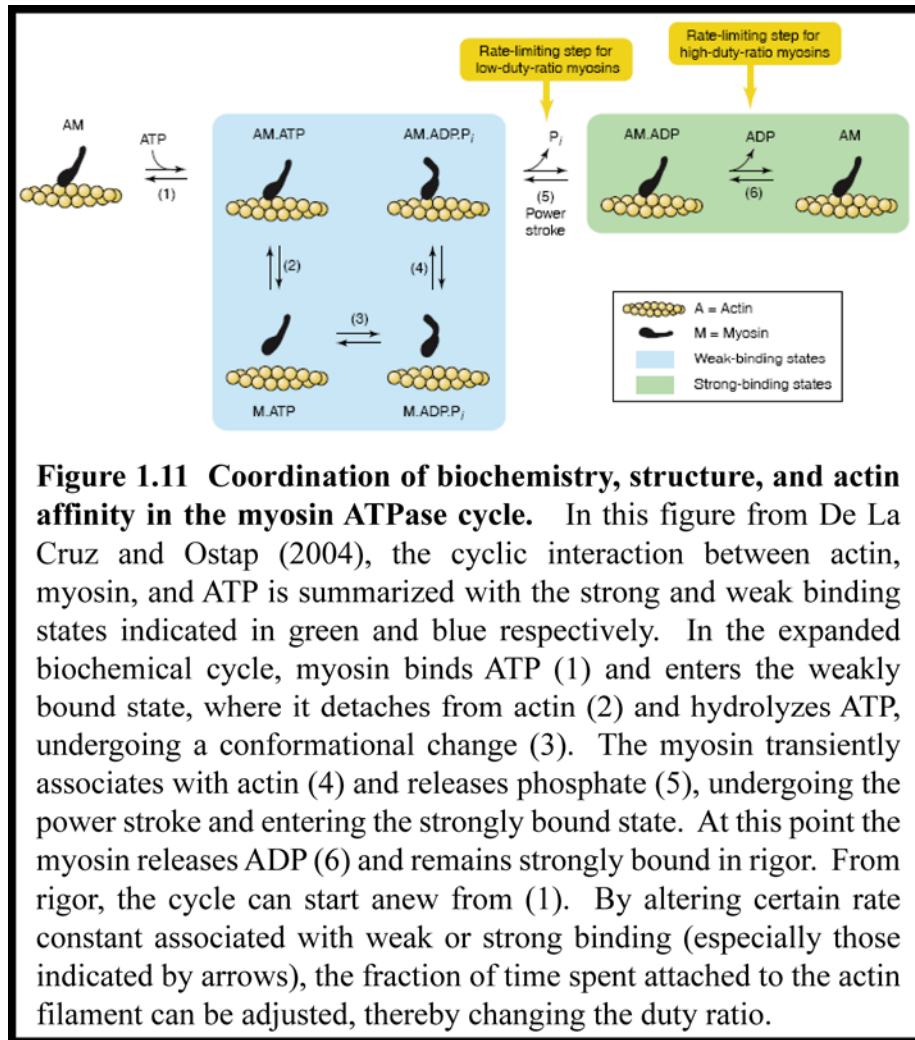


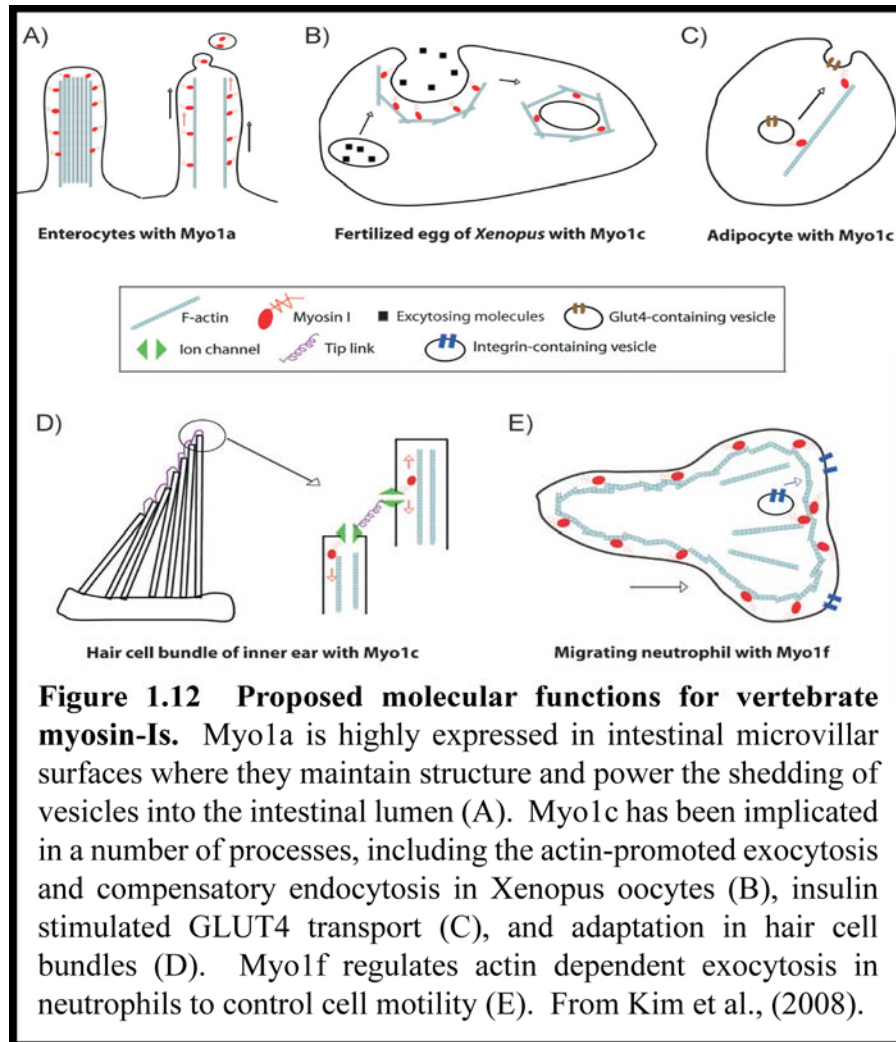
Figure 1.11 Coordination of biochemistry, structure, and actin affinity in the myosin ATPase cycle. In this figure from De La Cruz and Ostap (2004), the cyclic interaction between actin, myosin, and ATP is summarized with the strong and weak binding states indicated in green and blue respectively. In the expanded biochemical cycle, myosin binds ATP (1) and enters the weakly bound state, where it detaches from actin (2) and hydrolyzes ATP, undergoing a conformational change (3). The myosin transiently associates with actin (4) and releases phosphate (5), undergoing the power stroke and entering the strongly bound state. At this point the myosin releases ADP (6) and remains strongly bound in rigor. From rigor, the cycle can start anew from (1). By altering certain rate constant associated with weak or strong binding (especially those indicated by arrows), the fraction of time spent attached to the actin filament can be adjusted, thereby changing the duty ratio.

smooth and skeletal muscle (Pollard, Korn 1973). Like muscle myosin, the new ATPase was able to bind (and be activated by) actin in an ATP dependent manner. Notable differences however, include the inability of *Acanthamoeba* myosin to form bipolar filaments, a smaller molecular weight, and different amino acid composition. Purification of other myosins with similar activity soon followed in *acanthamoeba* (Maruta et al. 1979), simple eukaryotes, (Cote et al. 1985), and vertebrate brush borders (Mooseker, Pollard & Fujiwara 1978).

By screening an acanthamoeba genome library with a probe specific for a nematode myosin II, Hammer et al. identified and cloned the myosin-IB gene which, due to the size of its mRNA product, proved that the new myosins-I could not be degradation products of myosin II and were unique gene products (Hammer, Jung & Korn 1986). Amino acid sequence analysis demonstrated that the motor domains were highly conserved relative to conventional myosin-II and therefore the newly discovered unconventional myosin-Is represented “true” myosins.

1.8.2 General features of myosin-Is

Myosin-Is are widely expressed, single headed members of the myosin superfamily that bind to the plasma membranes of cells and participate in membrane structure and dynamics, and responses to signaling events (Kim, Flavell 2008). Myosin-Is can be loosely grouped into two subclasses based on the length of their tails. Eight myosin-I isoforms are expressed in humans, six short tailed forms (Myo1a, b, c, d, g and h) and two long-tailed (Myo1e and f) (Berg, Powell & Cheney 2001). Short-tailed myosins have a basic tail region called the tail homology 1 (TH1) domain, while long-tailed isoforms have, in addition to the basic region, a conserved tail homology 2 (TH2) domain rich in proline and alanine as well as an SH3 domain (Coluccio 1997). The neck region of myosin-Is consist of a variable number (0-6) of IQ motifs, which can bind calmodulins or calmodulin-like proteins in a calcium-sensitive manner.



1.8.3 Myosin-I tails

The highly divergent tails of myosin-I are largely responsible for their plasma membrane localization and some protein binding characteristics. The basic tail can bind to anionic phospholipids via electrostatic interactions (Hayden, Wolenski & Mooseker 1990, Adams, Pollard 1989) and generate force while associated with the membrane to power the movement of actin filaments in vitro (Zot, Doberstein & Pollard 1992). Using large unilamellar vesicles as model

membrane systems, Hokanson and Ostap measured the affinity for the myo1c tail to LUVs of varying phospholipid composition (Hokanson, Ostap 2006). While the myo1c tail bound weakly to physiological concentrations of phosphatidylserine (40%), the tail bound strongly to LUVs containing a physiologically relevant concentration (2%) of the important signaling lipid phosphatidylinositol 4,5-bisphosphate (PIP₂).

Both PS and PIP₂, being negatively charged (net charge -1 and -4 per headgroup at pH 7, respectively) would be expected to bind to the tail via electrostatic interactions, but by normalizing tail binding to the total negative charge, Hokanson and Ostap demonstrated that the tight binding of the myo1c tail is specific for PIP₂. This binding is inhibited by the soluble headgroup of PIP₂, inositol 1,4,5 trisphosphate (InsP₃), which is generated by cleavage of the PIP₂ by phospholipase C (PLC) in response to signaling events. Subsequent site directed mutagenesis and modeling studies demonstrated that the PIP₂ binding region of the tail was similar in structure and function to a pleckstrin homology (PH) domain, and that this putative PH domain is a common element among vertebrate myosin-Is (Hokanson et al. 2006).

Protein binding via the tail is best described in the long-tailed myosin-Is of lower eukaryotes. The tail domain of fission yeast myosin-I (myo1p) is able to influence actin dynamics at the cell cortex by binding to and activating the Arp2/3 complex, known for its ability to nucleate branched actin filaments and generate dendritic actin networks. (Lee, Bezanilla & Pollard 2000). Budding yeast myosin-Is

(myo3p and myo5p) influence actin dynamics in a similar fashion through binding of verprolin as mediated by the SH3 domain of their tails. Verprolin can then interact with Bee1p/Las17p which themselves activate the Arp2/3 complex. (Lechler, Shevchenko & Li 2000, Geli et al. 2000, Evangelista et al. 2000). Jung et al. used the SH3 domains of the dictyostelium myosin-I's myoB and myoC to look for potential binding partners by incubating a GST-SH3 resin with Dictyostelium cell extracts (Jung et al. 2001). They discovered a myosin-I binding partner, p116, which serves as a scaffold for binding to the Arp2/3 complex and actin capping protein. The protein was renamed CARMIL, which stands for capping protein, Arp2/3, myosin-I linker. Sequence analysis confirmed homologues of CARMIL in Acanthamoeba, Drosophila, C. elegans, mouse, and human, suggesting that the ability of myosin-I's to modulate Arp2/3 dependent actin polymerization through their SH3 domains may be more general.

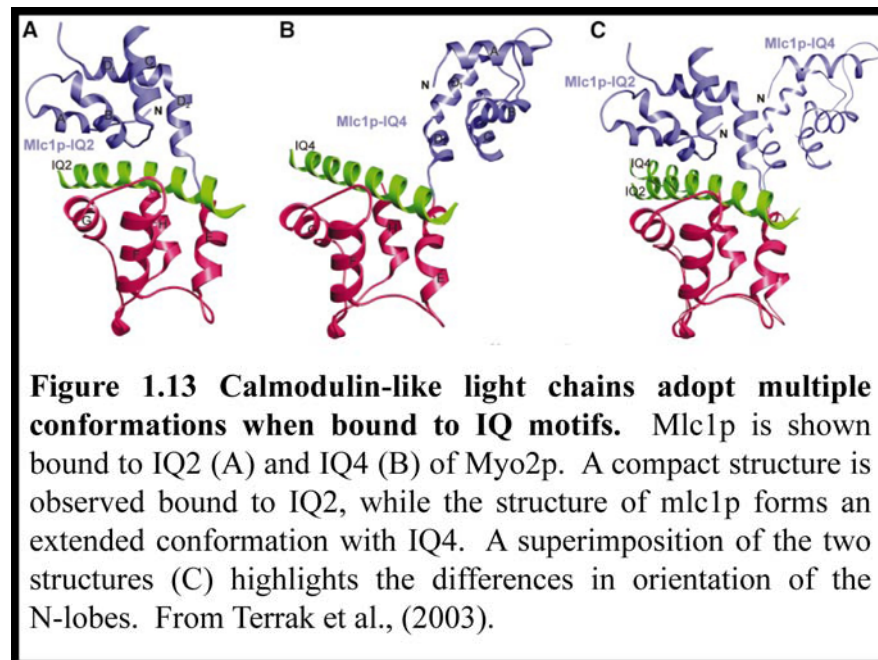
The variety in domain organization and binding mediated by the tail of myosin-I's is likely a consequence of the ancient evolutionary history of class I myosins (Richards, Cavalier-Smith 2005). Although this thesis does not deal specifically with the myosin-I tail and its binding partners, it is important to consider the tail in the context of myosin-I localization when we consider how force could affect myo1b function.

1.8.4 The myosin-I lever arm

The neck domains of myosin-I_s, also called the light chain binding domain (LCBD) are primarily made up of tandem repeats of IQ motifs, 20-25 residue sequences which contain the consensus sequence IqxxxRGxxxR. These motifs serve as target sites for the binding of calmodulin (CaM) or calmodulin-like proteins. Binding of light chains to IQ motifs is proposed to help stabilize the extended α -helical structure of the IQ motif to allow it to better serve as a lever arm (Bahler, Rhoads 2002). Thus, the number of IQ motifs along the myosin-I neck and the nature of their interaction with calmodulin has important effects on the mechanical properties of the myosin.

CaM is a small (~17 kDa) protein with two globular lobes separated by a flexible hinge region. Upon binding to IQ motifs, the α -helix of the hinge region partially dissolves, allowing the two lobes of CaM to wrap around the motif in a conformation stabilized by a number of hydrophobic interactions (Ikura et al. 1992). Specifically, the C-terminal lobe of CaM binds the IQxxxR portion of the motif while the N-terminal lobe is specific for the GxxxR half. Each lobe of CaM contains two EF-hand motifs, which in the absence of calcium adopt a “closed” conformation in which the hydrophobic core of each lobe is buried and inaccessible, otherwise known as apo-CaM. Binding of calcium to the EF-hand motifs causes a conformational change in which the lobe transitions to an “open” state, thus exposing the hydrophobic core (Grabarek 2006). CaM generally binds tightly to IQ-motifs in the calcium-free form of the protein, while binding of calcium

generally results in weak binding and eventually dissociation of one or more CaMs from the neck region of a myosin-I under increasing calcium conditions (Manceva et al. 2007, Lin, Tang & Ostap 2005). While the majority of light chain binding to myosin-I in cells is likely due to CaM, there exists evidence that alternative light chains could compete with CaM in the presence of calcium, with potential consequences on myosin targeting inside cells (Tang et al. 2007).



While atomic-level structural information regarding the binding of CaM to the IQ-motifs of myosin-I is lacking, a variety of conformations of bound CaM (and CaM like proteins) exist in complex with the IQ motifs from other unconventional myosins. Besides the general closed and open forms of CaM, a semi-open conformation allows partial exposure of hydrophobic residues for tight binding to the IQ motifs of myosin-V and may inhibit the binding of calcium to the EF-hands of CaM to prevent dissociation (Houdusse et al. 2006). Two different

structures of mlc1p (a CaM-like protein) are seen in x-ray crystallographic structures depending on the IQ motif of myosin-V to which it is bound. When bound to IQ2, both lobes of mlc1p interact extensively with the IQ-motif in a structure resembling the conventional apo-CaM interaction with an IQ-motif. However, the structure of mlc1p bound to IQ4 of the myosin is strikingly different, with the N-terminal lobe of CaM free from the IQ motif and loosely tethered to the bound C-terminal lobe (Terrak et al. 2003).

Binding specificity and calcium sensitivity of the CaM interaction with IQ motifs is highly dependent on not just the highly conserved residues of the IQ motifs, but also the more variable residues, resulting in inconsistent calcium sensitivity for IQ motifs along the regulatory domains of myosins with multiple IQ motifs. Differences in binding could also account for variation in the mechanical properties of the myosin lever, a possibility that will be investigated in this thesis by measuring the stiffness of the acto-myosin crossbridge as a function of the number of IQ motifs.

1.8.5 Potential functions of myosin-Is

The function of myosin-I described in 1.8.3 represents an incomplete picture of the range of potential functions for myosin-Is in the context of the cell. In addition to actin-polymerization activity, myosin-Is in yeast contribute to endocytic events and cell motility in collaboration with the actin cytoskeleton as described earlier in this thesis (section 1.6). Like vertebrates, yeast cells express multiple

class-I myosins with overlapping potential functions (Wessels et al. 1991, Jung, Wu & Hammer 1996). Inactivating mutations of single myosin-Is show little or no defect in endocytosis or cell migration, however inactivating multiple myosin-Is in the same cell has more profound functional consequences in these processes. It has therefore been proposed that the collective expression of multiple myosin-I isoforms contributes to overall efficiency of cellular processes in yeast.

How myosin-Is contribute in a general way to increased efficiency can potentially be understood by monitoring the effects of myosin-I expression levels on the forces produced by the dendritic network of actin filaments in the cell cortex, otherwise known as cortical actin tension. Using a micropipette aspiration technique, Dai et al., measured the relative cortical actin tension in *Dictyostelium* cells overexpressing myosin-I proteins and found them to have an increased cortical tension relative to control (Dai et al. 1999). Alternatively, the same measurements showed a decrease in tension in *Dictyostelium* cells lacking multiple myosin-Is, consistent with the prediction that myosin-Is are partially functionally redundant. The generation of cortical actin tension by myosin-Is in yeast is likely closely related to the established roles of myosin-I in actin polymerization and endocytosis (Titus 2000). Emerging evidence suggests that similar roles are carried out by myosin-Is in vertebrates (figure 1.12).

Myosin-Ia (*myo1a*), otherwise known as brush border myosin-I, has a well defined function in the apical microvilli of intestinal brush border cells, wherein *myo1a* connects the plasma membrane with the underlying bundle of cross-linked

actin filaments in each microvillus. Myo1a knockout mice, developed in the Mooseker lab, show disruption of microvillar architecture and loss of proper spacing between the actin cytoskeleton and the plasma membrane, in addition to a decrease in vesicle shedding from the microvilli into the lumen of the intestines (Tyska et al. 2005b, McConnell et al. 2009). These results, taken together, indicate that myo1a motor activity can generate tension in the intestinal microvilli, which is important for proper structure and overall function of the intestine.

In the case of myosin-Ic (myo1c), a more diverse range of functions has been described, involving vesicle trafficking, endocytosis, exocytosis, and adaptation in hair cell bundles (figure 1.12). The ability of a myosin to generate tension is proposed for models of hair cell adaptation in which myo1c functions to link membrane-associated ion channels with the underlying actin cytoskeleton (Batters et al. 2004c, Gillespie, Cyr 2004). In such a model, deflections of the hair cell bundles change the probability that a membrane-associated mechanosensitive ion channel will be open or closed depending on the direction and magnitude of the deflection. Myo1c has been proposed to move along the actin filament in response to bundle deflection, generating a force via motor activity which restores the resting tension between the mechanosensitive ion channel and the motor. Consistent with this model, myo1c mutants that are specifically inhibited by ADP analogs were expressed in mice, and these mutant mice showed adaptation defects (Holt et al. 2002).

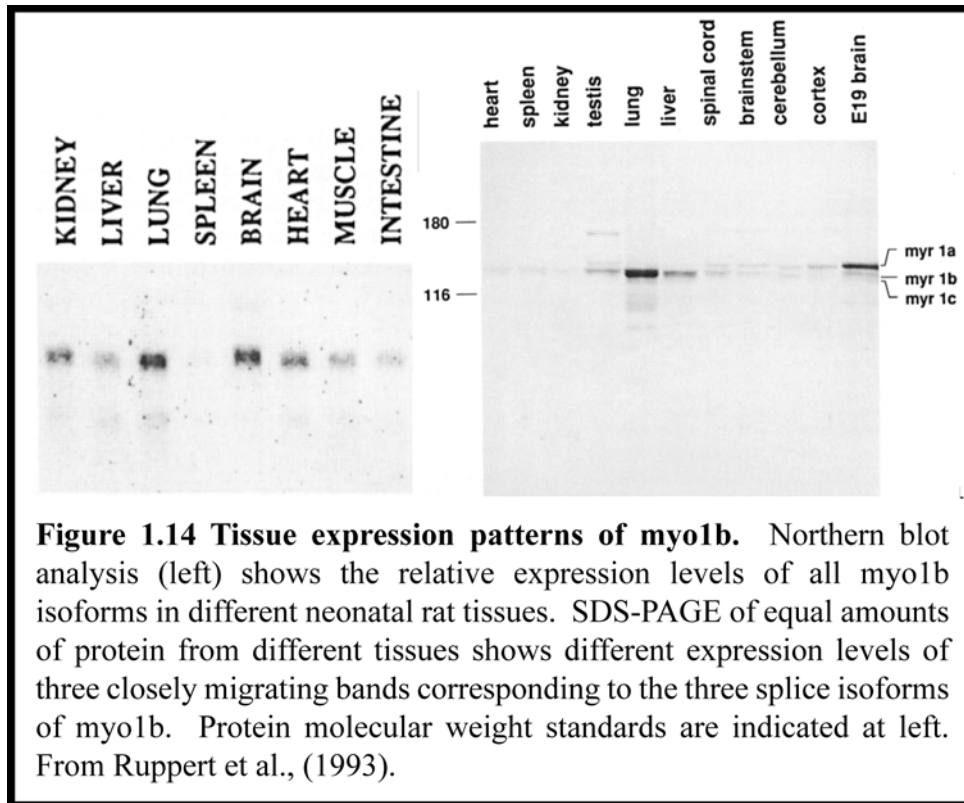
The proposed functions of myo1c and myo1a also highlight the importance of proper regulation of myosin function in the context of the cell. For instance, if myo1c indeed serves as the adaptation motor in inner ear hair cells, the activity of the motor must be regulated such that it is active at certain tension levels, and inactive at other tension levels. Additionally, while the motor is inactivated, it must maintain the connection between the membrane-bound ion channel and the actin cytoskeleton. How a motor is able to accomplish these functions is investigated in this thesis for the closely related motor protein, myosin-Ib.

1.9 Myosin-Ib

Myosin-Ib (myo1b, formerly MyrI) was originally discovered in rat tissues using an antibody specific for a synthetic peptide containing a highly conserved sequence from the brush-border myosin-I (BBMI/myo1a) motor domain. Amino acid sequence analysis showed a high degree of similarity between myo1a and the newly discovered myosin in the motor and tail domains, but expression patterns of the two proteins differed widely (Ruppert, Kroschewski & Bahler 1993). In contrast to myo1a, which is expressed specifically in the intestines, myo1b has a wide expression pattern both in neonatal and adult rat tissues. Myo1b exists in three different splice isoforms, (myo1b^{a,b,c}), which have 6,5 or 4 IQ motifs respectively along the neck domain of the protein. The three IQ motifs closest to the motor domain more closely resemble the canonical IQ motif discussed

earlier, while the distal three IQ motifs are more variable and predicted to bind calmodulin relatively weakly. Interestingly, the splice isoforms of myo1b differ in the composition of the three most distal IQ motifs, with alternative splicing generating “hybrid” IQ motifs containing parts of IQ motifs 4/5 in the case of myo1b^b, and 4/6 in the case of myo1b^c. It is interesting to speculate that the stiffness of the lever arm of myo1b may be modulated by changes in CaM (or other light chain) binding through alternative splicing (Lin, Tang & Ostap 2005), a possibility that will be investigated in this thesis.

Detailed transient kinetic characterization of myo1b was carried out by Coluccio and Geeves in 1999, and subsequently expanded upon by Lewis et al. in 2006, in an effort to kinetically characterize the various myosin-Is with the related goal, shared by many researchers of unconventional myosins, of relating biochemistry and function in myosin motors (Coluccio, Geeves 1999) (Lewis et al. 2006). The defining kinetic features, summarized in table 1.1, of the myosin are a slow overall ATPase cycle, with relatively slow ATP binding and release of hydrolysis products ADP and phosphate. Phosphate release from acto-myo1b (k_{+4}) is rate limiting at $\sim 0.58 \text{ s}^{-1}$ under solution kinetics conditions. As a result of the slow phosphate release kinetics, myo1b is predicted to exist predominantly in the weakly bound AM·ADP·Pi state, mostly detached from the actin filament under strain-free conditions. Therefore myo1b is predicted to be a low duty ratio motor under solution kinetics conditions.



Although myo1b is extremely well-described kinetically, the potential function(s) of this protein within the cell remain somewhat of a mystery. Electron microscopy studies show myo1b as an elongated monomer (with associated light chains) in solution that can potentially bundle actin filaments (Stafford et al. 2005). Consistent with this finding, myo1b localizes to dynamic cortical actin networks such as those found in the protruding lamellipodia of motile cells. Myo1b is highly expressed in ruffling membranes along the leading edge, which are known to be sites of actin polymerization during cell movement. In contrast to these findings, myo1b seems to be excluded from stable actin

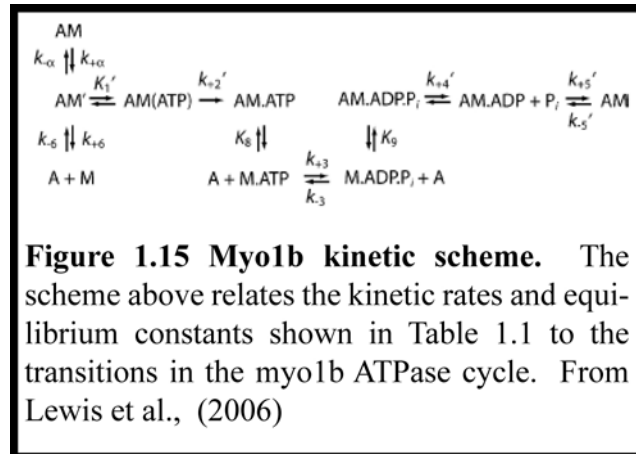
Actin Binding		Phosphate Release	
k_{+6} (s^{-1})	0.0044 ± 0.00010^b	k_{+4} (s^{-1})	0.58 ± 0.056^g
k_{-6} ($\mu M^{-1} s^{-1}$)	8.2 ± 0.32^b	K_9 (μM)	53 ± 9.8^g
K_6 (nM)	0.54 ± 0.024^c		
ATP Binding		ADP Release	
$1/K_1$ (μM)	330 ± 25^b	K_5 (μM)	0.84 ± 0.068^b
k_{+2} (s^{-1})	500 ± 15^b	k_{+5} (s^{-1})	6.7 ± 0.064^b
$K_1'k_{+2}$ ($\mu M^{-1} s^{-1}$)	1.5 ± 0.12^c	k_{-5} ($M^{-1} s^{-1}$)	8.0 ± 0.65^c
$K_1'k_{+2}$ ($\mu M^{-1} s^{-1}$)	$1.2 \pm 0.041^{b,d}$		
$K_1'k_{+2}$ ($\mu M^{-1} s^{-1}$)	0.64 ± 0.020^e		
ATP Hydrolysis		Nucleotide-Free Isomerization Step	
k_3^{app} (s^{-1})	41 ± 4.9^f	K_α	3.7 ± 0.65^b
		$k_{+\alpha}$ (s^{-1})	13 ± 1.0^b
		$k_{-\alpha}$ (s^{-1})	3.5 ± 0.67^c

Table 1.1 Rate and Equilibrium constants for myo1b at 37 degrees C. Rates for ATP binding and ADP release, referred to in results and discussion, are shown above from Lewis (2006). With rates derived from multiple experimental measurements as follows: ^b Pyrene-actin fluorescence. ^c Calculated. ^d Determined from a linear fit of the data at low ADP concentrations. ^e Light scattering in the presence of mantATP. ^f MantATP. ^g Phosphate-binding protein. Note that the rate constants were measured at 37 degrees C, whereas our experiments were conducted at 21 degrees C.

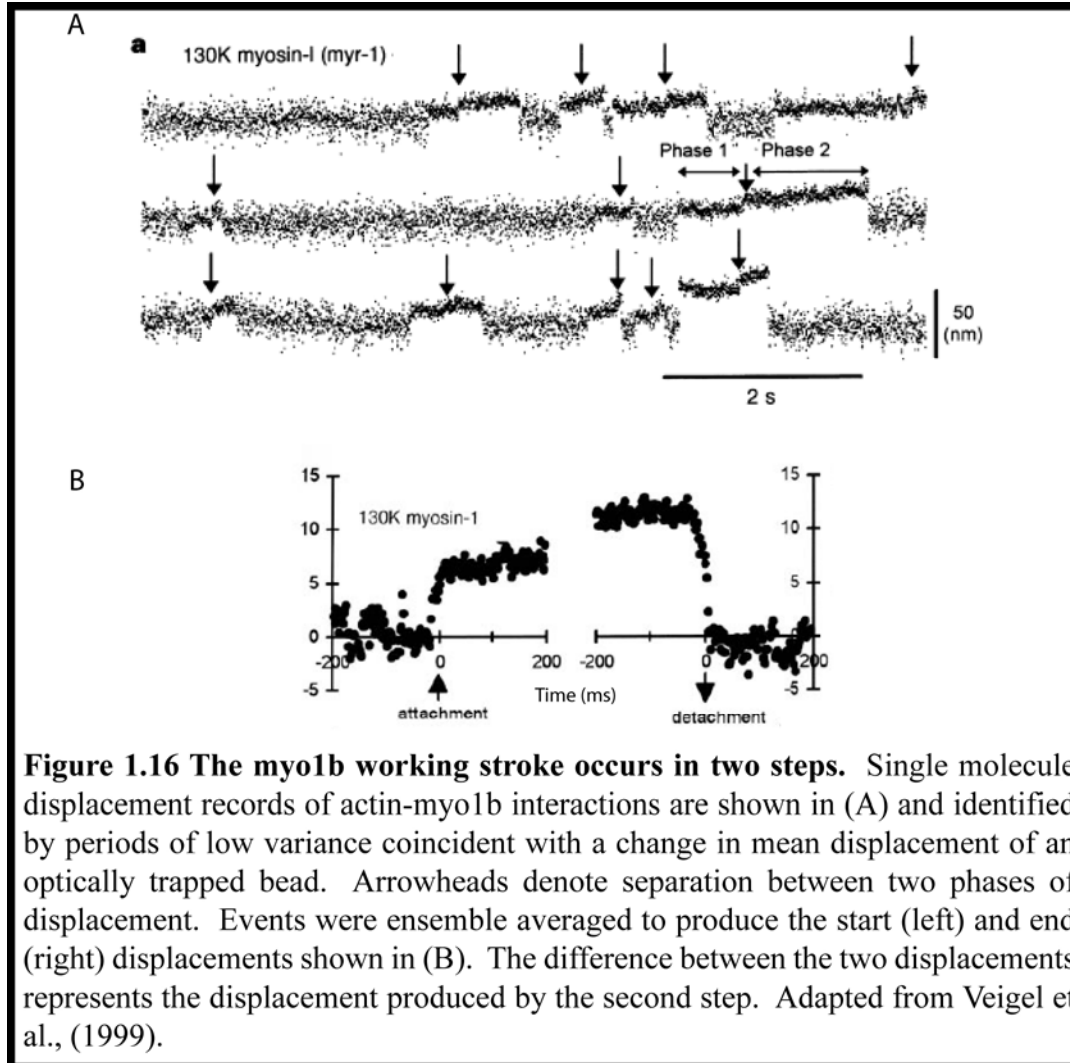
structures such as stress fibers. The mechanism of this exclusion likely involves tropomyosin binding to myosin target sites along the actin filament (Ostap 2008, Tang, Ostap 2001).

Both the motor domain and tail of myo1b are crucial for myo1b localization and therefore proper function. The actin networks within the lamellipodia are motile relative to the leading edge of the cell during cell movement, and move at a rate consistent with the velocities of actin sliding along a myo1b coated surface in a

conventional actin gliding motility assay. In light of localization, actin bundling, and solution kinetics studies, proposed cellular functions of myo1b include generating tension within cortical actin networks, powering retrograde flow of actin during motility, and powering movement of endocytic or other membrane-enclosed vesicles along actin tracks.



An important feature of the myo1b working stroke, with general relevance to the field of myosin molecular motors as a whole, was demonstrated in 1999 when Claudia Veigel et al. made detailed measurements of the forces and displacements produced by myosins undergoing their power stroke (Veigel et al. 1999). In a powerful demonstration of the applicability of single molecule techniques to the study of molecular motors, Veigel et al. suspended an actin filament held taut between two beads immobilized in optical traps (see section 1.9 and methods of this thesis) and lowered the actin filament over a surface with immobilized myosin. By measuring the deflection of the bead in the optical trap due to the myosin binding to actin and undergoing its power stroke, precise measurements of the displacement



produced by the myosin power stroke could be made (figure 1.16). They succeeded in showing that the displacement generated by the myo1b working stroke occurs in two steps totaling 11 nm.

The two-step mechanism was also found for the closely related myo1a, providing early evidence for the potentially widespread nature of the two-step working stroke. Future work, including the experiments presented in this thesis,

would relate the structural changes of the two-step working-stroke to biochemical states of myosins and shed light on how those biochemical and structural states could be regulated by strain on the myosin. Besides implications for the function of myo1b inside cells, these various sets of experiments shed light on a phenomenon originally observed in muscle and reported in 1923, called the Fenn effect.

1.10 Towards a molecular explanation of the Fenn effect.

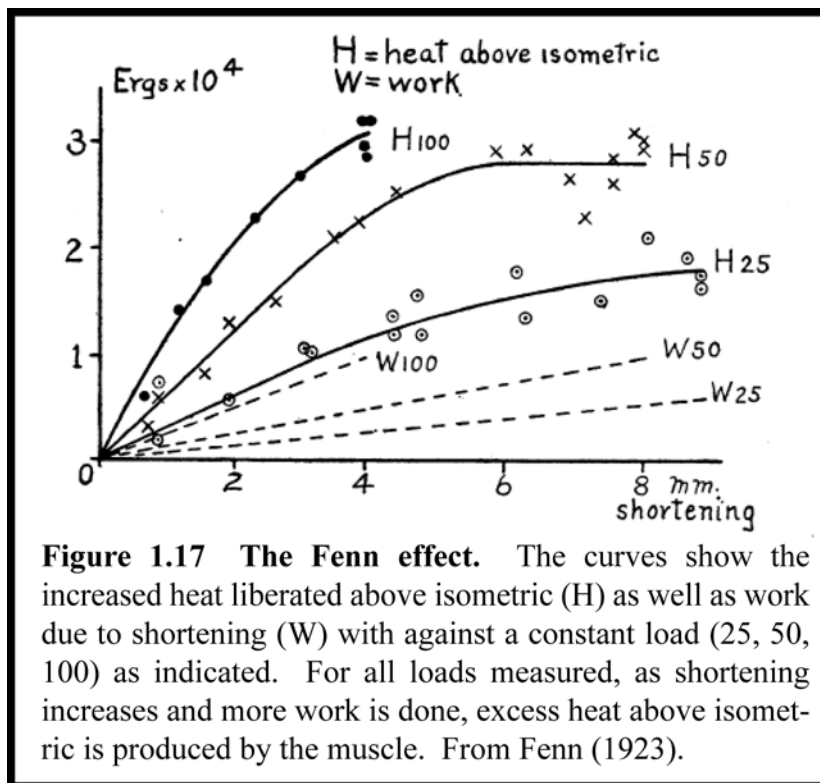
1.10.1 Experimental observation of the Fenn effect in muscle.

When a muscle hydrolyzes ATP, the energy released from the reaction produces force and heat. The force developed by the myosin motor generates stress between the myosin (thick) and actin (thin) filaments, which is resolved by the thin filaments sliding relative to the myosin in the thick filament in the direction of the power stroke. In 1922, W.O. Fenn conducted experiments in the basement of A.V. Hill's house in order to investigate the efficiency of muscle under different loading conditions (Rall 1982). In these experiments, Fenn measured the energy liberated by the muscle as a function of load subjected to and work produced by the muscle. In comparison to the amount of energy liberated during isometric contraction of muscle (without shortening), Fenn discovered that excess energy is produced when the muscle is allowed to shorten against a load, and in fact there is a direct relationship between energy liberated and work done by the muscle (Fenn 1923). These results can be roughly summarized by the following equation:

Equation 1

$$E \cong I + W + H$$

Where E is energy liberated by the muscle, I is isometric energy, W is work, and H is excess heat during shortening. The general conclusion from these landmark experiments in muscle physiology is that a muscle can respond to the mechanical environment via some form of feedback mechanism that regulates energy expenditure.



As it relates to the power stroke, it is possible to envision the Fenn effect as being due to a strain-dependent step in the chemo-mechanical crossbridge cycle. The prevailing hypothesis being that, if during stimulation the thin filament were prevented from sliding and relieving the stress imposed by the power stroke, as is

the case during an isometric contraction, the myosin head remains bound to the thin filament and unable to complete its ATPase cycle. Two candidates for strain-dependence from the Lymn-Taylor cycle (see figure 1.11) that would result in more efficient ATP hydrolysis during isometric contraction and also maintenance of the strong-binding state would be the slowing of the ADP release or ATP binding steps under strain (Nyitrai, Geeves 2004). Alternatively, if phosphate release were slowed, the myosin could produce force before releasing phosphate and detach from the filament (Takagi, Homsher, Goldman, and Shuman, 2006). The following will provide a brief summary of what is currently known about the molecular basis for strain dependence in molecular motors and the Fenn effect with particular emphasis on the emerging evidence from single molecule studies.

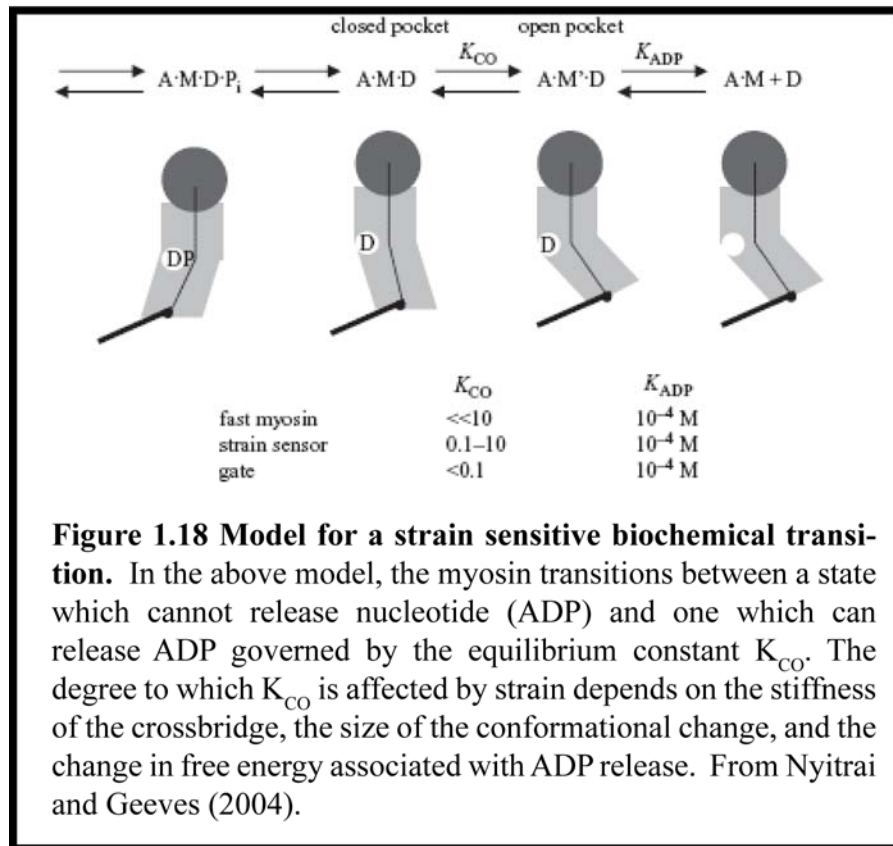
1.10.2 ADP release as it relates to muscle shortening

The rate constants for ADP release and ADP affinities of various skeletal muscle myosins varies substantially and would be expected to have consequences for the rate at which muscle shortens. Two papers related these kinetic measurements to the maximum shortening velocities of muscle fibers in an effort to show that the rate of ADP release for a muscle myosin limits the rate of shortening due to crossbridge cycling. Siemankowski et al. showed that the rate of ADP release was linearly related to the maximum shortening velocity of muscle, and that this effect could be correlated with changes in temperature, which affected ADP release and consequently muscle shortening velocity (Siemankowski, Wiseman &

White 1985). This result was further confirmed in 2001, when Weiss et al. measured ADP affinities for a variety of muscle isoforms and showed a similar relationship between ADP affinity and muscle shortening velocity (Weiss et al. 2001). This provided an evolutionary mechanism to tune muscles to work at different maximum speeds when stimulated, and strongly implicated ADP release as a potential biochemical strain sensing transition, but did not provide a direct observation of a strain-sensing mechanism.

1.10.3 Biochemical evidence for a nucleotide sensitive/insensitive transition

In 2000, Geeves et al. provided substantial biochemical evidence for a structural transition within the myo1b molecule whereby the nucleotide binding pocket exists in two conformations with differences in nucleotide affinity. By monitoring the fluorescence change associated with ATP induced dissociation of myosin from pyrene-labeled actin filaments, the timecourse of ATP binding could be determined for the myosin (Geeves, Perreault-Micale & Coluccio 2000). Surprisingly, the rate of ATP-induced dissociation was biphasic, consisting of an ATP concentration sensitive fast phase, and a separate slow phase. This suggested that myo1b exists in two states in solution, one which could readily bind ATP and one which was not able to bind nucleotide without first isomerizing to the ATP accessible state. Geeves et al. proposed a model for their data whereby the nucleotide binding site of myo1b existed in a “closed” state which was unable to bind or release nucleotide, versus an “open” state which could readily exchange



nucleotide, and that the transition between these two states was mediated by tilting or “rocking” of the lever arm of myo1b (Nyitrai, Geeves 2004). Comparable biphasic relationships for ATP induced dissociation of myosin were also found for myo1c, myosin-V, and smooth muscle myosin-II (Sweeney et al. 1998a, Batters et al. 2004b, Hannemann et al. 2005).

1.10.4 Direct measurements of myosin strain dependence

1.10.4.1 Single molecule measurements of strain-dependent ADP release

Another demonstration of a functional consequence of strain sensitivity is shown for the unconventional myosin, myosin V. Myosin-V, as opposed to myosin-I, is a two-headed multimer of heavy chains and associated light chains. Known to bind cargos such as melanosomes *in vivo*, myosin-V has been proposed to be a motor specifically adapted for the transport of cellular cargos along actin filaments (Mehta et al. 1999a, Wu et al. 1997, Wu et al. 2002). In order to “walk” along actin filaments, myosin-V takes alternating “hand-over-hand” steps along the actin filament in which the trailing head detaches from the actin filament and moves approximately 73 nm forward along the filament, powered in part by the power stroke of its partner head, to bind to the next “target zone” on the actin filament. (Yildiz et al. 2003). For myosin-V to undergo a large number of successive steps, it is necessary to somehow coordinate the biochemical cycles so that the trailing head detaches before the leading head, and that one head is always bound to the actin track.

Single molecule measurements of monomeric myosin-V step size (the displacement produced by the power stroke) showed that the power stroke for a single head/lever arm occurred in two substeps of ~16nm and ~5nm, suggesting a similar mechanism to what had been observed earlier for myo1b and myo1a (Veigel et al. 2002). This step size, however, is not large enough to account for the distance covered by myosin-V when stepping along actin filaments, which was measured to

be ~36 nm from single molecule tracking of processive myosin-V movement (Yildiz et al. 2003). A way to reconcile the two measurements and introduce a model that incorporated an asymmetric strain was proposed whereby the trailing head would detach from the actin filament and move forward due to the action of the power stroke of the leading head. The detached head could then undergo a rapid “diffusional search” due to random thermal motions which would lead to rebinding of the head at the next actin target binding site. The distance between actin binding sites for the heads would presumably stretch the molecule, imposing an asymmetric load on both of the bound heads. The (new) leading head would be experiencing a backwards load while at the same time trailing head would experience a forward load.

Consistent with this model, the stepping kinetics of a processive, two headed myosin-V were increased relative to those of a single headed construct (Veigel et al. 2002). Measurements of a single-headed construct, however, under external load imposed by the optical traps would provide a direct quantitative estimate of the strain dependence of the interaction. To accomplish this measurement, Veigel et al. modified the aforementioned optical-trap based assay used to measure myo1b and myo1a step sizes. By monitoring the positions of the optically trapped beads in their assay with fast (~1ms) time resolution, the investigators were able to rapidly impose either a “pushing” force in the forward direction of the power stroke or a “pulling” force opposing the power stroke of myosin-V by moving both optical traps after detection of an acto-myosin attachment event. They simultaneously

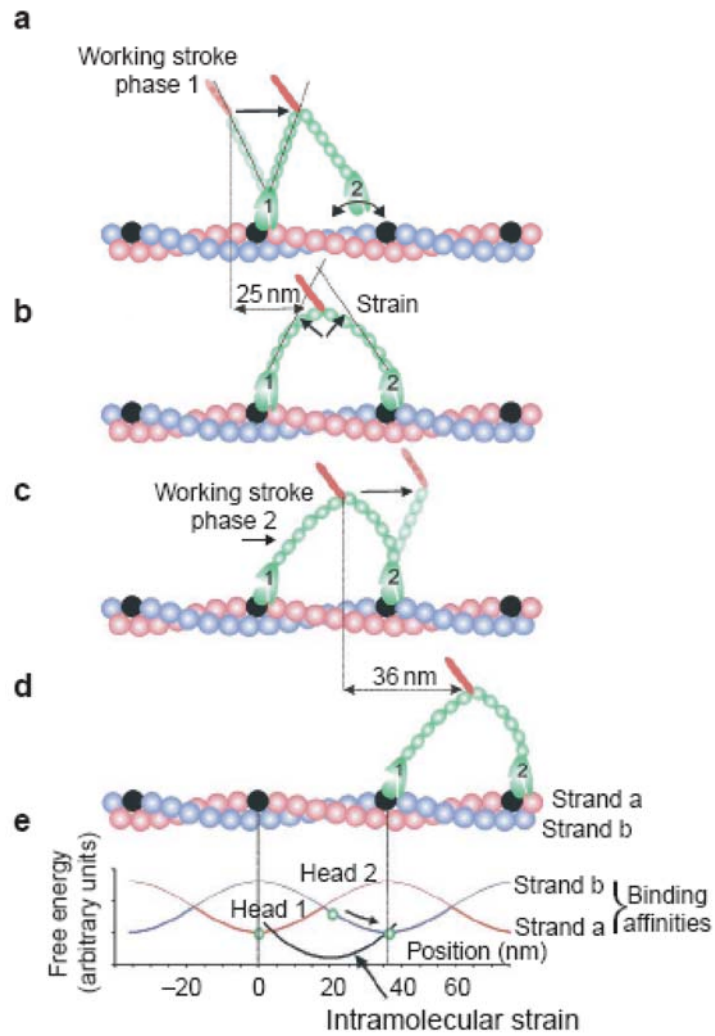
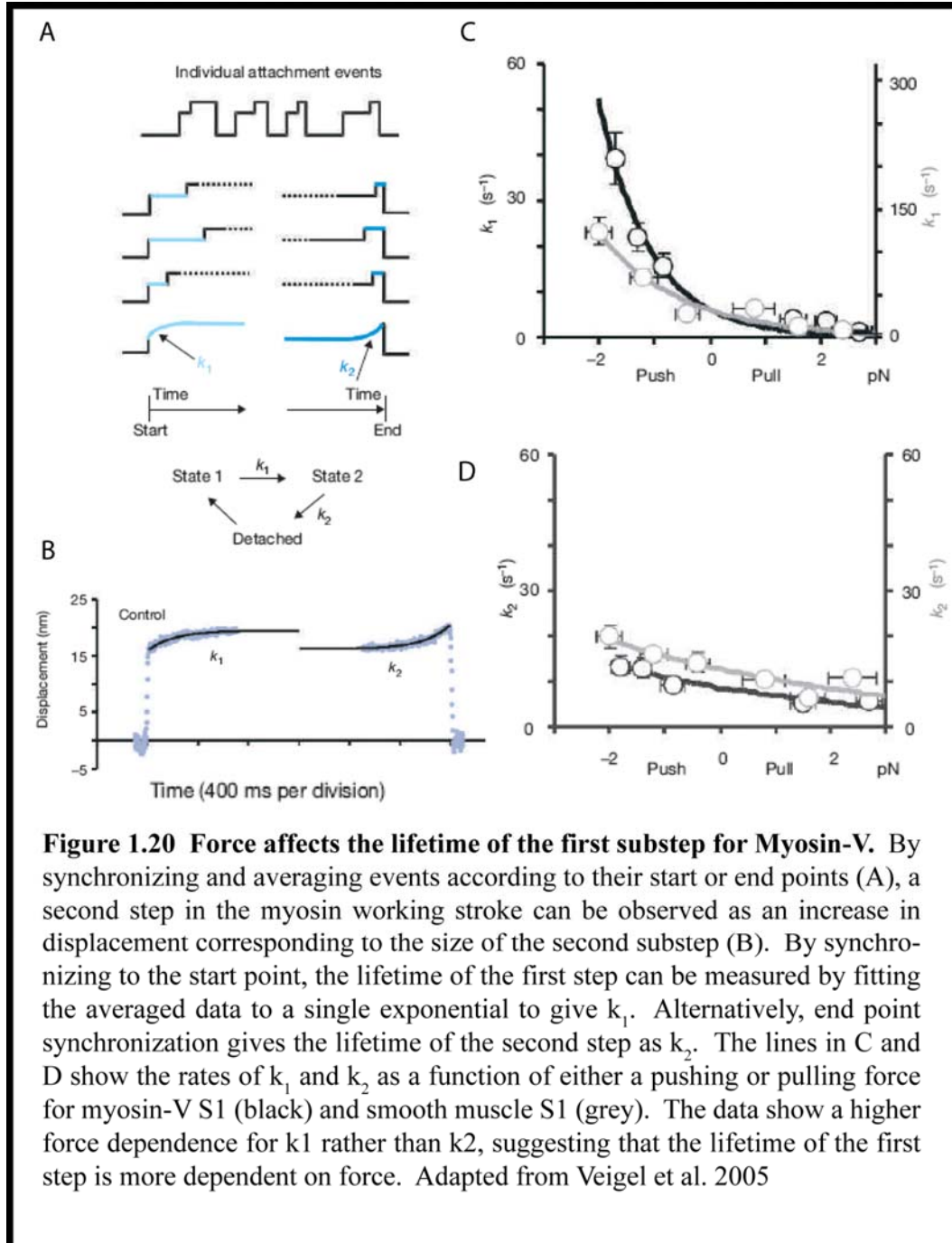


Figure 1.19 Model for strain-dependent Myosin-V processivity. a. The myosin head (1) attaches to the actin filament and undergoes a powerstroke which places the forward head (2) near the target actin binding site (black dots). b. The forward head (2) binds to the target actin site generating intramolecular strain (black line in e.) between the two heads. c. The elastic strain inhibits ADP release from the forward head (2) and accelerates ADP release from the rear head (1), causing the rear head to rebind ATP, detach from the filament, and allow the forward head to undergo its power stroke. d. The rear head becomes the new forward head and binds at the next forward actin target site, repeating the cycle. The relative binding affinities for each head to the actin filament are shown in e. Figure from Veigel et al. (2002).

measured the displacement produced by the myosin during the power stroke and developed a method to measure the rates of entry to and exit from the state seen in the second step of the working stroke (Veigel et al. 2005).

By synchronizing a large number of single attachment events to the beginning of each event and extending the end position to a predetermined limit, all the individual events could be averaged together to produce the records seen in figure 1.20. Besides a confirmation of a two step mechanism for the working stroke, the lifetime of the first step is measured as an exponential increase in displacement. Alternatively, by synchronizing the ends of the events and extending backwards, the lifetime of the second step is observed as an exponential increase in displacement directly prior to detachment. Veigel et al. measured the rates of entry to and exit from the second step in response to either a pushing or pulling force experienced by the myosin. They found that the rate of entry into the second step of the working stroke was decreased by a pulling force, and accelerated by a pushing force. If the rate of entry into the second step is governed by ADP release and further rotation of the lever arm, and the rate of exit by ATP binding and detachment, this would be compelling evidence for a strain-dependent ADP release.

As a further test of the model, Oguchi et al. measured the force at which single headed myosin-V detached from an actin filament at varying ADP concentrations and globally fit the histograms of unbinding forces to two gaussian distributions (Oguchi et al. 2008). These distributions presumably represent the detachment rates of $AM \cdot ADP \rightarrow A + M \cdot ADP$ for the lower force distribution and



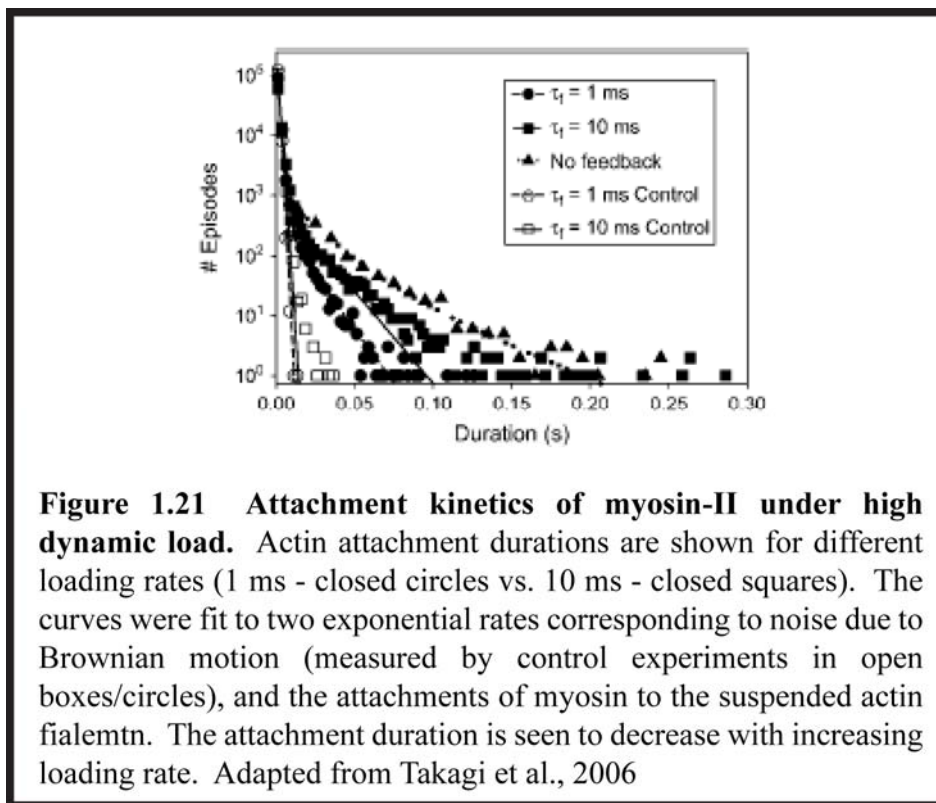
$AM \rightarrow A + M$ for the higher force distribution as the affinity for actin of $M \cdot ADP$ is less than that for myosin in rigor (no nucleotide). When subjected to a pulling force in the experiments (opposing the direction of the power stroke), the proportion of myosins in the $AM \cdot ADP$ state was increased suggesting a decreased rate of ADP release. In contrast, a pushing force in the direction of the power stroke accelerated ADP release. These experiments were an elegant demonstration of strain affecting the biochemistry of an unconventional myosin.

In addition to the compelling evidence for strain dependent coordination of the two heads for myosin-V, Veigel et al. repeated their measurements of the two step working stroke for smooth muscle myosin and added to their measurements an imposed load on the myosin as it produced force in the single molecule assay. In experiments similar to their myosin-V work, they correlated the two steps of the working stroke to changes in ATP concentration and measured the effect on the lifetimes of the working stroke substeps. They confirmed their two-step working stroke measurements for a conventional smooth muscle myosin-II and discovered that the lifetimes of the first and second steps have different sensitivities to ATP concentration. Specifically, the lifetime of the ATP-independent step was related to the force the myosin was exposed to (Veigel et al. 2003). As for myosin-V, when they “pulled” the myosin in the opposite direction of the power stroke, the rate of the ATP-independent step (likely ADP release) decreased while the opposite held true for a “pushing” force in the forward direction of the power stroke. These results represent some of the best direct evidence for a strain-dependent ADP

release mechanism for myosins (including muscle myosins) and imply that these findings may have some generality for many members of the myosin family of molecular motors, and perhaps also the kinesin family of molecular motors (Yildiz et al. 2008, Yildiz et al. 2004).

1.10.4.2 Strain-sensitive reversal of the power stroke.

In contrast to strain sensitive ADP release, another molecular explanation for the Fenn effect could be detachment of myosin from the actin filament after generating force, but with the products of hydrolysis still in the nucleotide binding pocket. Studies in isometrically contracting myofibrils show that Pi release is rate limiting in muscle (Lionne et al. 1995, Lionne et al. 2002), suggesting that perhaps there are multiple strain-dependent steps in the biochemical cycle of myosin. Consistent with this, Takagi et al., measured the detachment kinetics of skeletal muscle myosin-II at the single molecule level using a novel feedback-enhanced isometric force clamp (Takagi et al. 2006a), at high loading rates designed to mimic the load imposed on a single myosin-II crossbridge during isometric contraction. As they increased the loading rate on single molecules, they observed increased rates of detachment kinetics (figure 1.21) due to the effect of force on the myosin ATPase. They interpreted this result in terms of the Fenn effect as detachment of the M·ADP·Pi from the actin filament after force generation. Thus, energetic efficiency is increased since the myosin would be able to detach from the actin filament without ATP binding under load.



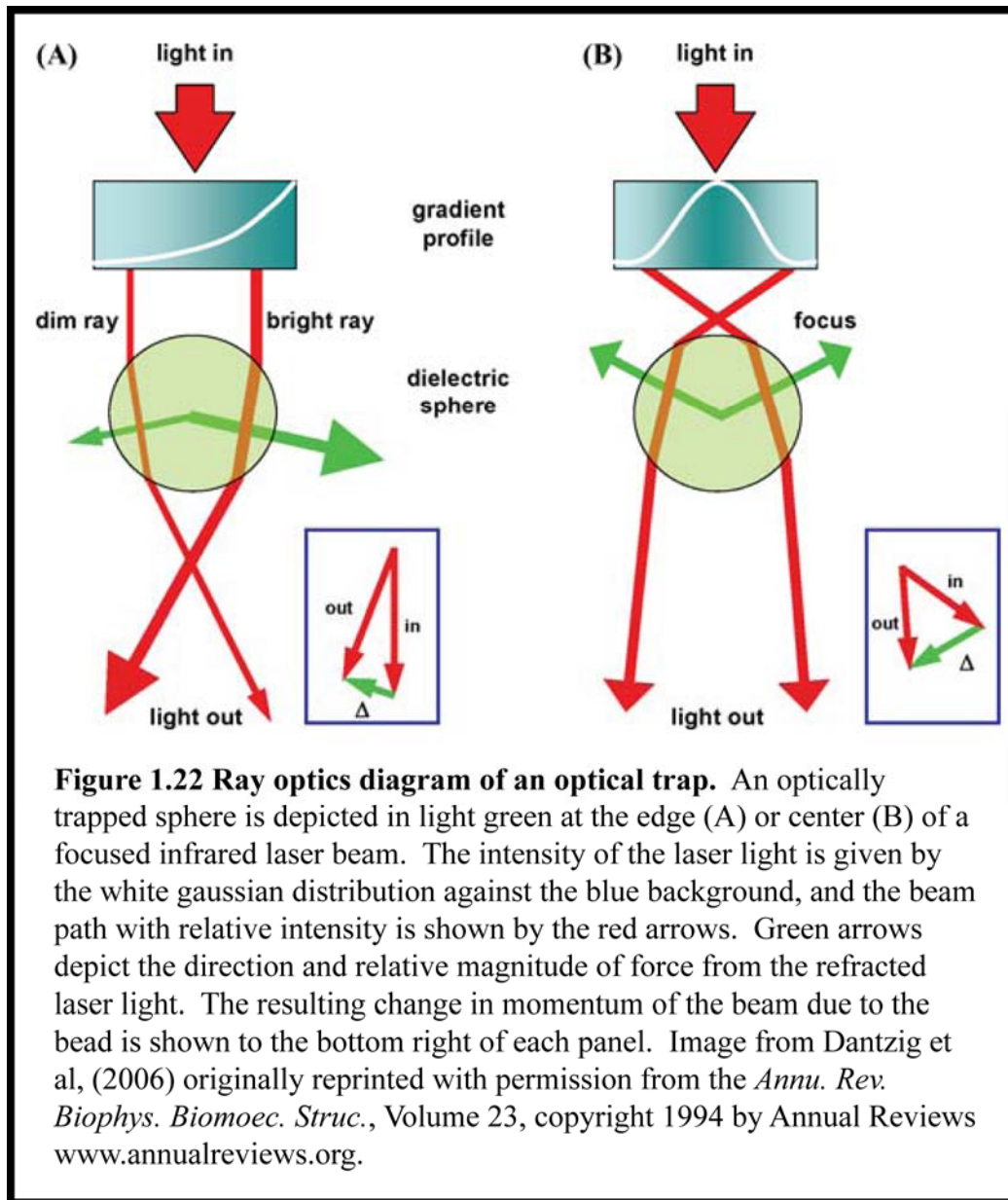
1.11 Optical Trapping Techniques

The increasing use of single molecule techniques has powered many exciting advances in our understanding of the function of motor proteins. Although single molecule techniques incorporate an increasing variety of methods to study dynamics of individual proteins, the experiments in this thesis deal primarily with the use of an infrared laser based optical trapping system, otherwise known as “laser tweezers”.

In 1975, Arthur Ashkin and J.M. Dziedzic were in the process of improving laser based methods for manipulating liquid droplets in air using laser radiation

pressure (Ashkin, Dziedzic 1975). Their methods eventually resulted in the development of optical trapping techniques in which tightly focused laser beams could prevent the diffusion of molecules away from the laser beam waist. Although the technique of optical trapping is perhaps most famous for the Nobel prize winning work demonstrating the use of laser radiation pressure in trapping individual sodium atoms, (Chu et al. 1985, Chu et al. 1986) biological applications of optical trapping were quickly developed to manipulate viruses, bacteria, whole eukaryotic cells, and even the plasma membranes of cells to create cytoplasmic extensions (Ashkin, Dziedzic 1989, Ashkin, Dziedzic 1987, Ashkin, Dziedzic & Yamane 1987).

The optical trapping studies used in this thesis will deal mainly with trapping of micron sized objects, the principles of which can be understood by the ray optics diagram in figure 1.22 (Dantzig, Liu & Goldman 2006). Briefly, a small object, such as the 1 micron polystyrene spheres used in this thesis, is brought in the vicinity of a focused infrared laser beam. The intensity of the laser light in the beam waist is described by a gaussian distribution with the greatest intensity of light in the center of the beam. When the sphere encounters the light of the laser beam, it refracts the light and changes its trajectory, thus exerting a force on the light. In accordance with the principle of conservation of momentum, the laser light exerts an opposing force of equal magnitude on the bead. When the bead moves outside the center of the beam waist in the x and y axes, the intensity of the light is greater on one side of the bead creating a net gradient force in the direction of the center of



the trap. When the bead is positioned directly below the focal spot of the laser, as in (B), the z-axis force on the bead acts in the opposite direction of the laser beam light, to counter the scattering force of the laser beam (the radiation pressure Ashkin and Dziedzic used to levitate droplets). As a result, the behavior of the bead in the

trap can be approximated by a linear Hookean spring with a stiffness dependent on the intensity of the laser beam (Svoboda, Block 1994).

Typical experimental geometries used in optical trapping studies of molecular motors include the single-bead assay, and the three-bead assay. In both sets of experiments, optically trapped micron-sized beads serve as “handles” to which the proteins to be interrogated are attached. The single-bead assay is particularly well-suited to studying dimeric processive molecular motors such as myosin-V, myosin-VI, conventional kinesin, and dynein, among others (Svoboda et al. 1993, Mehta et al. 1999b, Rock et al. 2001, Ross et al. 2006). In a typical single-bead assay, the motor protein is attached to a bead, usually through its tail domain via an antibody or a functional tag with a specific binding partner on the bead. A single bead can then be immobilized in an optical trap and brought in the vicinity of the binding partner for the protein on the surface of a glass coverslip, typically the characteristic filament track for the motor, i.e. microtubules for kinesin, f-actin for myosin. The position of the bead can simultaneously be tracked by conventional light scattering techniques or by projecting the refracted laser light from the trapping beam onto a four-quadrant photodiode. At sufficiently low motor protein densities, single interactions with the filament can be reported by changes in the bead position in the trap (during stepping for example) or by changes in the bead position variance due to Brownian motion (Svoboda, Block 1994, Svoboda et al. 1993). At low trap stiffnesses, relatively unrestricted movement of the motor along the track can be visualized by changes in the bead position in the trap. Alternatively, the trap

stiffness can be increased to examine the stepping behavior of the protein against an imposed load, similar to what a motor protein might experience inside a cell (Ross, Ali & Warshaw 2008).

An alternative experimental geometry, which will be used extensively in the experiments discussed in this thesis, is the three-bead assay, developed by Finer et al. (Finer, Simmons & Spudich 1994). In this type of experiment, the motor and track are inverted relative to the single bead assay. The use of two independently suspended beads in separate optical traps can allow binding of a filamentous track protein to both beads, which is stretched to create a bead-filament-bead “dumbbell”. The dumbbell is then lowered over the surface of a third bead, sparsely coated with the motor protein, on the surface of the experimental chamber, called a “pedestal” bead. The positions of both beads can be monitored in much the same way as for the single-bead assay.

In 1996, Simmons et al. demonstrated the use of a feedback-enhanced optical trapping system that could rapidly respond to the changes in force exerted on the trapped bead (Simmons et al. 1996). By coupling an acousto-optic modulator to the beam path of the trapping laser, the intensity of the laser and therefore the stiffness of the optical trap could be modulated to change the force on the bead. In order to measure the isometric force during attachment of myosin-II to actin, Takagi et al. developed an isometric force clamp which incorporated a feedback-enhanced optical trapping system in a three bead assay (Takagi et al. 2006b). In this experiment, one of the beads, termed the transducer bead, is monitored and any

change in bead position during, for example, an interaction between a myosin attached to the surface of a coverslip and a suspended actin filament, is rapidly communicated to the motor bead through a feedback loop.

By way of the feedback loop, the position of the trap opposite the transducer bead is driven in the opposite direction of the power stroke until the transducer bead is restored to its pre-power stroke position. Thus the actin filament length between the transducer bead and the myosin is held constant, and the dynamic stiffness of the dumbbell is higher, approximating the conditions a myosin might experience when generating isometric force against a load. The experiments presented in this thesis will take advantage of the experimental setup developed by Takagi et al. to impose a near-isometric load to an unconventional myosin. By monitoring the change in force necessary to restore the position of the transducer bead, we can estimate the force experienced by the myosin in the opposite direction of the power stroke and correlate the force with the lifetime of acto-myosin attachments to obtain information about the binding kinetics.

1.12 Thesis Overview

The broad goal of this thesis is to use single molecule techniques to address questions concerning the biochemistry, regulation, and mechanics of a motor protein, myo1b. Specific questions to be addressed include:

- What is the mechanical response of myo1b to an external load?

- How is myo1b regulated by alternative splicing?
- What signaling molecules regulate myo1b function and how could they affect the response of myo1b to load?
- Does the light chain binding domain act as a rigid lever?

Chapter 2 of this thesis will cover the appropriate methods and materials used to perform the experiments in this thesis. The experimental apparatus will be described and particular attention will be paid to the techniques used to select and analyze data. Chapter 3 will show the results of experiments used to address the questions above at the single molecule level. Chapter 4 will discuss our progress in achieving the aims detailed in section 1.2. Functional properties of myo1b will be addressed in terms of a model and our experimental results will be compared with other members of the myosin superfamily to highlight the diversity in function of these interesting molecular motors.

2. Methods

This chapter will introduce the proteins, apparatus, chamber preparation, and analysis techniques used in the experiments in this thesis. All chemicals are from Sigma unless otherwise noted.

2.1 Protein and reagent preparations

2.1.1 Buffer recipes

Lysis Buffer: 10 mM Tris, pH 7.5, 200 mM NaCl, 4 mM MgCl₂, 2 mM ATP, 5 mM DTT, 0.5% Igepal, 1 mM EGTA, 1 mM PMSF, 0.01 mg/ml aprotinin, and 0.01 mg/ml leupeptin.

Wash Buffer: 10 mM Tris, pH 7.5, 200 mM NaCl, 4 mM MgCl₂, 2 mM ATP, 5 mM DTT, 1 mM EGTA, 1 mM PMSF, 0.01 mg/ml aprotinin, and 0.01 mg/ml leupeptin.

Elution Buffer: 10 mM Tris, pH 8.0, 100 mM NaCl, 1 mM EGTA, 1 mM DTT, 0.01 mg/ml aprotinin, and 0.01 mg/ml leupeptin, 0.2 mg/ml FLAG peptide, 5 uM Calmodulin.

Column buffer: 10 mM Tris, pH 8.0, 50 mM NaCl, 1 mM EGTA, and 1 mM DTT.

Protein storage buffer: 10 mM MOPS, pH 7.0, 25 mM KCl, 1 mM DTT, 1 mM EGTA, 50% glycerol.

Buffer A: 2 mM Tris-HCl, pH 8.0, 0.2 mM ATP, 0.5 mM DTT, 0.1 mM CaCl₂, 1 mM NaAzide.

High Salt Buffer: 500 mM KCl, 4 mM MgCl₂, 1 mM EGTA, 20 mM KH₂PO₄, pH 7.2.

Motility Buffer: 25 mM KCl, 10 mM MOPS, pH 7.0, 1 mM EGTA, 1 mM MgCl₂ (Stored in 5x aliquots).

KMg25: 10 mM Imidazole, pH 7.0, 25 mM KCl, 2 mM MgCl₂, 1 mM EGTA and 1 mM DTT.

Activation buffer: 1x Motility buffer supplemented with 5 mM DTT, 1 mg/ml BSA, 1 mg/ml glucose, 20 μM CaM, 192 U/ml glucose oxidase, 48 μg/ml catalase (Roche). Variable amounts of ATP, free calcium, and phosphate were added as described in the text. DTT, BSA, and glucose were from freshly prepared stocks of 1M DTT, 10 mg/ml BSA, and 250 mg/ml glucose all solubilized in dH₂O.

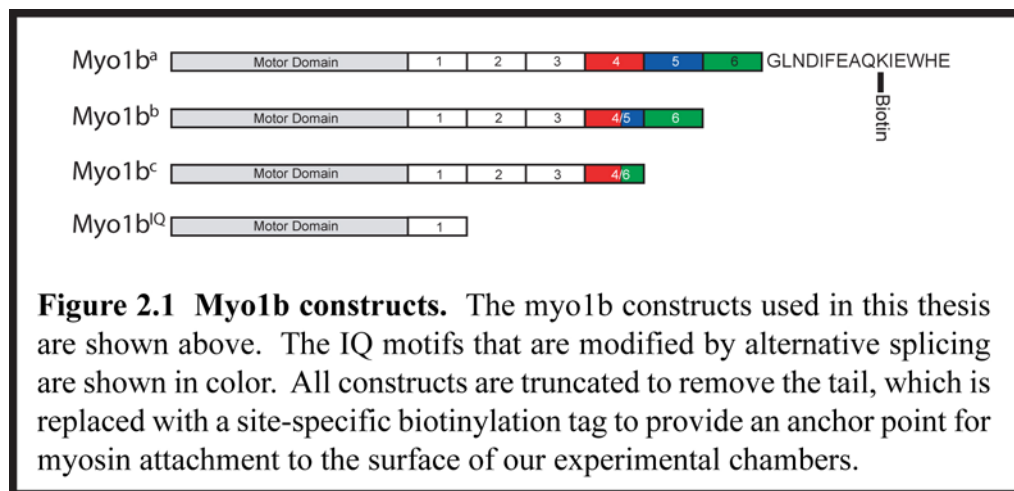
2.1.2 Coomassie Plus protein concentration determination.

Protein concentrations were determined using the Bradford assay via Coomassie Plus (Pierce). Protein concentration standards were prepared in duplicate using 0, 2, 6, 10, and 20 ng BSA in 95 μl H₂O. 5 μl Dialysis buffer was then added to each standard sample. An unknown concentration sample was prepared by adding 5 μl of the protein to be determined in 95 μl H₂O. 1.5 ml of Coomassie Plus reagent was then added to each sample, and tubes were mixed by brief vortexing. Absorbance at 595 nm was measured using a UV-visible spectrophotometer (Varian). A linear fit to the protein standard absorbance at 595

nm vs. known protein concentration was used to determine the concentration of the unknown sample.

2.1.3 Myosin constructs

Myo1b constructs were prepared as described in (Lin, Tang & Ostap 2005). All myo1b splice isoform constructs were truncated after the final IQ motif in the light chain binding domain, thus all constructs contained the motor and IQ motifs and excluded the tail domain (figure 2.1). An additional non-native construct (myo1b^{IQ}) consisting solely of the motor and first IQ motif was also prepared. A FLAG sequence for purification and a 15-amino acid AviTag sequence for site-specific biotinylation were inserted at the C-termini, and the constructs were subcloned into a baculovirus transfer vector (pBlue-Bac4.5).



Myo1b constructs were expressed and purified from Sf9 cells that were co-infected with virus containing recombinant myo1b and calmodulin (El Mezgueldi et

al. 2002). Four liters of Sf9 cells were pelleted by low-speed centrifugation, suspended in lysis buffer, and homogenized with 5 strokes in a Dounce homogenizer. Cell extract was spun at 100,000 x g for 1h in an LM-8 ultracentrifuge (Beckman). Supernatant was split into two equal volumes and loaded onto two 1.5 mL columns with FLAG resin that had been pre-equilibrated with wash buffer. After a 30 minute incubation, the column was washed with 5 column volumes of wash buffer. Bound protein was eluted with three column volumes of elution buffer by adding elution buffer to the column and stirring gently with a Pasteur pipette to mix the resin and buffer. Eluted protein was then loaded onto a Mono-Q column (Amersham Biosciences) equilibrated in column buffer. Myo1b constructs with bound CaM were eluted in a linear 50 mM – 1 M NaCl salt gradient. Fractions containing Myo1b were combined and concentrated by filtration through low speed centrifugal filter devices (Millipore). Concentrated protein was then site-specifically biotinylated with biotin ligase according to a kit manufacturer's protocol (Avidity). Site-specific biotinylation encouraged optimal orientation of the myo1b motor domain for interaction with actin filaments (Lin, Tang & Ostap 2005). Biotinylated protein was then dialyzed against 2 x 1 L protein storage buffer over two days. Protein concentration was determined using the Coomassie Plus based Bradford assay (see above). Typical protein concentrations were ~1.0 – 10 mg/ml. Protein integrity was determined by a standard gliding actin filament assay (Lin, Tang & Ostap 2005).

2.1.4 G-actin preparation

Monomeric g-actin was prepared from a protocol from Spudich and Watt (Spudich, Watt 1971) with modification. Acetone powder from rabbit back muscle was extracted on ice by gentle stirring in buffer A for 30 minutes. The remaining acetone powder was separated from extracted protein by centrifugation for 30 minutes at 7800 g in a SS-34 superspeed centrifuge rotor (Sorvall). The supernatant, containing the g-actin, was then filtered through a cheesecloth and the volume estimated. G-actin was then polymerized by adding salt to 50 mM KCl and MgCl₂ to 2 mM. After 1 hr at room temperature with gentle stirring, salt concentration was increased to 0.8 M KCl to dissociate contaminating tropomyosin filaments. After 30 minutes of gentle stirring at room temperature, the actin filaments were pelleted by centrifugation in a 50.3-Ti rotor for 2 hours at 88000 g in an LM-8 ultracentrifuge (Beckman). The supernatant was discarded and the actin-containing pellet was washed briefly and then resuspended in ~3 ml of buffer A by pipetting with a Pasteur pipette. Actin filaments were depolymerized by dialyzing the protein into 1 L buffer A over two days vs. three changes of buffer A. The depolymerized actin was then clarified by centrifugation in a 50.3-Ti rotor (Beckman) for 2 hours at 88000g in an LM-8 ultracentrifuge (Beckman). The top 2/3 of the supernatant, containing the g-actin monomers, was collected and stored for up to 90 days at 4°C. Concentration was determined by absorbance at 290 nm. Of note is the omission of a final gel filtration step, we found that removing this final step improved the stability of our actin filaments under pretension.

2.1.5 Rhodamine-phalloidin labeled f-actin (RPFA) preparation

F-actin stocks were prepared from g-actin by diluting the g-actin stock into 5x motility buffer and dH₂O to make 2 μM f-actin in 1x motility buffer.

Rhodamine-labeled phalloidin (Sigma) was added to 10 μM and the actin was allowed to polymerize for 30 minutes at room temperature. Each RPFA preparation was used for up to two weeks at a time, at which point the rhodamine fluorescence was too dim to easily visualize actin filaments.

2.1.6 N-ethyl maleimide(NEM) modified myosin-II

NEM-myosin II was prepared according to the method of Veigel et al. (Veigel et al. 1998). Myosin-II prepared from rabbit back muscle, provided by John Beausang from Yale Goldman's lab, was diluted 1:10 into dH₂O to form filaments. At a protein concentration of 16.5 mg·ml⁻¹, 78 μl of protein was diluted into 722 μl of dH₂O in a 1.5 ml plastic centrifuge tube. The polymerized protein was spun at 13,000 rpm for 30 minutes at 4°C in an eppendorf 5415 R desktop centrifuge. The supernatant was discarded and the myosin was resuspended in ~110 μl high salt buffer to depolymerize the protein. N-ethyl maleimide (Sigma) was dissolved in high salt buffer to 50 mM and 12 μl of this stock solution was added to the depolymerized myosin to give ~5 mM NEM. The mixture was allowed to react at room temperature and stopped after 90 minutes with the addition of 1 ml of 20 mM

DTT in dH₂O. NEM-myosin, having repolymerized, was spun at 13,000 rpm for 30 minutes and the supernatant was discarded. NEM-myosin was resuspended in ~400 µl high salt buffer + 50% glycerol and stored for up to one month at -20°C.

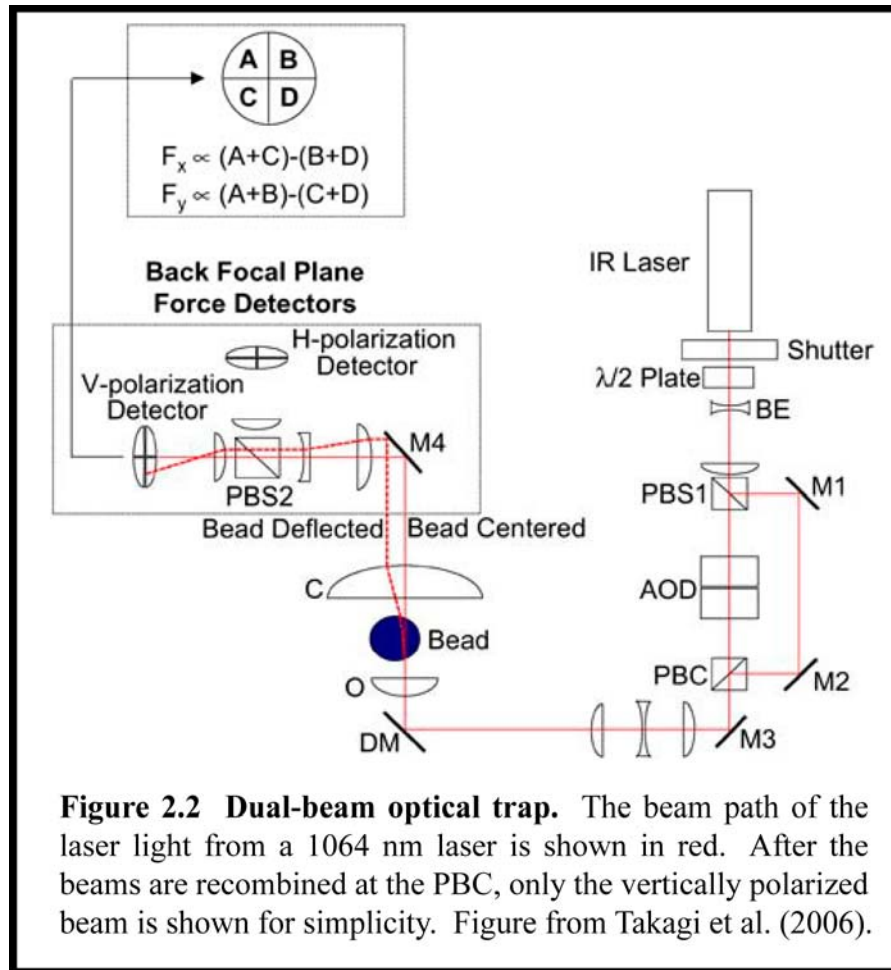
2.1.7 NEM-myosin-II coated beads

2 µl of polystyrene beads (1.1 µm mean diameter, Sigma, LB-11) were washed twice in 250 µl dH₂O to remove surfactant in storage solution. The beads were resuspended in ~15 µl dH₂O by brief sonication in a bath sonicator and ~80 µl of the NEM-myosin-II stock solution was added to the beads. The beads + myosin were incubated for two hours at 4°C. Two 1.5 ml plastic centrifuge tubes were pre-coated with 1mg/ml BSA for at least 15 minutes in high salt buffer for one and motility buffer for the other. Pre-coating the tubes with BSA for at least 30 minutes prevented adsorption of the NEM-myosin-II beads to the wall of the tubes. The coated beads were added to the tube containing 1 mg/ml BSA in high salt buffer and mixed gently to depolymerize long myosin filaments on the beads. The beads were collected by low speed centrifugation (7 minutes @ 8000 rpm on a desktop centrifuge) and resuspended in 1 mg/ml BSA in motility buffer (from the second tube). The beads were collected by another round of low speed centrifugation in the second coated tube and resuspended in ~200 µl motility buffer. Coated beads were stored at 4°C and used for up to 10 days.

2.2 Apparatus

2.2.1 Optical Trap

A detailed description of the optical trap setup developed by Takagi, Goldman, and Shuman can be found with details on calibration and design principles from (Takagi et al. 2006a). A diagram of the setup is shown in figure 2.2. The setup is based on an inverted microscope (Olympus) mounted on a 6' by 4' Vibration isolation optical table (I-2000 Stabilizer, Newport) to reduce mechanical noise transmitted to the sample chamber from the surroundings. The trapping laser consists of a single Millennia IR laser diode ($\lambda = 1064$ nm, Spectra-Physics Lasers) split by polarization into two beams via a polarizing beam splitting cube (Newport), the relative intensities of which can be adjusted with a half wave plate which allowed for equivalent trapping strengths (within 10%). Although both beams can be controlled with separate 1-dimensional Acousto-optical deflectors (AODs) (Brimrose), allowing rapid ($3 \mu\text{s}$) x-axis positional control of the trap, the experiments in this thesis will only use the AOD controlling the trap from the horizontally polarized light as depicted in the figure. Both beams can also be controlled, together or individually, by adjusting the angles of mirrors along the beam path. The laser light is recombined at a second polarizing beam cube, and the combined beams are directed to the specimen plane by way of periscoping mirrors. At this point the laser intensity is attenuated (with the exception of the stiffness experiments) to 40% by a neutral density filter (Thorlabs) in order to reduce trap



stiffness in all experiments except actomyo1b stiffness measurements. The beams are focused to two diffraction-limited spots by the objective lens (Olympus, UPlanApo/IR 60x) and used to trap beads in solution. After interacting with the beads, the laser light is collected and collimated by a condenser lens (Olympus PlanApoUV 60x). The beams are directed to another polarizing beam splitter by a mirror at an angle 45° to the optical axis of the microscope. The horizontally and vertically polarized light, representing the motor and transducer traps respectively, are collected separately on the two 4-quadrant photodiodes (Current Designs). The

distribution of laser intensity on the photodiodes reports the magnitude of the force acting on the bead, which can be converted to distances by dividing by the known trap stiffness. Signals are filtered and amplified (Frequency Devices) and recorded using an analog-to-digital converter board (National Instruments). An EMCCD camera (Andor) mounted on the side-port of the microscope stage allows sensitive fluorescence imaging of the specimen during attachment of RPFA to NEM-myosin-II coated beads. Positional stage control in x, y, and z axes is provided by a piezoelectric controller (Mad City Labs).

For measurement of stage position fluctuations, an additional infrared laser beam ($\lambda = 930$ nm, Point-Source) was installed on the same beam path as the trapping laser, with the exception that after being collected and collimated by the condenser objective the light was directed to a separate 4-quadrant photodiode. The position of this laser was controlled manually by tilting mirrors and set to the center of the pedestal bead used during experiments. The changes in stage position due to drift or mechanical vibration of the instrument are reported by deflections in the laser light by the pedestal.

2.2.2 Calibration of the Optical Trap

To determine the trap stiffness and detector sensitivity, the following calibration measurement was performed for each experiment. A single bead was brought in the vicinity of each optical trap and the trapped beads were directed away from the area of the chamber containing beads. The x-axis voltage signals from the

4-quadrant photodetectors were recorded for 5 seconds at a 20 kHz sampling rate. The resulting power spectra for both signals were plotted as shown in figure (2.3) and fit to a Lorentzian function using the equation:

Equation 2

$$S_v(f) = S_0 \frac{1}{1 + \frac{f^2}{f_c^2}} + k$$

where S_v = power spectrum in units V^2/Hz , f = frequency, and k represents an electronic noise cutoff. The roll off frequency (f_c) is related to the trap stiffness (κ) by the following equation:

Equation 3

$$\kappa = 2\pi\gamma f_c$$

where π = Pi (mathematical constant), and γ is the viscous drag coefficient of the trapped bead in $N \cdot s \cdot m^{-1}$. γ can be determined from first principles by:

Equation 4

$$\gamma = 3\pi\eta d$$

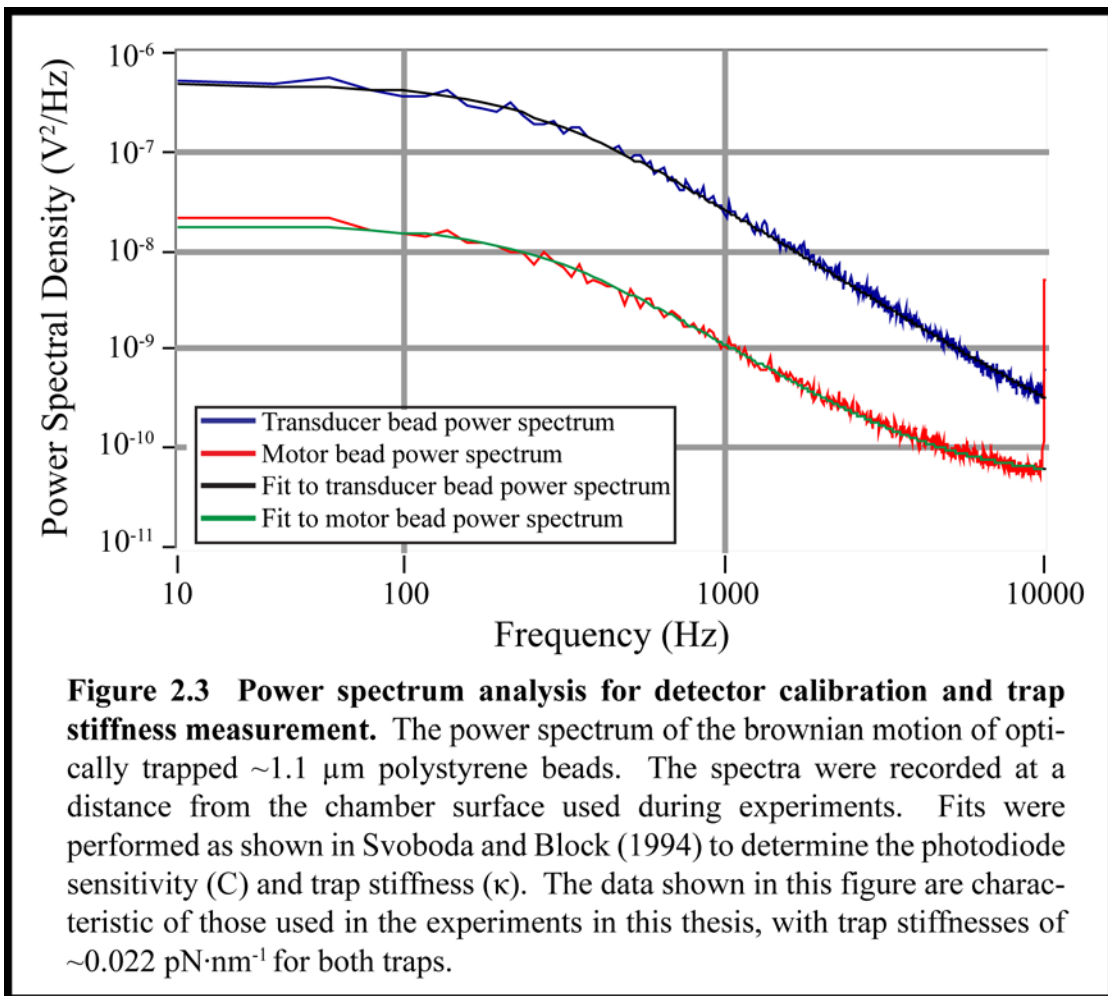
where d is the diameter of the trapped bead (the mean particle diameter used in the experiments in this thesis is 1.1 μm), and η is the dynamic viscosity of the solvent (for water = 0.001 $N \cdot s \cdot m^{-2}$).

Over the range of frequencies where the power spectrum is approximately constant ($f \ll f_c$) the calibration constant to convert the voltage measurement from the photodiode to force (the detector sensitivity) can be determined from the following equation:

Equation 5

$$S_V(f) = S_0 = \frac{4\gamma k_B T}{C^2}$$

where k_B = Boltzmann's constant ($\sim 1.38 \times 10^{-23} \text{ J}\cdot\text{K}^{-1}$), γ = the viscous drag coefficient of the trapped bead in $\text{N}\cdot\text{s}\cdot\text{m}^{-1}$, T = temperature in K, and C = the calibration constant for the photodetector (in $\text{pN}\cdot\text{V}^{-1}$). This calibration data was recorded for every bead-actin-bead dumbbell used in experiments.



2.2.3 Isometric force feedback

In order to apply varying loads on the acto-myosin crossbridge, a feedback loop was incorporated which acts to keep the position of one of the beads (termed the “transducer” bead) at a predetermined force level in the optical trap by driving the position of the other bead (termed the “motor” bead). As shown in figure (2.4) originally from Takagi et al. 2006, stretching the actin filament between two beads in the three-bead assay geometry places a pretension force on the two beads in the trap. The force on either bead is given by the difference signal $[(A + B) - (C + D)]$ from the respective 4-quadrant photodiode. Zeroing the voltage output of the photodiodes after pretensioning the filament and then engaging the feedback loop keeps the force on the transducer bead constant during an experiment.

During force feedback experiments, the myosin binds to the actin filament, undergoing a power stroke and producing force in the direction of the pointed end of the actin filament (left, as shown in the figure). The change in x-axis voltage difference signal from the transducer bead is sent through an integrating amplifier that directs the motion of the motor trap, and consequently the trapped bead, in the opposite direction of the power stroke. The motion of the motor bead drives the bead-actin-bead dumbbell in the opposite direction of the power stroke until the transducer bead is restored to its pre-power stroke position (dotted line in figure 2.4), closing the feedback loop. The force on the motor bead, and therefore the myosin, is reported by the resulting x-axis voltage difference signal from the motor trap 4-

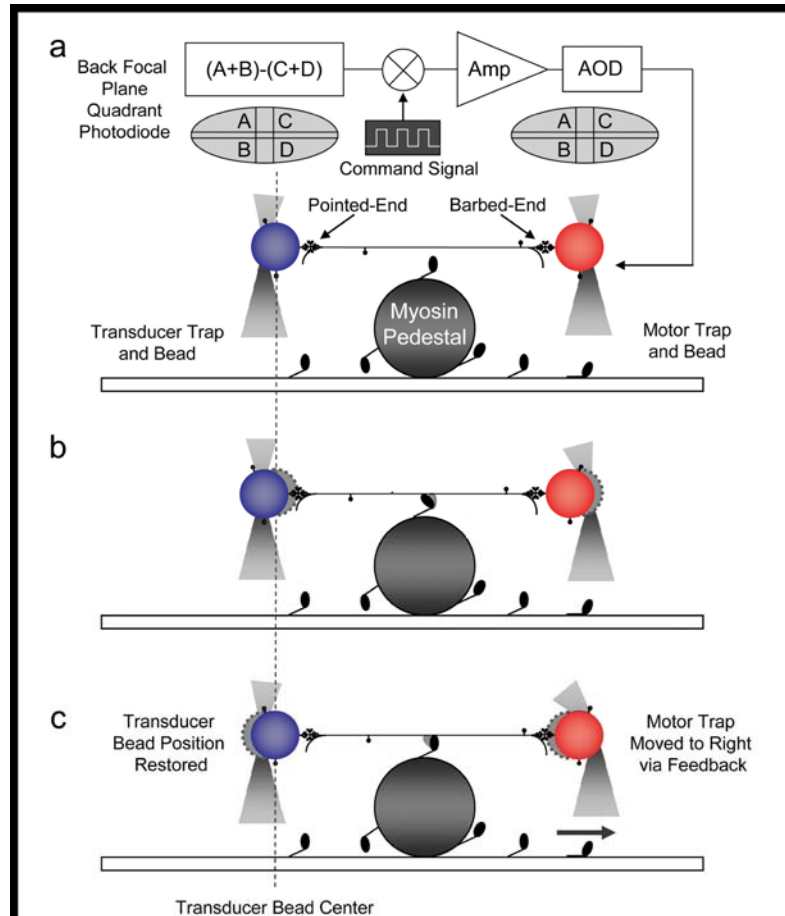


Figure 2.4 Motion of the isometric force clamp during an actomyosin attachment. In panel a, the myosin is detached from the actin filament and the beads are stably trapped with the stretched actin filament between them. The zeroed position of the transducer bead is shown by the dashed line. The pretension force on the filament is given by the displacement of the beads from the center of the trap as recorded by the photodiodes. In b, during an attachment event, the myosin power stroke moves the bead attached at the pointed end of the actin filament towards the center of the trap. The displacement signal recorded by the transducer photodiode is sent through an integrating amplifier which drives the AOD controlling the motor bead until the transducer is restored to its original position (c). From Takagi et al. (2006).

quadrant photodiode. The resulting forces reported in the experiments in this thesis therefore, are simply a result of the myosin undergoing its power stroke, and the distributions of forces are due to variation in the length of the power stroke, stiffness of the myosin, and binding position of the myosin to the actin filament.

2.2.4 Stage position feedback

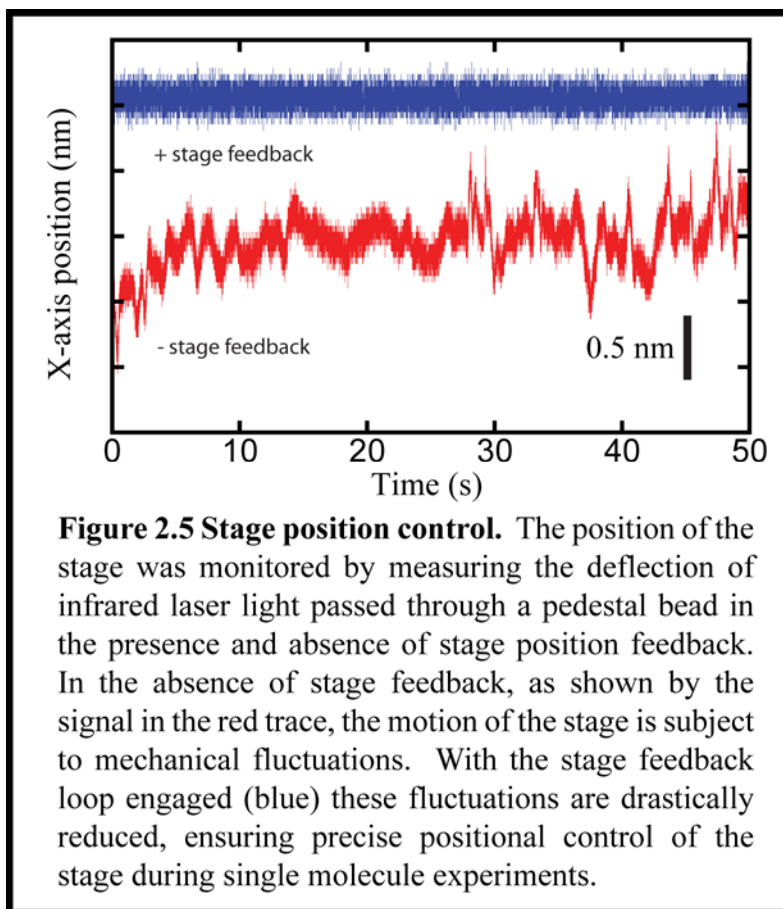
We have designed a method to measure stage position fluctuations by adding an additional infrared laser beam to the experimental apparatus described above. This laser is on the same beam path as the trapping laser, except its position is controlled manually and centered on the pedestal bead on the surface of the sample chamber. The light, after interacting with the pedestal bead, is projected onto the 4-quadrant photodiode which measures changes in stage position as the light is deflected by the pedestal bead during movement of the stage (for example, due to drift). The signal from the photodiode is then sent through an integrating amplifier to a piezo stage controller which moves the stage until the signal on the photodiode is returned to zero. By incorporating this stage feedback system into our experiments, we can reduce fluctuations in the x-axis position of the stage (figure 2.5 and 3.16) due to drift or other mechanical vibration. Additionally, by injecting a sinusoidal command signal into the summing junction of the x-axis position detector we can use the feedback loop to oscillate the stage during stiffness measurement experiments (see 2.4.4).

2.2.5 Calibration of the isometric force feedback loop

Calibration of the feedback response can be accomplished by adjusting the gain of the integrating amplifier of the feedback loop described above. Briefly, an actin filament was stretched between two trapped beads, and the x-axis voltage signals from both beads were zeroed by adjusting the position of the photodiode detectors. The feedback loop was engaged and a 2 Hz square wave command signal was injected into a summing junction of the transducer bead x-axis position signal. The feedback response was recorded and the time required for the transducer signal to return to zero was measured. The integral loop gain was adjusted so that the half time for the response was ~50 ms for force feedback experiments. For stiffness measurements the feedback gain was increased to allow a half time of ~5 ms. Proportional and differential feedback controls were not used in the experiments in this thesis.

2.2.6 Calibration of the stage feedback loop

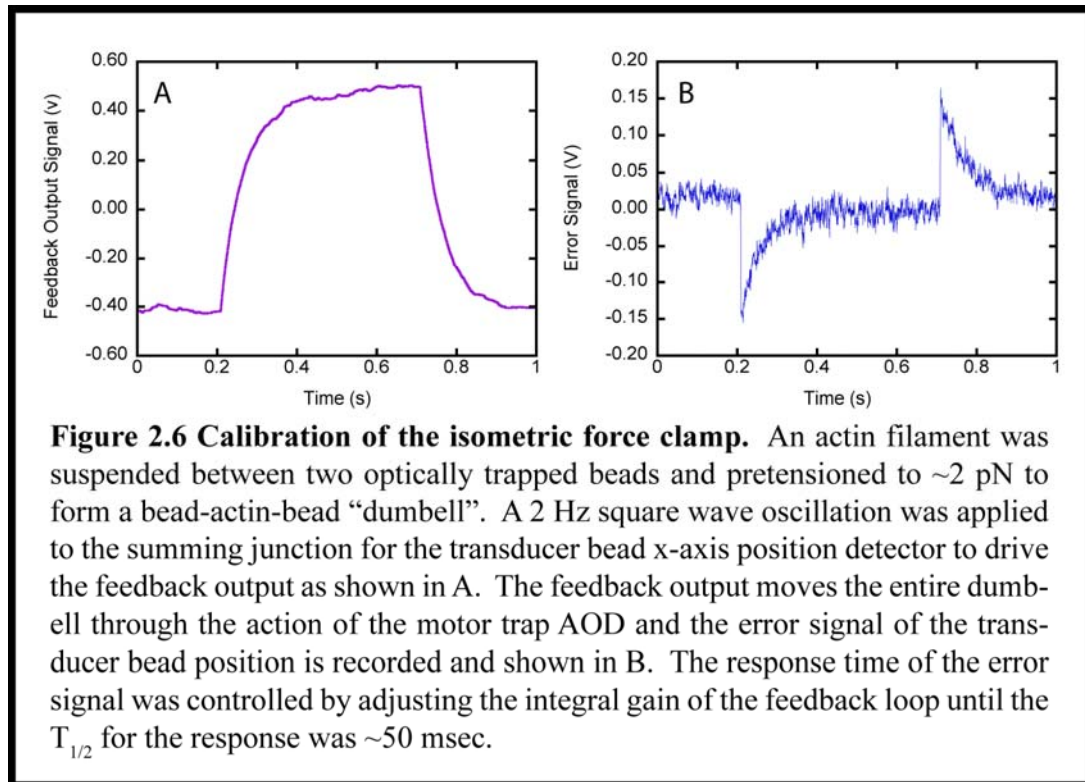
In order to calibrate the stage feedback loop and obtain the calibration to convert feedback output voltage to distance moved by the stage we first measured the input voltage required to drive the stage piezo controller by known amounts. A stage micrometer was used to compare voltage sent to the piezo controller to



distance between successive 1 μm marks on the stage micrometer. 1 V was found to correspond to 788 nm of stage movement.

Before every experiment involving stage feedback, the output voltage from the x and y-axis difference signals from the 4-quadrant photodiode for the 930 nm position detection laser were zeroed at the center of a pedestal. A 1 Hz square wave corresponding to ~ 10 nm of stage motion was injected into the summing junction of the stage laser photodiode x-axis position signal, and the response of the feedback loop was recorded. The x-axis signal was recorded and the time required to restore the x-axis signal to zero was adjusted using the integral gain much the same way as

for the isometric feedback loop. For all experiments the time required for half signal restoration was set to ~ 10 ms. As for the isometric force feedback loop, proportional and differential controls were not used.



2.3 Experimental protocol

2.3.1 Motility chamber preparation

Coverslips (22 x 40 – 1.5 – Fisher) were prepared by coating with a 1% nitrocellulose in amyl acetate (Fullam) solution to which 2 μ l of 1.9 μ m silica beads (Bangs Laboratories, 1% initial volume) in amyl acetate were added to serve as pedestals. Coated coverslips were stored in a plastic petri dish and left to dry for 30 minutes at room temperature. Motility chambers were prepared by applying double

sided tape to each end of an uncoated coverslip and tracing the inside tape edge of each side with a thin strip of silicon vacuum grease (Dow Corning). A coated coverslip was placed on top of the vacuum grease and gentle pressure was applied to form a thin motility chamber of approximate volume 20 μ l.

Solutions were added sequentially to the chamber as follows: 0.1 mg/ml streptavidin in water (3 min), 1 mg/ml BSA in motility buffer (2 x 5 min) to block nonspecific binding of protein to the nitrocellulose-coated surface, 1 – 5 nM biotinylated myo1b in motility buffer + 20 μ M CaM (5 min), 1 nM RPFA in activation buffer. NEM-myosin-II coated beads were added to one side of the chamber to replace \sim 1/4 the volume of the chamber. The chamber was sealed with vacuum grease and used for up to 90 minutes in experiments.

2.3.2 Data Collection

For each experiment, two NEM-myosin-II coated beads were separately immobilized in optical traps and brought away from the bead-infused area of the experimental chamber. Calibration of trap stiffness was performed as described above for each experiment. Fluorescent actin filaments were observed in the camera display, and a bead-actin-bead dumbbell was prepared by moving the stage until a fluorescent actin filament was brought into contact with one of the beads. By moving the stage, the other end of the actin filament could be brought into contact with the other bead. Care was taken to avoid long “overhangs” from bead attachment positions too close to the center of the filament. Additionally, filaments

were selected for length, with only filaments between ~ 5 and $15 \mu\text{m}$ used in experiments.

After forming a dumbbell, the actin filament was stretched manually by adjusting the tilt of a mirror that controlled the x-axis position of one of the beads. The force applied to the filament could be estimated by observing the change in voltage signal from both beads and multiplying by the calibration factor (C) from the calibration described above. For most experiments the pretension force on the beads was $\sim 2 - 3 \text{ pN}$. The stretched actin filament would then be brought close to the surface of the coverslip, and the stage piezo controller was used for all further adjustments of the stage relative to the dumbbell position. At this point the stage was moved to position the center of the actin filament directly over the pedestal. The stage was then raised, bringing the actin filament into contact with the pedestal, which caused the actin filament to flex in response to pressure from the pedestal. Flexing of the actin filament caused a change in force on the beads, which was reported in the voltage signal. The stage was then lowered slightly until the actin filament was no longer bending over the pedestal. Each pedestal was “scanned” by moving the stage in 100 nm increments, allowing the actin filament to sample multiple areas of the pedestal for 5-10 second intervals. At the myosin densities used for single molecule experiments, $\sim 50\%$ of scanned pedestals showed interactions with a myosin. Interactions were detected visually by observing the voltage signals from trapped beads in real time. During an interaction between myosin and the suspended actin filament, a change in system stiffness results in a

decrease in Brownian noise in the bead voltage signals. Additionally, the power stroke of the myosin causes a change in the average voltage signal on the bead. Upon observation of interactions, voltage signals were recorded for 6 – 10 minute intervals at a 2 kHz sampling rate. Drift was corrected manually in the y and z axes by visual observation of the relative positions of the three beads before and after each experiment.

For force feedback experiments, the experimental protocol is much the same with some exceptions. After collecting the first set experimental data set, the direction of the power stroke was determined by looking at the direction of the change in voltage signal during acto-myosin interactions. During an interaction, the powerstroke causes the stretched dumbbell to move in one direction, thus the voltage changes on the two beads are equal in magnitude (when converted to force) but opposite in direction, since one bead moves towards the center of its trap while the other moves further from the center of its trap. Force feedback experiments require that the direction of the force is always away from the center of the motor trap to result in a “pulling” force opposing the power stroke, so for roughly half the experiments it was necessary to switch the orientation of the dumbbell. This was accomplished by moving the stage away from the actin filament and shuttering the trapping laser light (Uniblitz), after which the stage was rapidly moved manually so that when the laser light was re-introduced by releasing the shutter one of the beads was immediately trapped in the trap opposite its original orientation. The other bead was then immobilized in the remaining laser trap by stage movement, thus

switching the orientation of the filament. After checking the orientation of the filament, the voltage signals from the two photodiodes were zeroed and the feedback loop was engaged. Pedestals were scanned and interactions were observed in the same way as for the no-feedback experiments.

For experiments in which the stage position feedback was used, pedestals were scanned in the absence of stage feedback until the filament orientation was determined and a myosin was found. The position of the stage position detection laser was manually adjusted by way of a mirror along the beam path before it converged with the trapping laser beams. When the beam was positioned roughly at the center of the pedestal bead (visualized by looking at the reflected laser light in the digital camera projection) the voltage output signals from the stage position photodiode were zeroed in both x and y axes. The feedback loop was then engaged and the voltage output from the feedback loop was monitored and recorded with all data to observe the corrections for drift and stage fluctuations made by the feedback loop.

2.3.3 Steady state ATPase

The steady state ATPase of myo1b^{IQ} was assessed using the NADH enzyme linked assay as described (De La Cruz, Sweeney & Ostap 2000) (Furch, Geeves & Manstein 1998) in KMg25 using an Applied Photophysics (Surrey, UK) SX.18MV stopped flow instrument. 5 μ M Myo1b^{IQ} was added to one syringe of the stopped-flow instrument, while the other syringe contained 0.5 mM DTT, 0.5 mM ATP, 0.4

mM NADH, 1 mM phosphoenolpyruvate , 40 U/mL lactate dehydrogenase , 200 U/mL pyruvate kinase, and varying actin concentration. The time courses of NADH reduction were monitored by absorbance change at 340 nm with a 400 nm long pass filter and converted to ADP concentration produced by the Beer-Lambert law using the extinction coefficient for NADH ($\epsilon_{340} = 6220 \text{ M}^{-1}\text{cm}^{-1}$) and a cuvette path length of 0.2 cm. The actin dependence (activation) of the observed ATPase rate was fit to a rectangular hyperbola in accordance with standard Michaelis-Menten kinetics. Experiments at each actin concentration (0 – 100 μM) were done in triplicate at 23°C

2.3.4 Transient Pi release

Transient phosphate (Pi) release was measured in the stopped flow apparatus described above using the coupled assays system containing the fluorescently labeled mutant of phosphate binding protein (PiBP) as described (Lewis et al. 2006, Brune et al. 1994). The instrument and syringes were incubated for at least 2 hours in a phosphate “mop” containing 1 mM 7-methylguanosine and 0.2 U·mL⁻¹ nucleoside phosphorylase, to remove contaminating inorganic Pi. During experiments, one syringe contained 5 μM Myo1bIQ, 2 μM CaM, 10 μM PiBP, in KMg25 containing 2.5 μM ATP. After a brief aging period to allow formation of the AM·ADP·Pi complex, the solution in the first syringe was rapidly mixed with the actin solution in the second syringe containing 0.02 U·mL⁻¹ apyrase, 2 μM CaM, and 2 μM PiBP, and varying [actin] in KMg25. The fluorescence enhancement of Pi

binding to labeled PiBP was recorded using a 425 nm excitation wavelength and a 440 nm long-pass filter

2.4 Data Analysis

2.4.1 Selection of events

Events were selected using the covariance thresholding method as described in Takagi et al., (2006) with modification. All software used for analysis was written in Labview (National Instruments) by Henry Shuman. The average covariance (*cov*) of the motor, F_m , and transducer, F_t , force signals was calculated for a 85 ms time window centered on each data point of the force traces using the equation,

Equation 6

$$\text{cov}(F_t, F_m) = \langle (F_t - \langle F_t \rangle)(F_m - \langle F_m \rangle) \rangle = \langle F_t F_m \rangle - \langle F_t \rangle \langle F_m \rangle$$

where $\langle \rangle$ is an average over the time window. The means of F_t , F_m and $F_t \cdot F_m$ are given by,

Equation 7

$$\langle F_t \rangle = \frac{1}{2n+1} \sum_{-n}^{+n} F_t; \quad \langle F_m \rangle = \frac{1}{2n+1} \sum_{-n}^{+n} F_m$$

and

Equation 8

$$\langle F_t F_m \rangle = \frac{1}{2n+1} \sum_{-n}^{+n} (F_t F_m)$$

The covariance was then smoothed over a 50 ms sliding-window to generate the covariance histograms (figure 2.7) used to select attachment events. A typical covariance histogram was bimodal, with one peak of higher covariance corresponding to the detached state, and one lower covariance peak corresponding to actomyosin attachment events.

Two methods, based on covariance thresholding, were used to determine the start and ends of actomyosin attachments. Selection method #1 was used to minimize false positives in the attachment-duration measurements. For this method, attachment starts were defined as the point when the covariance decreased from the peak of the distribution of covariances assigned to actin detached from myosin (point A in figure 2.6) and reached the peak of the covariance distribution assigned to actin bound to myosin (point B in figure 2.6). Attachment ends were defined as the point when the covariance returned to the peak of the detached covariance distribution.

Selection method #2 was used to optimize the time resolution of the time courses of the ensemble averages. Attachment starts were defined as the point when the covariance decreased below a point between the attached and detached covariances where the histogram of covariances was at a minimum (point C in figure 2.6). Since these selection criteria resulted in a greater number of false positive events, that are expected to have zero net displacement, the total ensemble

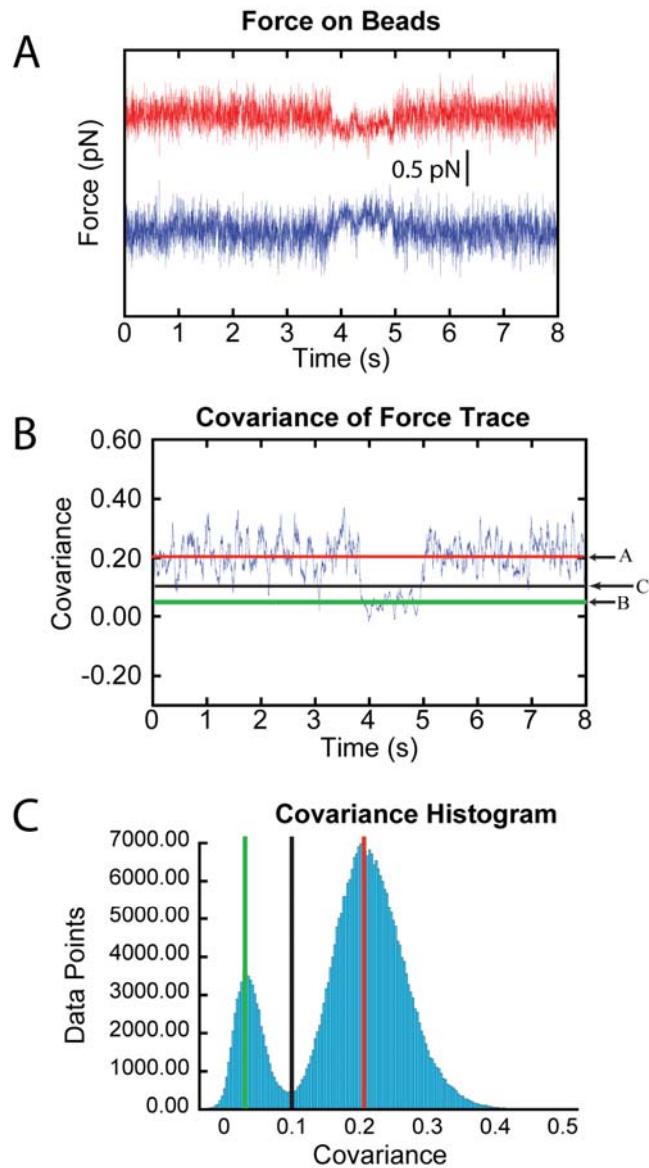


Figure 2.7 Selection of actomyo1b interactions. (A) Forces on the two trapped beads holding a single actin filament during an actomyo1b interaction. (B) Covariance of the trapped beads calculated for the trace shown above. Points A, B, and C correspond to the covariances identified on the histogram below. (C) Distribution of the covariances from a sample data trace, which includes the interaction shown above. The histogram is bimodal with the higher covariance distribution corresponding to the detached state and the lower distribution corresponding to the actomyo1b attached state. The cutoff thresholds discussed in the text for the two types of analyses are shown as colored bars. From Laakso et al. (2008)

averaged events were normalized to the number of events identified by selection method #1, by multiplying the displacements by the ratio of events collected by the two methods.

A particular exclusion was made for events collected with the isometric feedback loop engaged that showed an initial positive deflection in force which was immediately followed by a rapid “reversal” to a negative force (figure 2.8). These types of events were not analyzable for the experiments presented in this thesis as the rapid change in force saturated the feedback loop in the direction of the power stroke, with the transducer bead having moved back to the center of the optical trap. While these reversals may represent an interesting phenomenon, we have not quantitatively developed an explanation for their occurrence. These events are very similar to the observations of “bipolar” attachment events observed by Takagi et al., (Takagi, Shuman & Goldman 2004) and we consider them to be more likely to occur at higher gain settings (see discussion).

2.4.2 Ensemble Averaging

Ensemble averaging of synchronized interactions were performed according to the method of Veigel et al. (2003). Events were synchronized to the start or end of each event according to selection method #2 (see 2.4.1). Events were extended forwards in time by extending an average of the force value immediately before detachment over 50 ms (see panel C of figure 1.19). Alternatively, the events were extended backwards in time by extending the force value immediately after

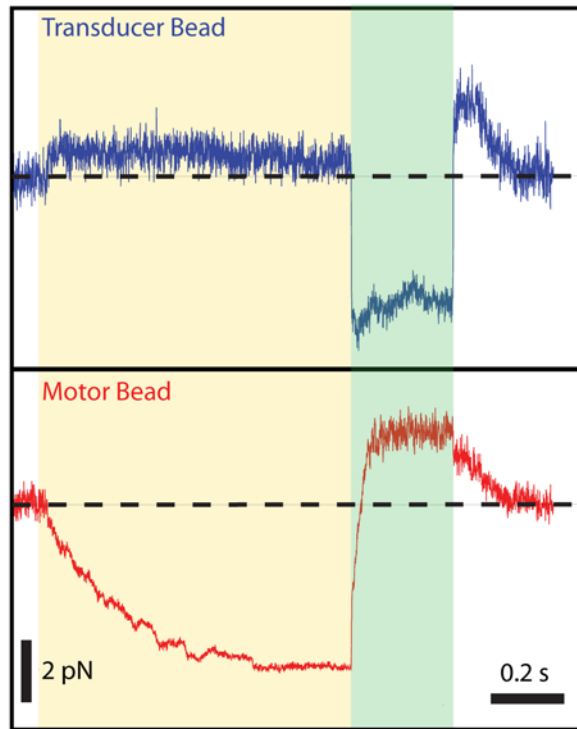


Figure 2.8 Observation of “reversal” events. A single actomyo1b attachment event is shown undergoing a rapid reversal. The zero force position (representing the pretension force on the beads) is indicated by the dashed line. The yellow shaded area represents the “normal” phase of the interaction where force is generated by the myosin and opposed by the movement of the motor bead driven by the AOD. At the intersection between the green and yellow shaded areas, the force on the bead rapidly reverses and saturates the feedback loop due to compliance in the actin filament. The filament goes slack between the myosin and the transducer bead, indicated by the movement of the transducer bead to the center of the trap (top panel) and the increased variance of the motor bead (bottom panel). These events could represent a similar transition to the “bipolar” actomyosin events observed by Takagi et al., (2004) for myosin-II.

attachment over 50 ms. Selecting this force value removes the error associated with calculating the covariance over a sliding window during attachment or detachment.

Time courses of the ensemble averages were fit using Kaleidagraph (Synergy Software) to a single exponential rate function

Equation 9

$$k_{\text{obs}} = \text{Amplitude}(1 - e^{-\text{rate} \cdot \text{time}})$$

Best fit parameters and standard errors of the fits are reported. For feedback event sorting, ensemble averages of event starts and ends were binned by the force value 50 ms prior to detachment.

2.4.3 Maximum likelihood estimation

Bootstrap Monte Carlo simulations were performed to generate data for Maximum Likelihood Estimations (MLEs) of the log-likelihood of equation 10 in Labview by John Lewis. A range of all applicable parameters was tested to find the peak in the log likelihood, and the parameters corresponding to this peak were reported as the best-fit values. Errors were assessed at a 97% confidence level. The calculated MLEs from the simulated data were normalized according to the MLE from the original data set. If the value was less than 2 standard deviations away, it was rejected. The parameters from the accepted set were collected and the maximum and minimum values were recorded. Errors were obtained by subtracting the maximum and minimum values from the respective parameters.

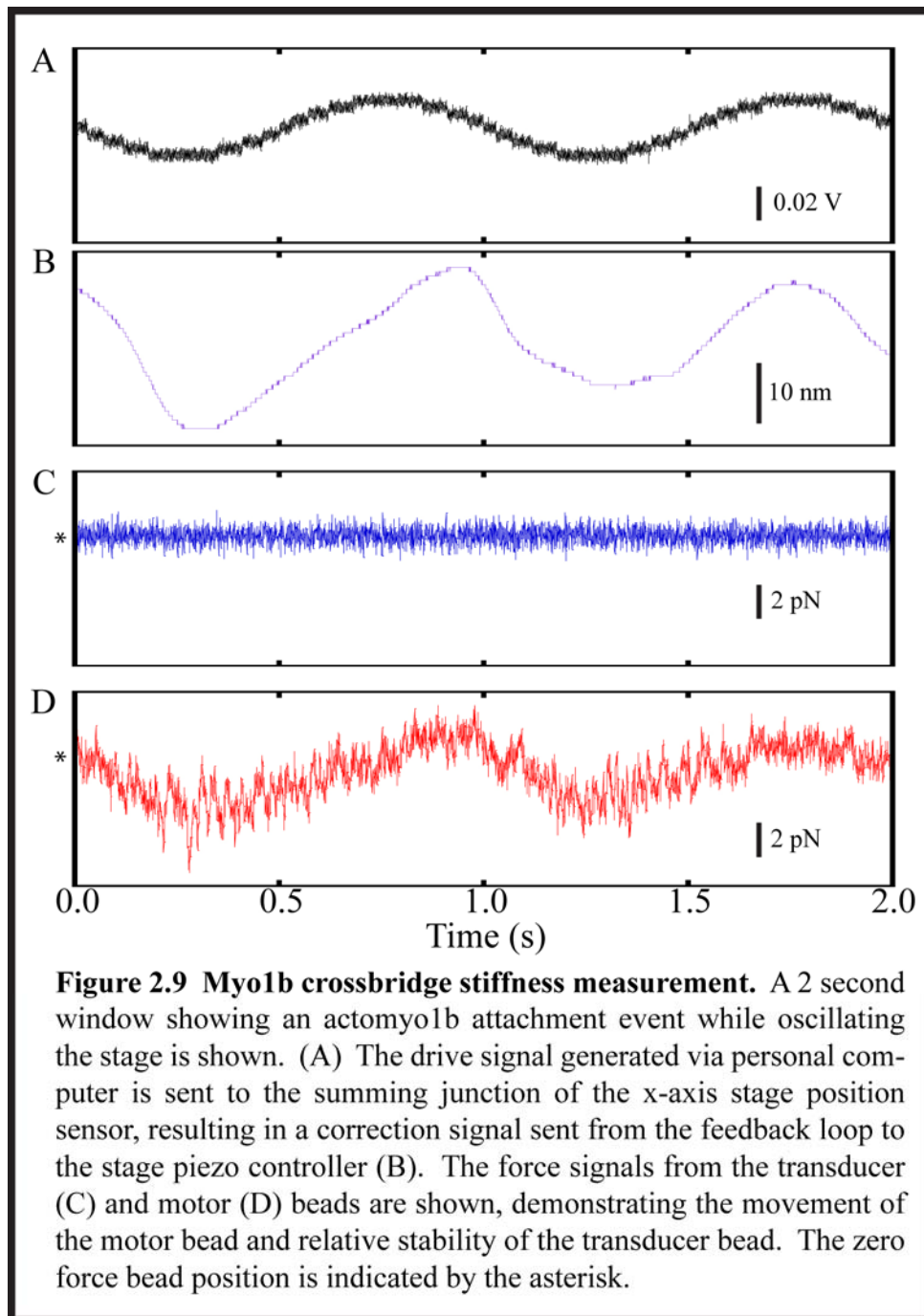
2.4.4 Stiffness measurements

We measured the stiffness of actomyo1b crossbridges by the simultaneously measuring the position of the stage during a controlled oscillation and recording the

force on the motor bead due to stretching of the actomyosin crossbridge while attached to actin. The three bead assay was performed as described earlier in 2.3.2 with the isometric force clamp engaged, with the exception that a 1 Hz sinusoidal drive signal was injected into the summing junction of the x-axis detector of the stage position sensor. Using the isometric force clamp maintains a constant pretension force on the actin-transducer bead linkages, removing the need to correct for bead-actin compliance in the stiffness measurement.

Using stage feedback, the drive signal (figure 2.7 A) generated an error signal in the output of the stage feedback loop, which was then sent to the piezo stage controller. The piezo controller moves the stage to correct the error signal, closing the feedback loop, and thus oscillating the stage. The voltage output of the feedback loop was recorded and converted to distance according to the conversion factor measured above in 2.2.6. The force signals of the motor and transducer beads were collected and the gain of the isometric force clamp feedback loop was adjusted to minimize movement of the transducer bead (usually ~ 5 ms), ensuring that the motor bead force trace faithfully reported the force due to stretching of the myosin crossbridge. Every 2000th point was averaged for both the force and stage position to generate an average over 1 second, and the force on the motor bead was plotted against the stage position to generate a phase plot (see results, figure 3.22), the long axis of which was fit to a straight line, the slope of the line giving the stiffness of the interaction in $\text{pN}\cdot\text{nm}^{-1}$. Events were selected using the covariance method #2

described earlier, and no events less than 3 seconds or greater than 35 seconds were used.



3. Results

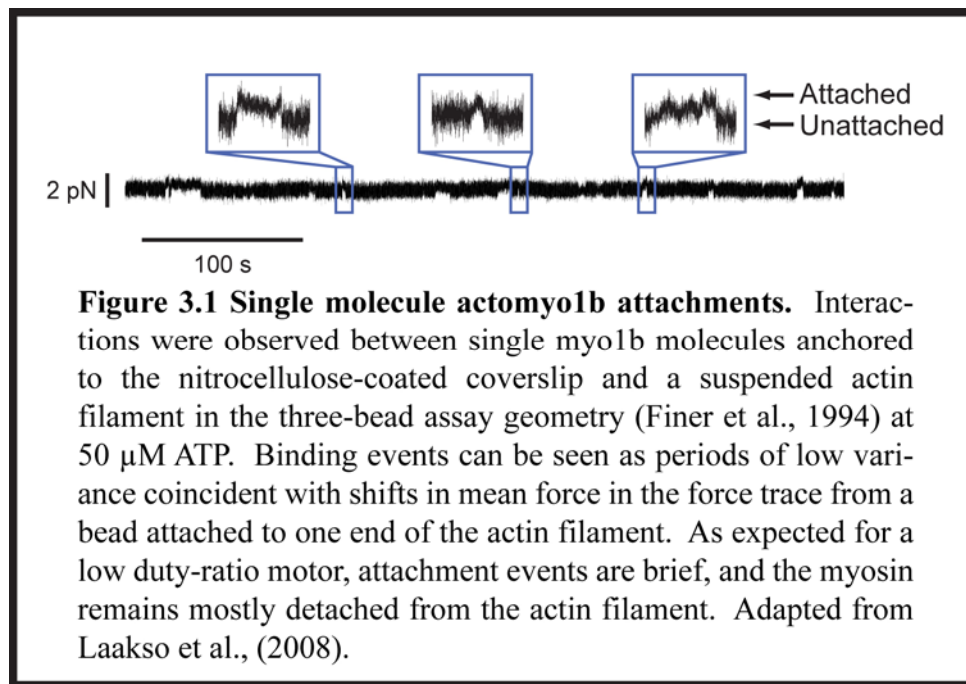
3.1 Myosin-Ib can act as a molecular tension sensor

In the first part of the results section of this thesis, we set out to examine the response of myo1b to an external load resisting the power stroke, similar to what an individual myo1b molecule or cluster of myo1b molecules working together might experience in a cellular environment. We examined the lifetimes of actomyo1b attachment durations as a function of force at the single molecule level using the isometric force clamp developed by Takagi, Goldman and Shuman (Takagi et al. 2006a). We then used ensemble averaging to confirm the two-step nature of the myo1b working stroke (Veigel et al. 1999) and show that ADP release corresponds to the highly sensitive transition for myo1b. This work will show in detail how myo1b mechanochemistry changes due to an imposed load, providing in vitro evidence that it could potentially function as a tension sensor.

3.1.1 Detection of single molecule interactions

The first series of experiments in this thesis sought to examine the mechanics and force sensitivity of myo1b at the single molecule level using the three-bead assay geometry. For the following experiments, a myo1b construct containing five IQ motifs along the LCBD was used. The activity of myo1b was assessed in the three bead assay configuration by observing interactions between the

suspended actin filament and the site-specifically biotinylated myosin (anchored via a biotin-streptavidin linkage) on the surface of the experimental chamber. Data were collected at low trap stiffness ($\sim 0.022 \text{ pN}\cdot\text{nm}^{-1}$) to reduce the load imposed on the myosin by the optical trap. A series of

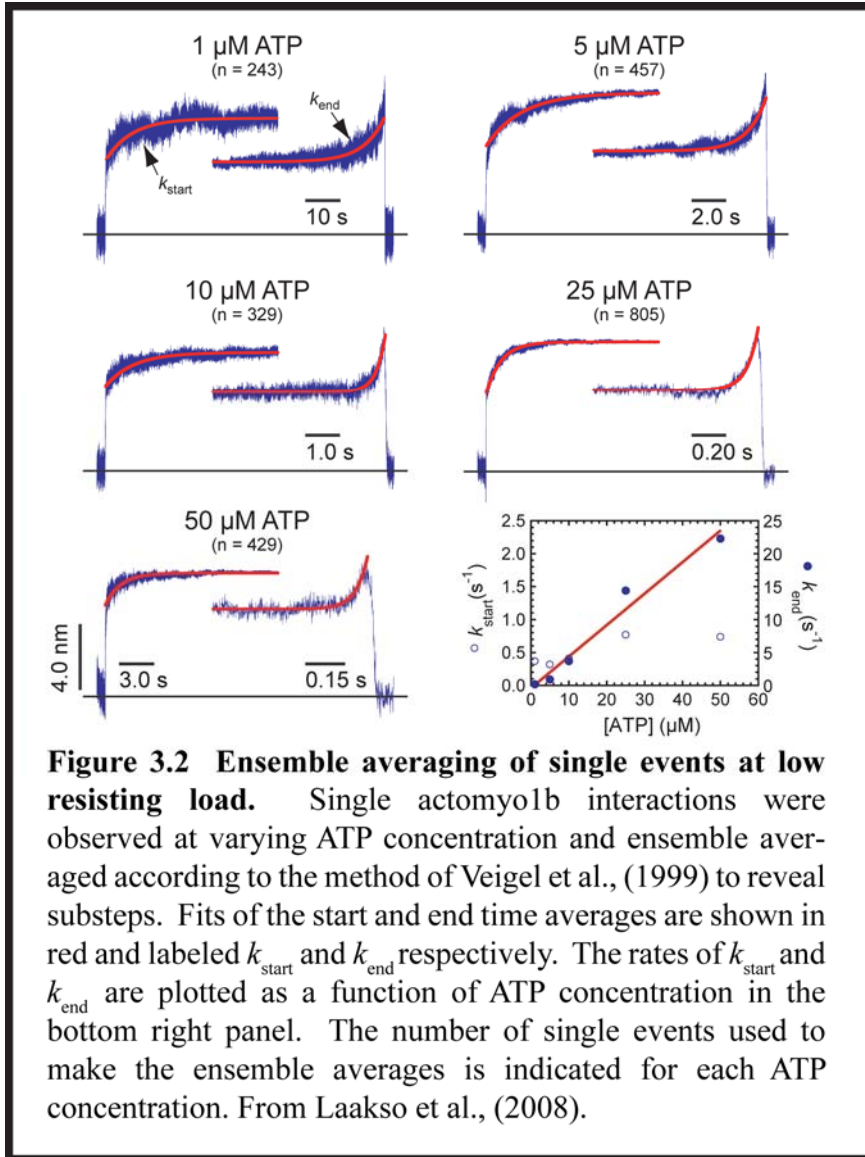


sample interactions collected at $50 \mu\text{M}$ ATP is shown in figure 3.1. Binding events between the actin and myosin can be observed as changes in the variance of the force trace due to an increase in system stiffness, with a simultaneous change in mean force acting on the bead in the optical trap due to the motion of the myo1b power stroke. The start and endpoints of events were determined by the covariance thresholding methods described previously (Takagi et al. 2006a).

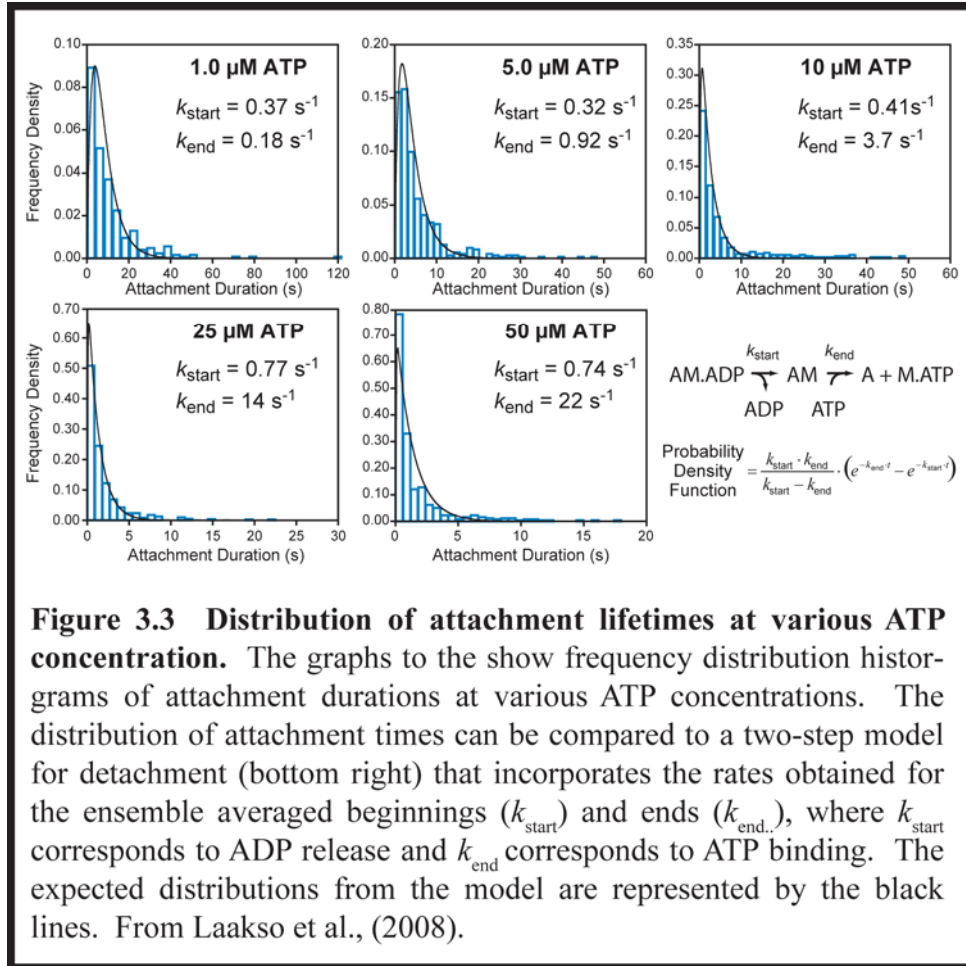
3.1.2 Kinetics of Myo1b substeps

To detect the presence of substeps in the myo1b working stroke, we used the method of ensemble averaging as described by Veigel et al. (Veigel et al. 1999). Briefly, by selecting events according to covariance method 2 (see methods) and synchronizing to the start of each event and extending the recording of the end immediately prior to detachment, a second substep can be observed as an increase in displacement after the initial substep that occurs within the time resolution of the instrument. For the start time averages, the rate of the increase in displacement is related to the lifetime of the first substep (k_{start}). Alternatively, by synchronizing the ends of the events and extending backwards in time immediately after attachment, a similar increase in displacement is observed, with the rate corresponding to the lifetime of the second step (k_{end}). Displacements in nm were calculated by dividing the forces recorded in the ensemble averaged traces by the known trap stiffness. As shown in figure 3.2 the ensemble averages of myo1b^b at various ATP concentrations show a rapid initial substep of 5.1 ± 0.43 nm that takes place within the time resolution of our instrument. This first substep is followed by a slower 3.3 ± 0.35 nm increase to the final displacement (errors represent standard deviations of the distribution of individual step sizes). The start and end time averages both showed similar changes in displacement.

We fit the ensemble averaged start and end time courses to a single exponential function to measure the lifetimes of the first and second step respectively. A plot of the rates of the start and end time averaged data versus ATP



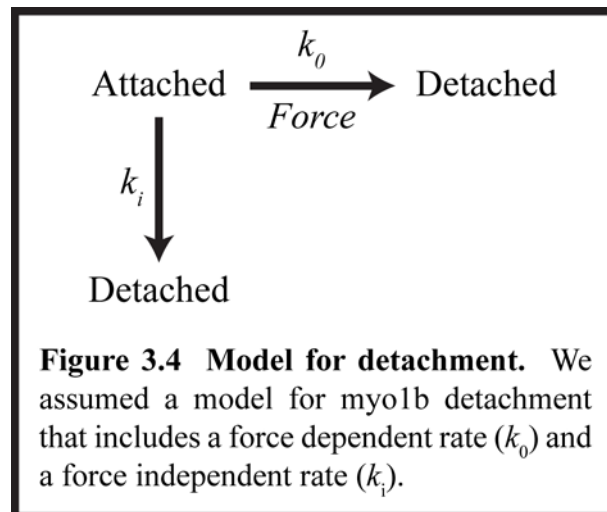
concentration is shown in the bottom right panel of figure 3.2. The rates of the start time averages had little ATP concentration dependence, varying from 0.37 s^{-1} to 0.77 s^{-1} . The rates of the end time averages, however, were linearly related to the ATP concentration with a slope of $0.48 \mu\text{M}^{-1}\text{s}^{-1}$. The rates of the start and end time averages, therefore, are consistent (within a factor of three) with the known rates of



ADP release and ATP binding described in Table 1.1 when corrected for temperature considerations, with ATP dependent kinetics that would be expected for the lifetimes of the AM·ADP and AM(rigor) states respectively. The overall lifetimes of actomyosin attachment can be approximated by the lifetimes of the two substeps as determined by k_{start} and k_{end} . As shown in figure 3.3, histograms of attachment lifetime, plotted as frequency densities, can be well described by the predicted probability distribution generated by using the values for k_{start} and k_{end} in the two step model shown in the bottom right panel.

3.1.3 Myo1b is a high duty-ratio motor under load

Using the isometric force clamp described in methods, we were able to subject myo1b^b to a variety of loads resisting the motion of the power stroke. As shown in panel B of figure 3.5, we observed dramatic increases in attachment duration under loads of up to 4 pN in the presence of 50 μ M ATP. A scatter plot of data collected from 12 different myosins is shown in figure 3.6, where the actin attachment lifetime is seen to increase in response to increasing force up to ~ 1.5 pN, after which the lifetimes appeared to be force-independent. We assumed a model for the rate of actomyo1b detachment that includes force-dependent and force-independent pathways:

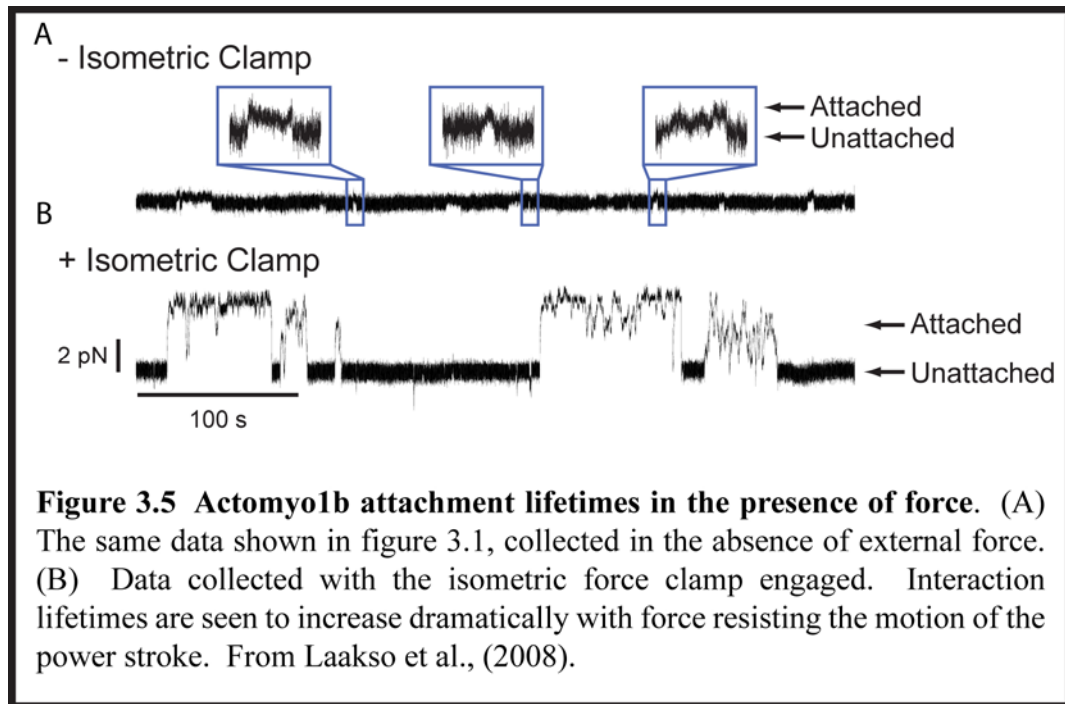


where k_g is a force-dependent rate constant and k_i is a force-independent rate constant for actomyo1b dissociation. The force dependence of the detachment rate can be calculated by fitting our data to the following model:

Equation 10

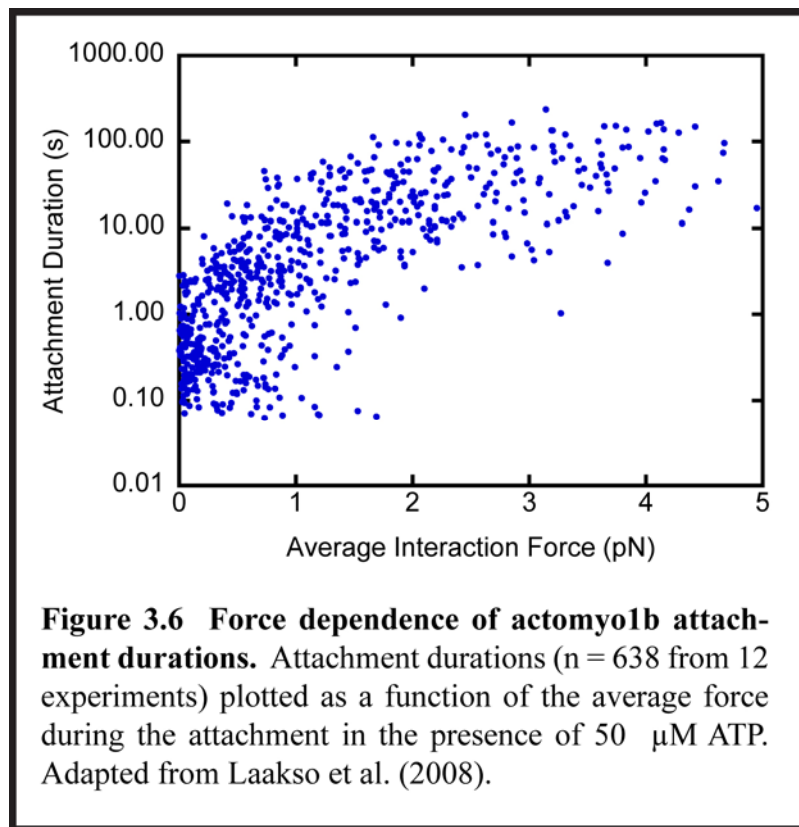
$$k_{\text{det}}(F) = k_0 + k_i = k_{g0} e^{\frac{-F \cdot d_{\text{det}}}{kT}} + k_i$$

where k_{g0} is the rate of k_g in the absence of force, d_{det} is the distance parameter (the distance to the transition state of the force dependent step, or the distance over which the force acts), F is force, k is the Boltzmann constant, and T is the temperature. Because the attachment durations at each force are expected to be exponentially distributed, we used bootstrap monte carlo simulations to generate data for maximum likelihood estimations (MLEs) which were used to determine the values and confidence limits of the parameters that describe the distribution of attachment lifetimes.



From the MLEs, the best-fit value of $k_{g0} = 1.6 \text{ s}^{-1} (+0.5/-0.35 \text{ s}^{-1})$ is consistent with the rate of ADP release as measured via solution biochemical

methods (1.8 s^{-1}) (Lewis et al. 2006) which is expected to limit detachment from the actin filament in the absence of force. The distance parameter, $d_{\text{det}} = 12 \text{ nm}$ ($+1.6/-3.0 \text{ nm}$), is extraordinarily large and distinguishes myo1b as an extremely strain-sensitive molecular motor. The force independent rate of detachment k_i , representing the rate of detachment at forces $> 1.5 \text{ pN}$, was found to be 0.021 s^{-1} ($+0.007/-0.004 \text{ s}^{-1}$). The errors of the fit parameters represent the 97% confidence limits of 250 bootstrap Monte Carlo simulations of our data, calculated as described in Methods.



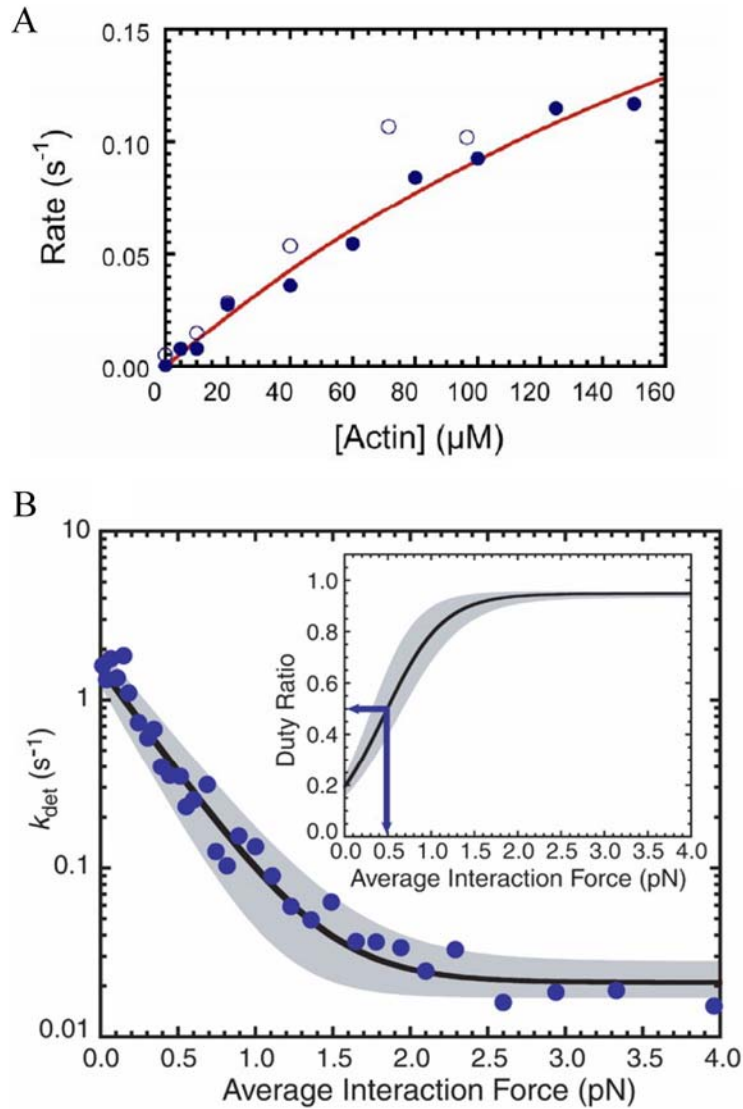


Figure 3.7 Myo1b is a high duty ratio motor under load. Panel A shows the steady-state ATPase activity and transient phosphate release from actomyo1b. The actin dependence of the ATPase rate is shown in closed circles. The actin dependence of the rate of phosphate release is shown in open circles. The solid line is a fit of the steady-state ATPase rates to the Michaelis-Menten equation. Panel B shows the detachment rate as a function of force for the data in figure 3.6. Inset shows the predicted duty ratio according to equation 11 using values for k_{det} from the data above and k_{att} estimated from phosphate release in panel A. Grey shaded areas represent the 97% confidence limits as described in the text. Adapted from Laakso et al., (2008)

To determine the predicted duty ratio as a function of force, we measured the steady-state ATPase and transient rate of phosphate release from actomyo1b. The actin dependence of both the ATPase rate and Pi release rate from actomyo1b is shown in figure 3.7 (panel A). The solid line is a fit of the steady-state ATPase rates to the Michaelis-Menten equation, yielding $V_{\max} = 0.38 + 0.14 \text{ s}^{-1}$ and $K_M = 310 + 160 \text{ }\mu\text{M}$. The overlaid graphs show that the steady state rate ATPase of myo1b is dominated by rate-limiting phosphate release from actomyo1b.

A plot of the detachment rate as a function of force is shown in panel B of figure 3.7. The blue dots represent the inverse averages of 20 consecutive points (by force), where the black line is the fit of the model above to the raw data. The inset shows the predicted duty ratio as a function of force, according to the equation:

Equation 11

$$\text{duty ratio}(F) = \frac{k_{att}}{k_{att} + k_{det}(F)}$$

where $k_{det}(F)$ is our measured rate of detachment at force F (figure 3.7B), and k_{att} is the rate of entry into the strong binding states estimated by the rate of Pi release at saturating actin concentration (figure 3.7A). Myo1b, therefore, transitions from a low duty ratio motor to a high duty ratio motor when working against loads greater than 0.5 pN.

3.1.4 ADP release is the predominant strain-sensitive transition in the myo1b biochemical cycle

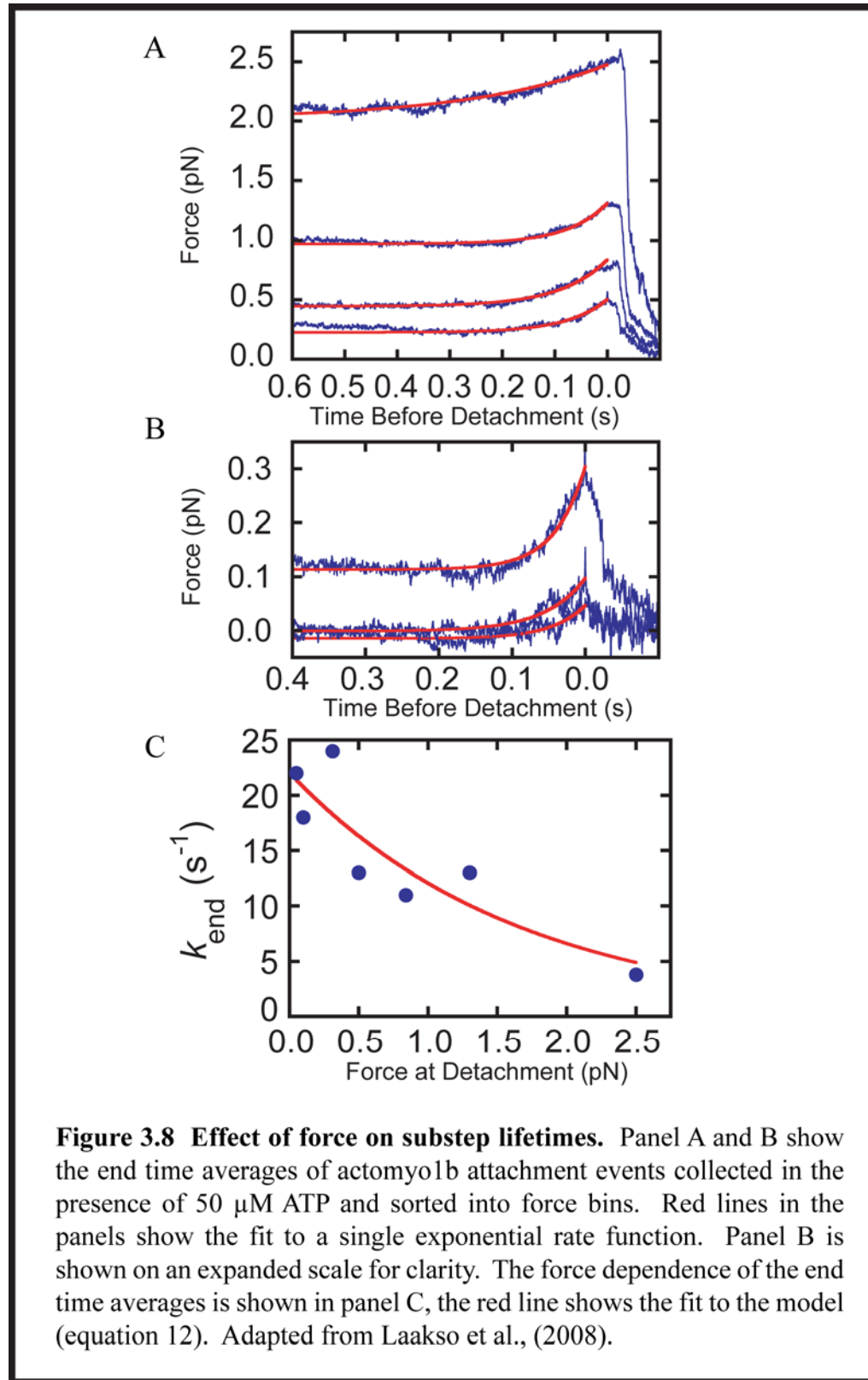
The two biochemical steps that could be modified to increase the lifetime of the strongly bound state in the myo1b ATPase cycle are inhibition of ADP release from the AM·ADP state or inhibition of ATP binding to the rigor complex. To distinguish between these two potential biochemical steps, we investigated the effect of force on the lifetimes of the working stroke substeps. Interactions acquired in the presence of 50 μM ATP with the isometric force clamp (see methods) engaged were binned by force immediately prior to detachment into groups corresponding to all events between 0 to 0.125, 0.125 to 0.25, 0.250 to 0.50, 0.500 to 0.750, 0.75 to 1.0, 1.0 to 2.0, and 2.0 – 4.0 pN. We ensemble averaged the force binned events according to the end points of the interactions and observed transient increases in force in the $\sim 500\text{ms}$ immediately preceding detachment (figure 3.8). Single exponential fits of the ensemble averaged ends yielded rates that decreased with increasing force, and the force dependence of the rates was fit to the equation

Equation 12

$$k_{\text{end}}(F) = k_{\text{end}0} e^{\frac{-F \cdot d_{\text{end}}}{kT}}$$

where $k_{\text{end}0}$ is the rate of the time course in the absence of force and d_{end} is the distance parameter of the substep.

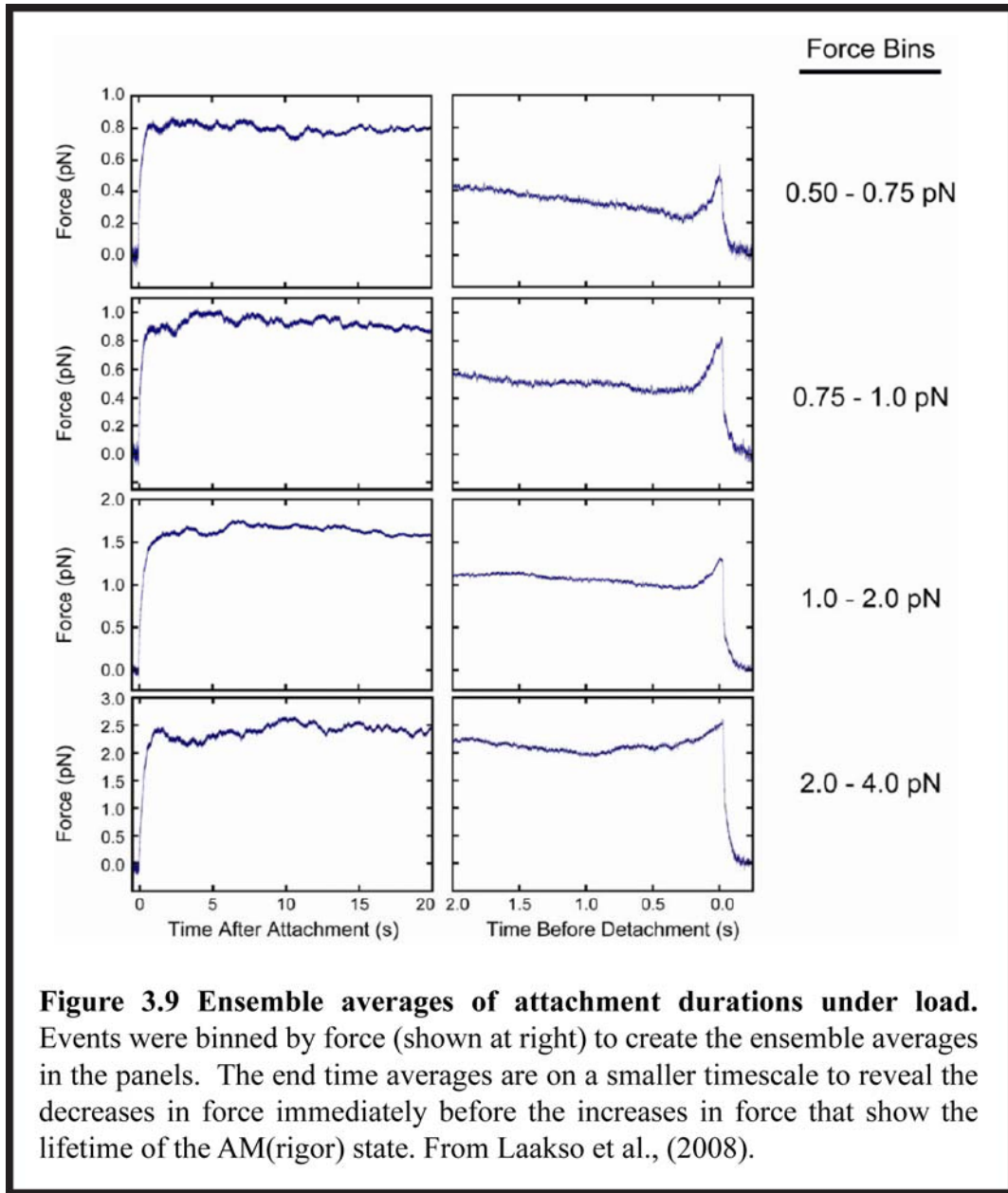
The best fit rate of $k_{\text{end}0}$ ($22 \pm 2.5 \text{ s}^{-1}$) is in agreement with the rate of ATP binding at 50 μM ATP as determined by the fit to the end-time averages of data collected without the isometric force clamp engaged ($k_{\text{end}} = 24 \text{ s}^{-1}$, figure 3.2).



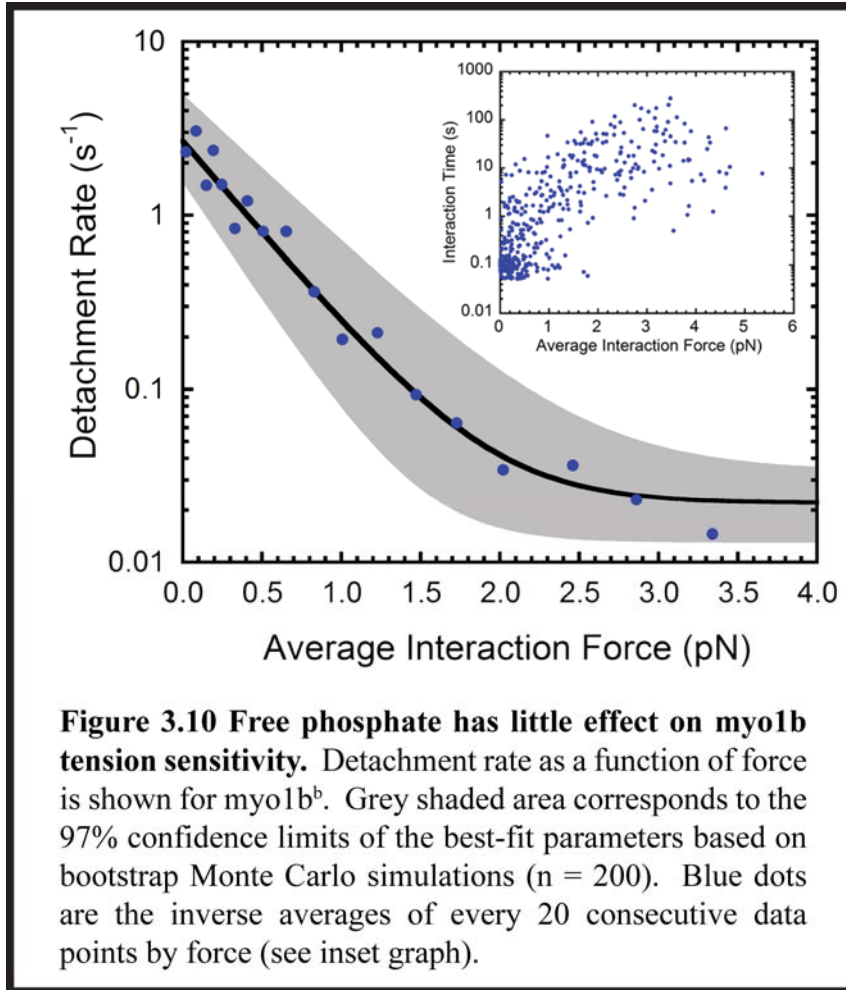
Taken together these data suggest that the transient increases in force describe the lifetime of the same transition (ATP binding and detachment) as the unloaded data. The rate of k_{end} decreases with force, however the best fit value for d_{end} ($2.5 \pm 0.83 \text{ s}^{-1}$) is much smaller than d_{det} . Therefore the predominant force sensitive transition most likely responsible for the large value for d_{det} is not restriction of ATP binding to the AM(rigor) state, but rather inhibition of ADP release. Additionally, we observed decreases in force immediately prior to the rapid increases in force immediately prior to detachment in expanded ensemble averages (figure 3.9). These decreases in force may represent fluctuations due to mechanical vibrations of the stage prior to detachment, a potential artifact corrected for in later experiments (see discussion).

3.1.5 The myo1b force sensitive state is not reversible by phosphate rebinding

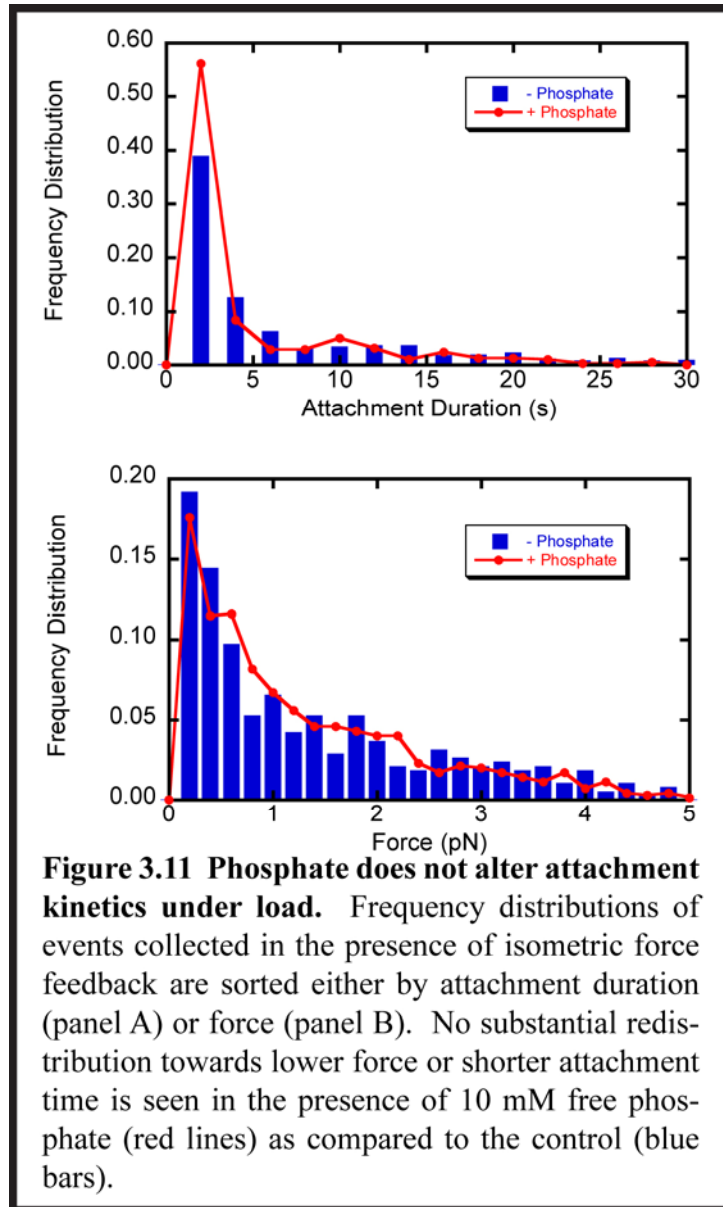
Given that the predominant force-sensitive state is likely AM·ADP, we sought to test if reassociation with phosphate could occur and drive the myosin into a weakly bound AM·ADP·Pi state as has been shown for myosin II (Hibberd et al. 1985). By repeating our force dependence measurements for myo1b in the presence of a large excess of free phosphate, we can examine the effect of phosphate on the lifetime of interactions as a function of force. Specifically, if phosphate could reassociate with myo1b in the AM·ADP state, we would expect to see a decrease in the force sensitivity of myo1b.



Single molecule interactions between myo1b and actin in the three-bead assay were observed under the same conditions as described in 3.1, with the exception of 10 mM free phosphate added to the final motility buffer. A summary of the force dependence of the lifetimes of attachment is shown in figure 3.10. The data were fit to the model in equation 10, and the associated errors for the



parameters were determined by the 97% confidence limits of 200 bootstrap Monte Carlo simulations of the data. From the fit, k_i was determined to be 0.022 s^{-1} ($+0.009/-0.012 \text{ s}^{-1}$) and k_{g0} was determined to be 2.7 s^{-1} ($+1.1/-2.3 \text{ s}^{-1}$). The force sensitivity, estimated by d_{det} , was 10 nm ($+2.1/-2.6 \text{ nm}$). The parameters are not significantly different from data collected in the absence of excess free phosphate (compare with figure 3.6). We then tested the force and attachment duration distributions to determine if phosphate could increase the fraction of short, low



force events. The data shown in figure 3.11 do not show any large redistribution of events, either in force or duration, with the addition of phosphate. These data together suggest that myo1b is still able to function as a high duty ratio motor, when subjected to a resisting load against the power stroke, at the free phosphate concentrations that exist inside a cell.

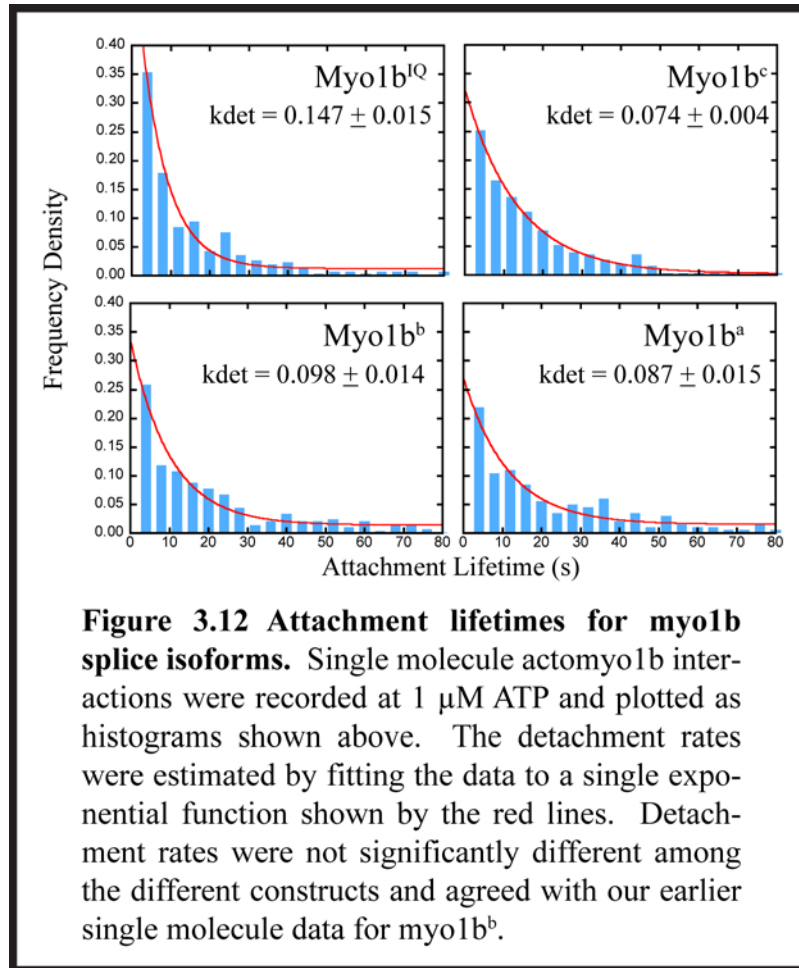
3.2 Force sensitivity can be tuned by alternative splicing of the myo1b LCBD

The following experiments will test the contribution of the LCBD to the force sensitivity of myo1b. The LCBD, or lever arm of myo1b is naturally alternatively spliced to generate constructs with 4, 5, or 6 IQ motifs. The experiments described in 3.1 of this thesis dealt entirely with the 5 IQ motif splice isoforms, myo1b^b, generating an incomplete picture of the remarkable tension sensitivity of this protein. In the following experiments, we repeat our measurements of the step and substep sizes of the various natural splice isoforms, as well as a non-native construct with a single IQ motif. We also test the force sensitivity of myo1b as it relates to the mechanical parameters of the LCBD/lever arm. In all following results, we have improved the accuracy and resolution of our single molecule measurements by incorporating a stage feedback loop, which corrects for experimental error due to mechanical fluctuations of the stage (see methods and discussion). These results test the hypothesis that the myo1b force sensitivity, demonstrated in 3.1, could be tuned by alternative splicing as a possible mechanism for a cell to modify its tension sensing machinery.

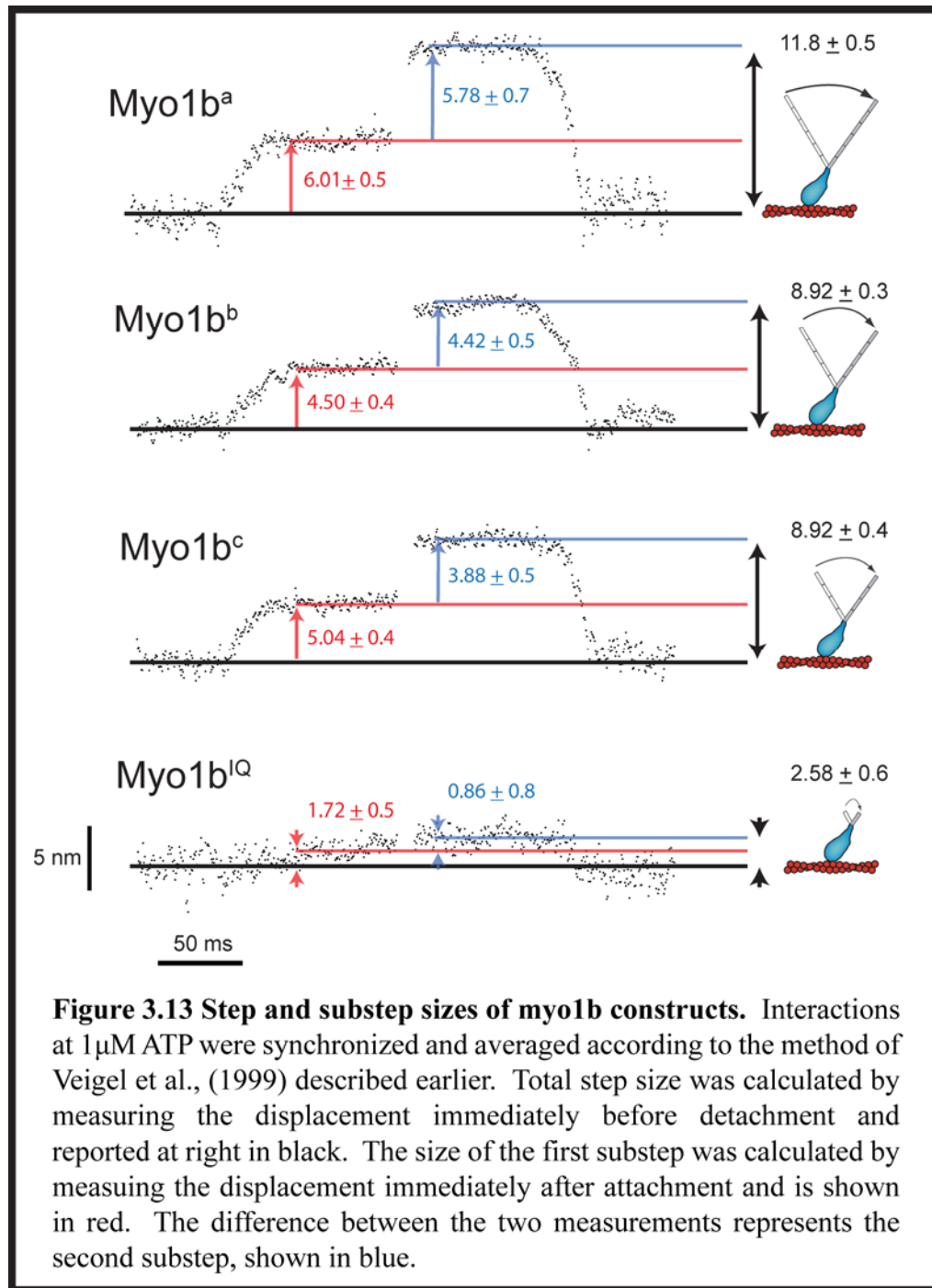
3.2.1 Step and substep sizes of myo1b splice isoforms.

In order to examine the effect of alternative splicing along the light chain binding domain (LCBD) on myo1b mechanochemistry, we examined the forces and displacements produced by single myo1b constructs containing the head and LCBD of myo1b at low load under the same experimental conditions as in 3.1. Single actomyosin interactions were recorded at 1 μ M ATP for the three naturally occurring myo1b splice isoforms (myo1b^{a-c}) as well as a non-native myo1b construct containing a single IQ motif (myo1b^{IQ}). To obtain a rough comparison of the detachment rates for the various splice isoforms, we fit the histograms of attachment lifetimes to a single exponential function. The lifetimes of the interactions of all constructs were consistent with each other, and consistent with predicted rates of detachment at 1 μ M ATP (Lewis et al. 2006)(figure 3.12).

To examine the magnitude of the total power stroke of the myo1b constructs, as well as the substeps, single actomyosin attachment events were selected by covariance thresholding and synchronized according to the method of Veigel et al. (1999) to generate the ensemble start and end averages shown in figure 3.13. Forces in pN were converted to distances in nm by dividing by the known trap stiffness for each experiment. Confirming our previous measurement of the myo1b^b construct with 5 IQ motifs, we observed that the total working stroke of myo1b occurs in two substeps for all constructs. An initial step, likely corresponding to Pi-release, occurs within the resolution of the instrumental setup and accounts for a larger proportion of the total working stroke. A second, smaller step, believed to correspond to ADP-

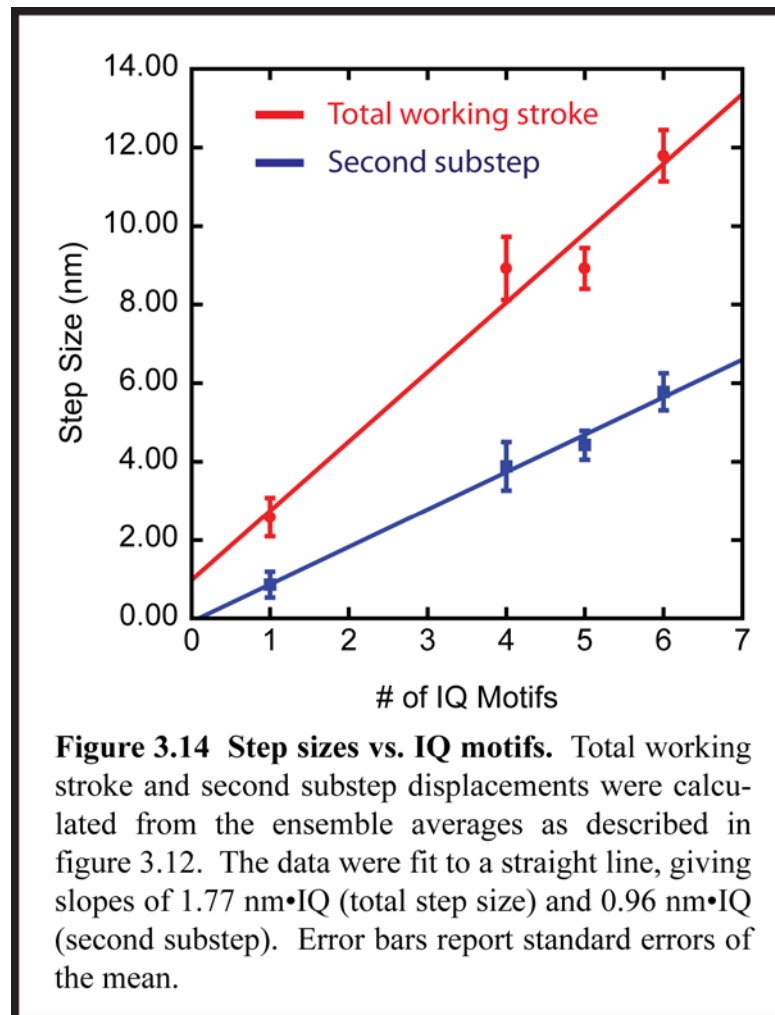


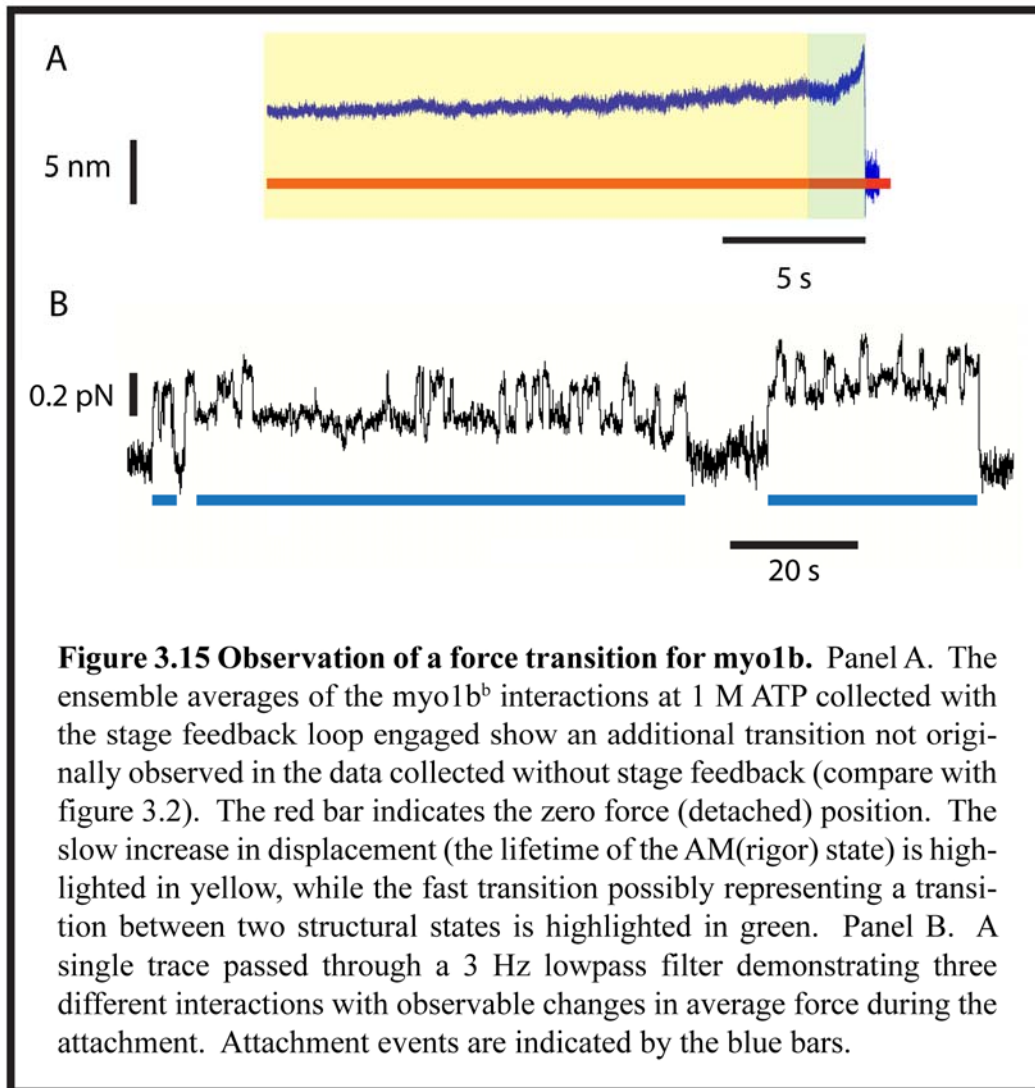
release, follows the first as shown by the difference in start and end-time averages for each construct. The total step sizes for each construct are shown in black, calculated by averaging 100 data points in the plateau of the end time ensemble averages prior to detachment. The size of the first substep, shown in red, was generated by averaging 100 data points in the plateau immediately after attachment. The second substep, in blue, is the difference in size between the displacement of the total working stroke and first substep. Error bars are standard deviation of the distributions of the 100 points used to generate step sizes. A plot of step size vs. the number of IQ motifs was generated and fit to a straight line in shown in figure 3.14.



The relationship between step size and number of IQ motifs in the LCBD suggests that the total working stroke and substep sizes are a result of amplifications of small changes in the converter region of the motor domain via the LCBD. Interestingly, a

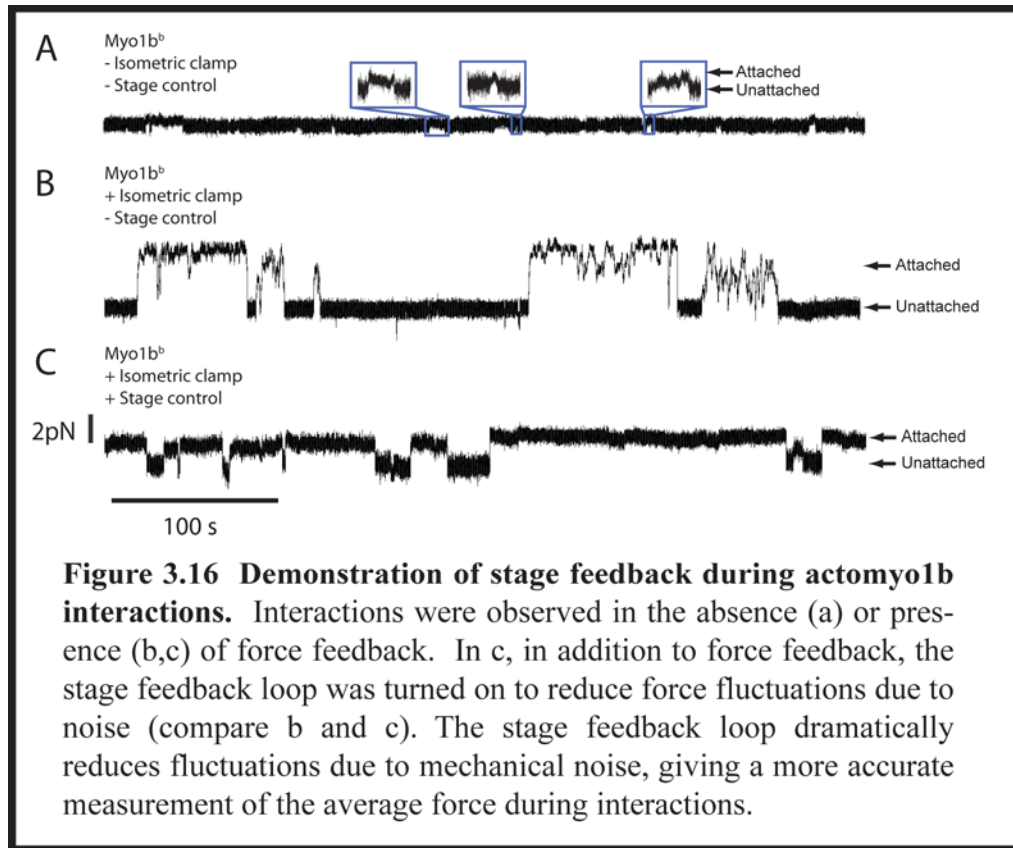
fast transition is observed in the presence of stage feedback in the ensemble averages over expanded timescales (figure 3.15 A). A filtered sample trace (figure 3.15 B) shows that the interactions show a rapid transition between two force states. If the myosin detaches mostly from the higher force state, this force “flicker” could account for the fast transition seen in the ensemble averages of the data in the presence of stage feedback.



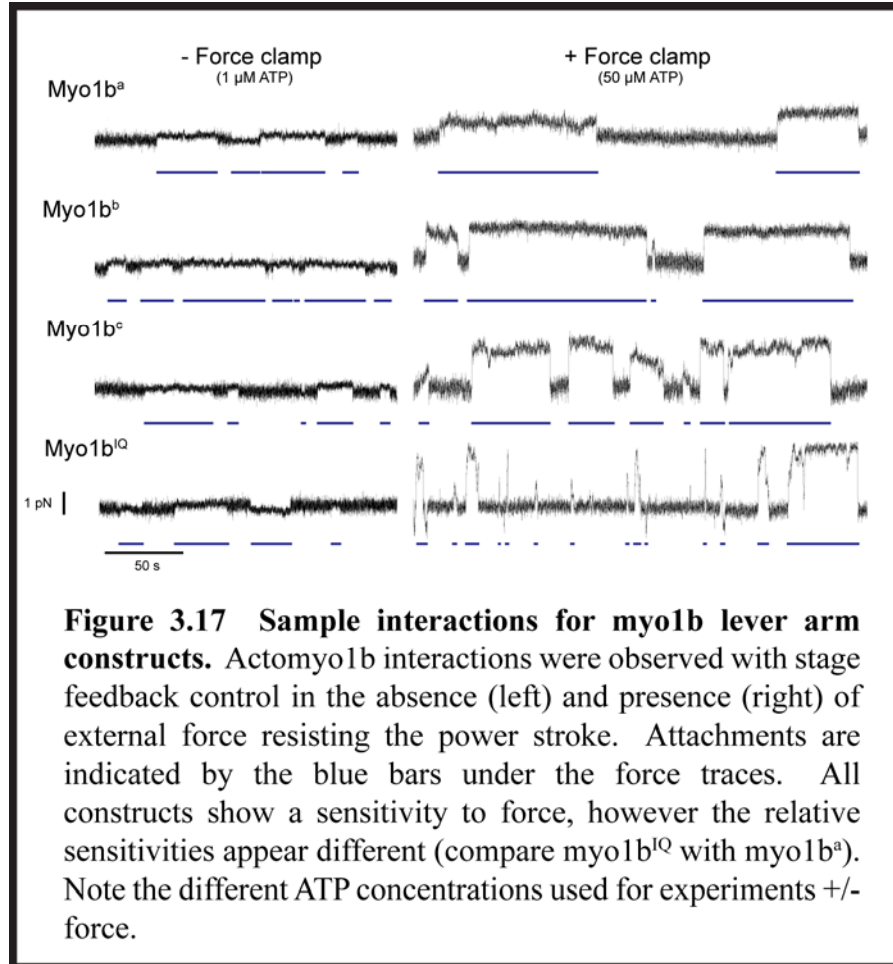


3.2.3 Force sensitivity of myo1b splice isoforms

In the following experiments, we measured the response to force of the attachment kinetics of myo1b constructs with varying #IQ motifs along the LCBD. Excess calmodulin was included in all solutions to ensure complete occupancy of all IQ motifs.



The force dependence of actomyo1b^(IQ,a,b,c) attachment lifetime was measured as described in 3.1 in the presence of 50 μ M ATP with both the isometric force clamp and the stage control feedback loop engaged. The stage feedback gave an improved measurement of the average force during an actomyo1b interaction (figure 3.16). The resisting force, however, was capped at a specific voltage level using a digital limiter corresponding to ~ 2.5 pN of total force to limit the proportion of extremely long-lived events. Precise control of stage x-axis position through rapid feedback limits fluctuations in force due to mechanical vibration or other noise sources, ensuring an accurate and consistent measurement of the average force on the actomyo1b crossbridge. A series of



sample interactions at comparable forces resisting the power stroke for each myo1b construct are shown in figure 3.17.

Scatter plots of attachment lifetime vs. force for each construct are shown in the inset panels of figure 3.18. Confirming our previous result for 5 IQ motif splice isoforms (myo1b^b), the attachment kinetics are highly force dependent, with load on the myosin increasing the attachment lifetime until a plateau is reached, at which point the detachment rate is force-independent. The force at which the plateau is reached varies according to the number of IQ motifs in the construct, indicating that

the force dependence of the constructs is modulated by the number of IQ motifs along the LCBD.

We globally fit our data for all myo1b constructs to the same model described in equation 3.10 that includes the same force-dependent detachment rate (k_g) and force-independent detachment rate (k_i) as alternative pathways for detachment. Using Maximum Likelihood Estimations (MLEs) of 10000 bootstrap monte carlo simulations of our data, we generated the associated errors reported as 97% confidence intervals. The values for the kinetic parameters k_i and k_{g0} are reported in table 3.1, along with the distance parameters for the myo1b constructs as well as the error values from the MLEs.

Kinetic Parameters	Best Fit Value	Min Error	Max Error
k_{g0}	0.544 s ⁻¹	0.144 s ⁻¹	0.19 s ⁻¹
k_i	0.01 s ⁻¹	0.002 s ⁻¹	0.002 s ⁻¹
Distance Parameter	Best Fit Value	Min Error	Max Error
Myo1b ^a (n = 219)	18.41 nm	3.92 nm	4.93 nm
Myo1b ^b (n = 327)	14.85 nm	3.45 nm	4.56 nm
Myo1b ^c (n = 179)	10.23 nm	2.28 nm	2.20 nm
Myo1b ^{IQ} n = (219)	3.72 nm	0.74 nm	0.94 nm

Table 3.1 Kinetic parameters and force sensitivity of myo1b constructs. Best fit parameters were according to the model in equation 10. Errors were calculated as 97% confidence limits generated by Maximum Likelihood Estimations of 10000 bootstrap Monte Carlo simulations of the data in figure 3.18 (insets).

The force response of myo1b, as described by d_{det} , is sensitive to the number of IQ motifs along the LCBD. Fits of the detachment rate of myo1b constructs to the model above are shown by the red lines in figure 3.18. The myo1b constructs demonstrate a range of force sensitivities which are best described in a plot of d_{det} vs second step (figure 3.19). The force sensitivity of myo1b (d_{det}) shows a roughly linear relationship with the second step size, suggesting that the force sensitivity can be modulated by alternative splicing along the LCBD.

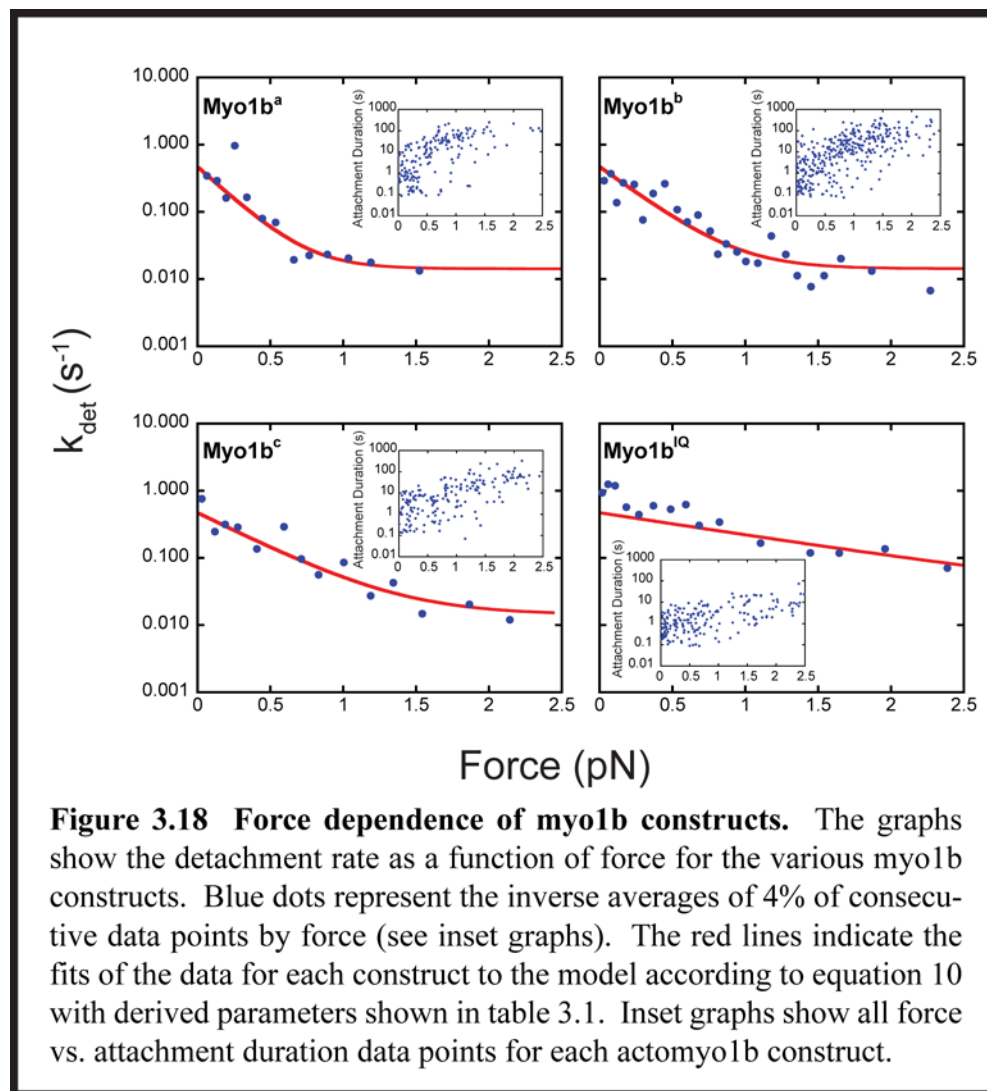
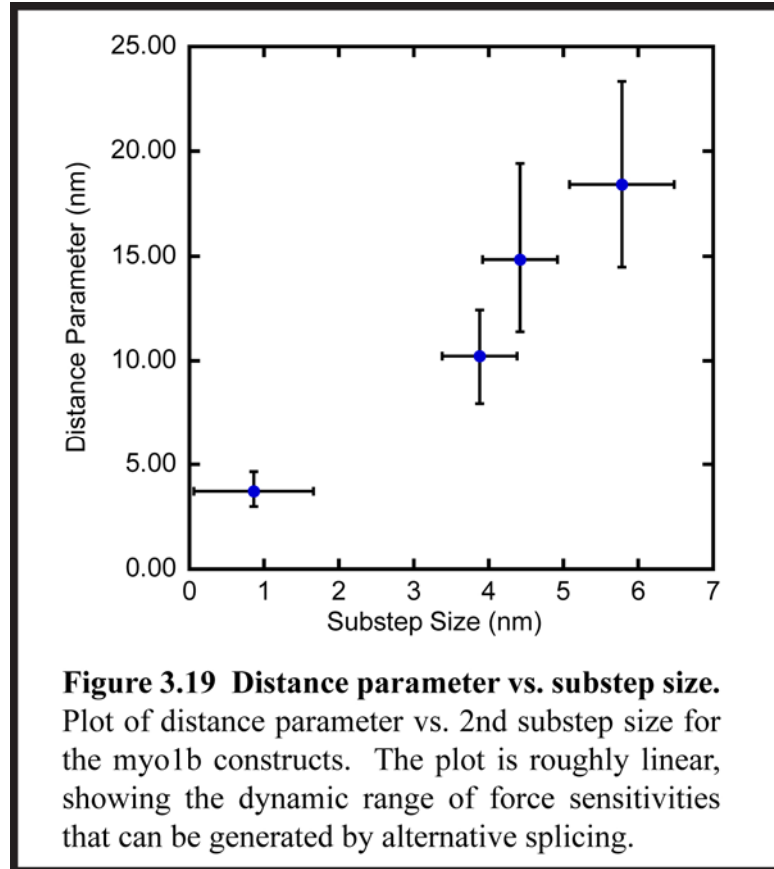


Figure 3.18 Force dependence of myo1b constructs. The graphs show the detachment rate as a function of force for the various myo1b constructs. Blue dots represent the inverse averages of 4% of consecutive data points by force (see inset graphs). The red lines indicate the fits of the data for each construct to the model according to equation 10 with derived parameters shown in table 3.1. Inset graphs show all force vs. attachment duration data points for each actomyo1b construct.



3.3 Calcium regulation of myo1b mechanochemistry

If myo1b were behaving as a tension sensor in vivo, there could exist regulatory mechanisms to allow myo1b to switch from a high duty ratio to a low duty ratio, such that clusters of myo1b on an actin filament would transition from a static structure to active motility. As shown in the previous section, all of the naturally occurring splice isoforms are sufficiently sensitive to load that they can stall themselves simply through the force generated by their own power stroke. In

the following section, we tested a potential mechanism through which the force resisting the motion of the lever arm could be uncoupled from the force dependent steps in the myo1b biochemical cycle.

3.3.1 Free calcium reduces myo1b step size

Free calcium is predicted to directly influence calmodulin binding to the LCBD of myosins containing IQ motifs. More specifically, the binding of calcium to the lobes of calmodulin induces a conformational change that weakens the affinity of calmodulin for the IQ motif (Manceva et al. 2007, Lin, Tang & Ostap 2005). If calmodulin serves to reduce the compliance of the myo1b LCBD, then calcium could have an effect on the step size of the myosin in single molecule measurements by decreasing the stiffness of the myo1b LCBD. The decrease in stiffness would prevent the LCBD from serving as a suitable lever arm to amplify conformational changes in the motor domain.

We recorded displacements produced by actin-myo1b^a interactions in the presence of 0, 1, and 9 μM free calcium and plotted the step sizes as histograms in figure 3.20. An intermediate effect is observed at 1 μM free calcium, where the average step size is 2.96 nm compared to 11.8 nm for myo1b^a in the absence of calcium. At 9 μM free calcium, the myo1b^a average step size is close to zero (0.62 nm), with the entire lever arm essentially uncoupled from any motion in the motor domain. Based on these results, we can conclude that calcium results in a motor that is not suitable for generating motion along the axis of the actin filament.

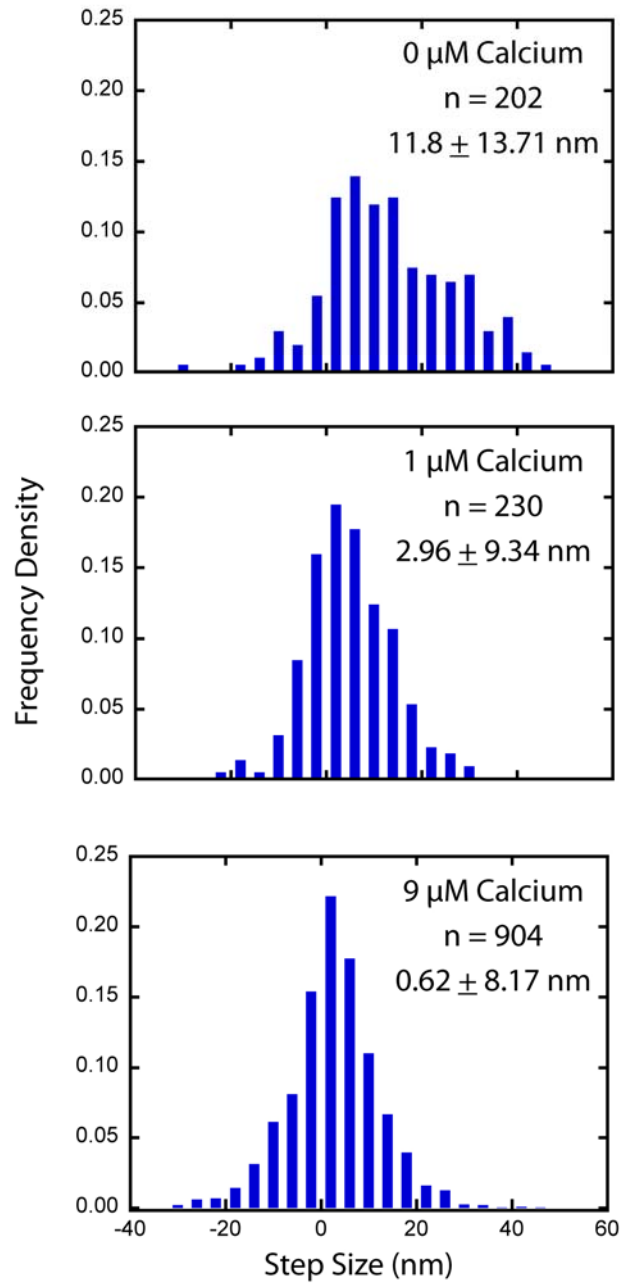


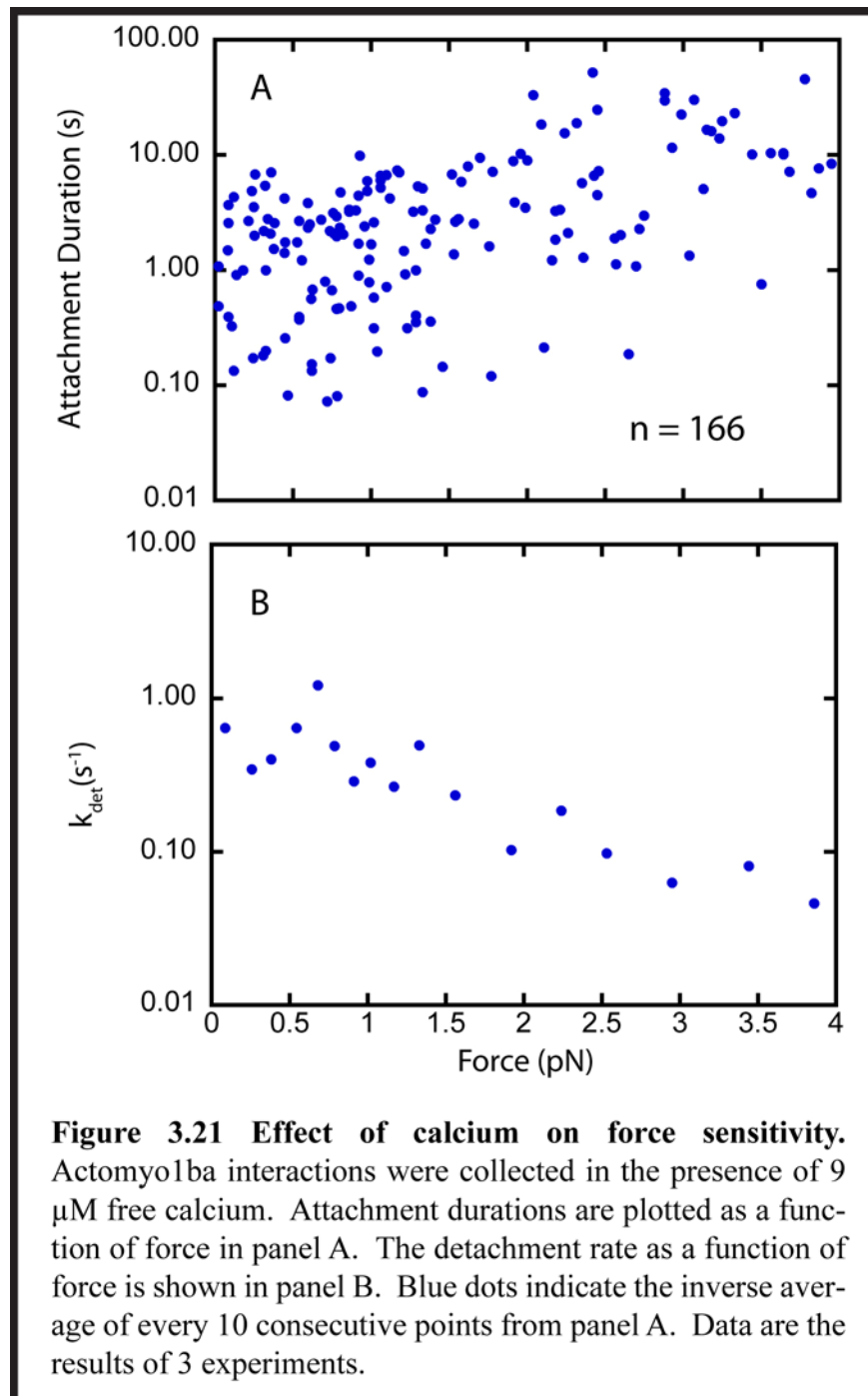
Figure 3.20 Effect of calcium on myo1b step size. Frequency density histograms of myo1b^a step size in the presence of indicated amounts of free calcium are shown. Histogram bin width is 4nm. The average step size is shown, with the associated error values representing the standard deviation of the distribution.

3.3.2 Effect of calcium on myo1b force sensitivity

The reduction in step size of myo1b^a may result in an effect on the tension sensitivity of myo1b as measured in our single molecule assays. An increase in compliance of the lever arm could reduce the ability of the LCBD to transduce force to the motor domain, allowing free rotation of the converter domain and release of ADP. Additionally, calcium is known to have effects on the kinetic parameters of myo1c, particularly increasing the rate of ADP release (Adamek, Coluccio & Geeves 2008). Therefore, through both increasing the compliance of the lever arm and altering kinetic parameters of the myo1b ATPase, calcium could serve to decouple the force imposed on the lever arm from mechanochemistry of the motor domain, thus acting as a chemical switch to turn myo1b from an extremely force-sensitive motor to a force-insensitive motor.

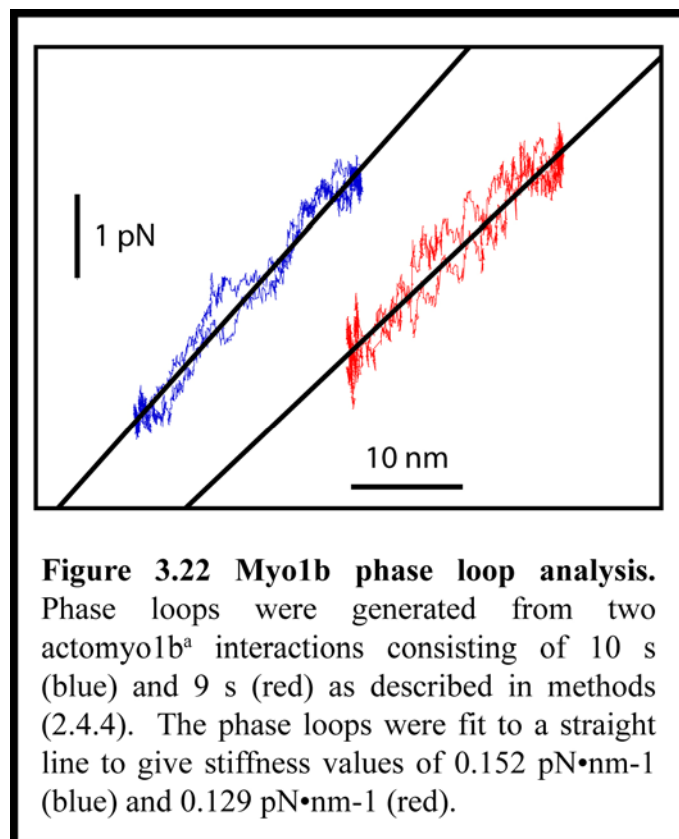
We tested the effect of free calcium on the force sensitivity of myo1b^a by repeating our single molecule measurements using the isometric force clamp in the presence of 9 μM free calcium. Forces and attachment lifetimes are plotted in figure 3.21. Although we were able to show a range of forces in the presence of calcium over which myo1b would be expected to be highly force sensitive, there was minimal change in the attachment lifetime as a function of force (compare with 3.18). Myo1b^a, in the presence of 9 μM free calcium, is as force sensitive as myo1b^{1Q}, suggesting that the lever arm is nearly completely uncoupled from the movements in the motor. This result strongly suggests that an intracellular calcium

signaling event could cause the myosin to rapidly detach from the actin filament and undergo repeated ATPase cycles without generating force and tension.



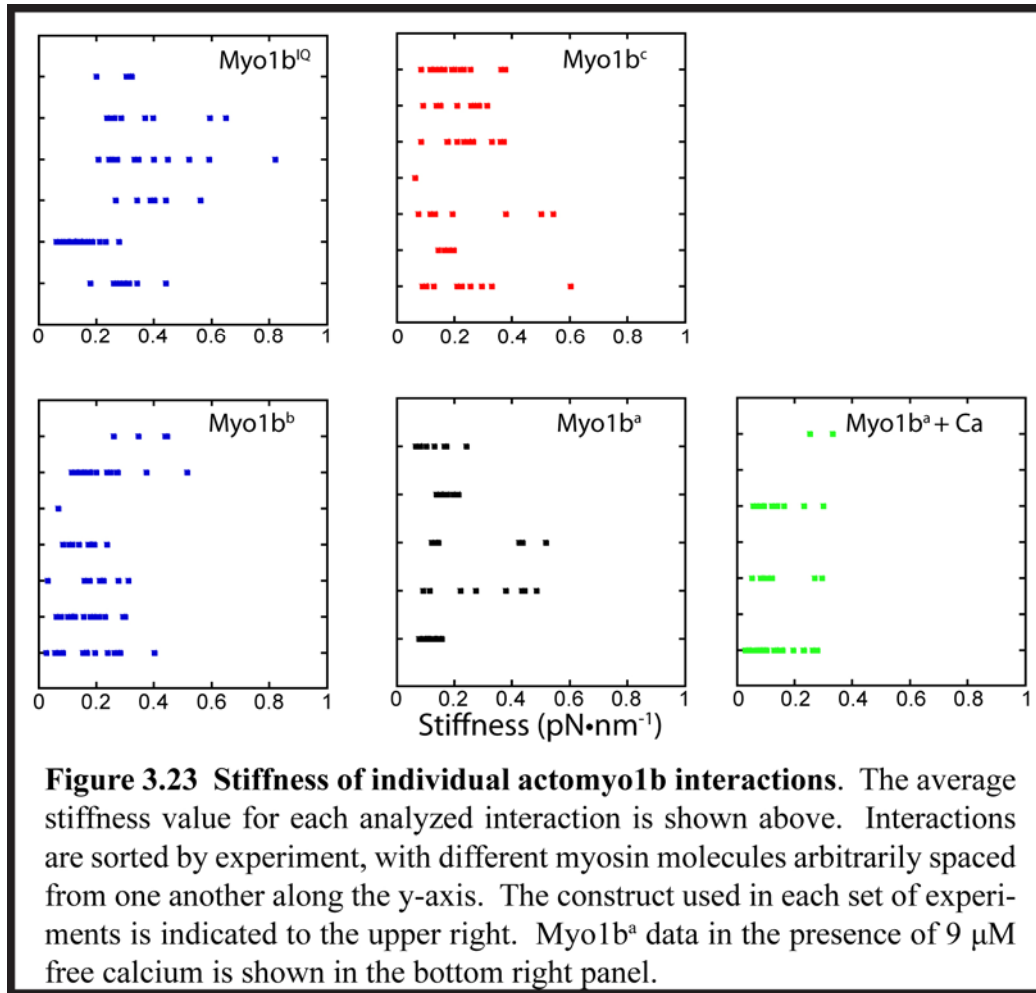
3.4 Stiffness of myo1b constructs

Our myo1b constructs allow us the unique opportunity to test a fundamental mechanical property of the LCBD of a myosin. By directly measuring the stiffness of the actomyo1b crossbridge as a function of the number of IQ motifs for myo1b, we can test the hypothesis that the myo1b LCBD serves as a rigid lever arm or an elastic cantilever, and if there are any high-compliance elements within that lever arm or within the motor domain (Warshaw et al. 2000b, Uyeda, Abramson & Spudich 1996b).



3.4.1 The stiffness of the actomyo1b crossbridge is linearly related to the lever arm length.

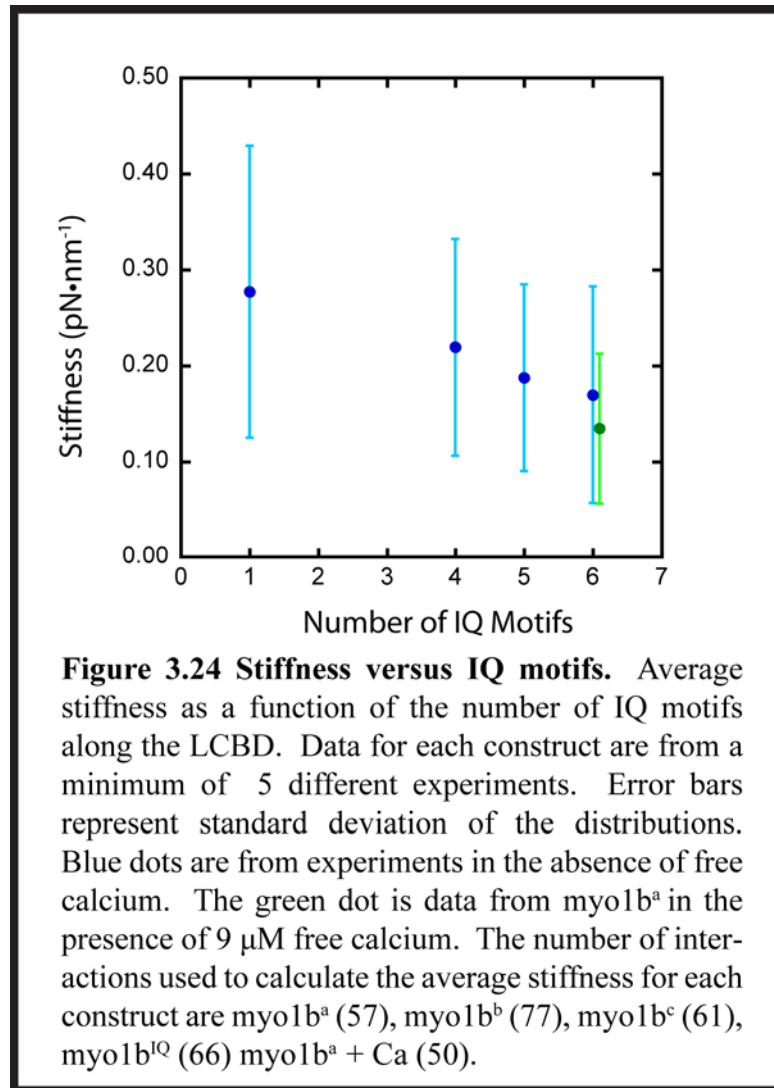
By making a slight modification to our single molecule experiments in the presence of both the isometric force clamp and stage feedback, we can oscillate the stage during our experiments by known amounts and simultaneously record the force during stretching of a single myo1b molecule attached to an actin filament. We therefore tested the stiffness of the myo1b lever arm as a function of the number of IQ motifs by recording the force and displacement during our single molecule experiments while oscillating the stage at a frequency of 1 Hz. The force and displacement data were averaged as described in Methods (2.4.4) to generate phase loops like the examples shown in figure 3.22. Phase loops were fit to a straight line to give the average stiffness over the entire interaction in $\text{pN}\cdot\text{nm}^{-1}$. The stiffness for each interaction was calculated and plotted in figure 3.23. The average stiffness values were then calculated for each construct and plotted in figure 3.24. As shown, the stiffness is roughly linear with the number of IQ motifs along the lever arm, with the shorter lever arms having a higher average stiffness. The error in our measurement, however, is relatively high and it is possible that there is no real difference in stiffness between the different isoforms.



3.4.2 The average stiffness of myo1b in the presence of calcium.

To test if calcium binding to calmodulin causes an increase in the compliance of the myo1b lever arm, phase loop analysis was used to measure the average stiffness over the course of actomyo1b^a interactions in the presence of 9 μM free calcium. Stiffness values are plotted in figures 3.23 and 3.24. Surprisingly, even at calcium concentrations which reduce the step size of myo1ba to nearly zero, the average crossbridge stiffness was not significantly different at 0.134 pN·nm⁻¹. From this data we conclude that the uncoupling of the myo1b lever arm from force

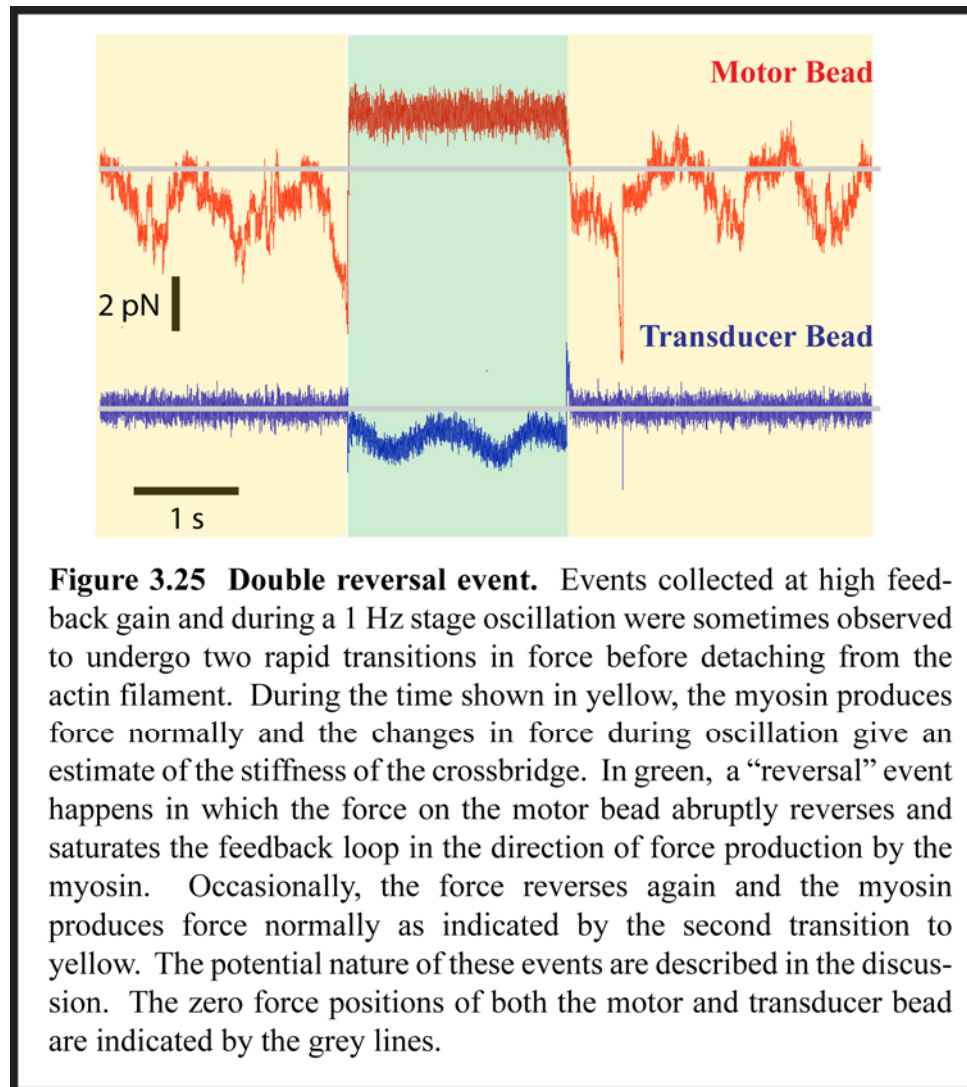
generation and force sensitivity is not due to a large compliance change along the LCBD of the myosin.



3.4.3 Double reversal events during forced oscillations.

Occasionally, an interesting phenomenon is observed where the myosin undergoes a reversal (see figure 2.8 in methods) while the stage is oscillating, however unlike the events observed at high feedback gain in the absence of stage

oscillation, the myosin remains attached to the actin filament and “re-reverses” to undergo normal force production (figure 3.25). Although these events are rare (estimated to be < 1% of total events), they may deserve special consideration given the movement of the stage and stretching of the lever arm in both directions.



4. Discussion

4.1 Summary of results

The broad goal of this thesis is to use biophysical tools to study the effects of force on motor protein function at the single molecule level. Using a dual-trap optical trapping system, we were able to measure the size of the two-step working stroke of myo1b and assign specific biochemical states to each step. We then measured the force sensitivity of myo1b using a feedback-enhanced isometric force clamp, and found it to be an extremely force sensitive motor. By repeating these types of experiments both for a variety of myo1b constructs and different chemical perturbations, we were able to draw broader conclusions about potential myo1b function and regulatory properties. Furthermore, we demonstrated the use of a stage position clamp, and how that stage control could improve resolution of our step and substep sizes. Finally, we used the stage control feedback loop to apply an oscillation to the stage during actomyo1b interactions to measure the stiffness of the actomyo1b crossbridge.

In the final chapter of this thesis, I discuss how our progress in achieving the goals outlined in the specific aims relate to the possible molecular functions of myo1b inside a cell. Attention is paid to regulatory properties of myo1b through tension sensitivity, and higher-level regulation of that sensitivity by various means.

Also, I explain our new understanding of the interesting properties of myo1b in the context of the myosin superfamily as a whole and how this particular protein may be specifically tuned to perform a role as a molecular tension sensor.

4.2 Data collected at low resisting loads

4.2.1 Validation of single molecule data

A primary concern for any experiment that involves making measurements at the single molecule level for motor proteins, is ensuring that analyzed interactions are the result of one protein instead of multiple molecules. Appropriate care was taken in all experiments to control the concentrations of myo1b and actin in solution, such that multiple filaments were not bound to the trapped beads at the same time. Validation of the single molecule nature of our interactions was accomplished in the following ways.

The covariance selection criteria outlined in materials and methods in this thesis requires that there are two peaks in the covariance histogram for each recorded experiment, corresponding to the attached and detached states. Multiple myosins, or nonspecific interactions between the coverslip surface and the actin filament would be expected to increase system stiffness and further decrease the covariance of the bead motion, resulting in multiple peaks in the covariance histogram. Therefore, all experiments showing greater than two covariance peaks

were not included in our analysis. Additionally, kinetic rates derived from our measurements at low load would be expected to agree with solution kinetics experiments, which are essentially unloaded. From the start and end time ensemble averages of single actomyo1b interactions at varying ATP concentration, we measured rates of ADP release and ATP binding respectively, which are in line with solution kinetics measurements (Coluccio, Geeves 1999, Lewis et al. 2006). This kinetic evidence, combined with covariance records, provide strong evidence that our conclusions are the result of interactions between single actin filaments and single myo1b molecules.

4.2.2 The myo1b working stroke is composed of two substeps

Biochemical, structural, and kinetic evidence suggest that the myosin-I working stroke is composed of two substeps (Jontes, Wilson-Kubalek & Milligan 1995, Veigel et al. 1999, Nyitrai, Geeves 2004, Geeves, Perreault-Micale & Coluccio 2000, Veigel et al. 2002, Oguchi et al. 2008). We therefore first set out to confirm the two-step working stroke for myo1b originally demonstrated by Veigel et al. (1999). Two-step interactions can be discerned by eye in the single molecule force records highlighted in figure 3.1, and ensemble averaging of synchronized events shows two increases in displacement as expected for a two-step working stroke. Increased stage control via the stage feedback loop allows a detailed inspection of the various substep sizes of the myo1b constructs, including the small steps of the single IQ construct. With the exception of the non-native single IQ

construct, the second substep accounts for up to 50% of the total displacement generated by the myo1b working stroke. This is similar to measurements made for other myosin isoforms (Veigel et al. 2002, Veigel et al. 2003), as well as earlier studies of myo1b (Veigel et al. 1999).

The total step sizes are roughly linear with increasing number of IQ motifs, as expected given the fact that the LCBD is proposed to serve as a rigid lever arm, (Sakamoto et al. 2003), and the size of the second step is more clearly linear with the number of IQ motifs along the LCBD. This shows that whatever conformational changes in the motor domain occur, they are faithfully translated by the LCBD to amplify those changes and produce larger displacements. Therefore the LCBD behaves as a rigid lever arm regardless of alternative splicing, and the effect on second step size would be predicted to have a proportional effect on the force sensitivity of myo1b if it serves as the predominant thermodynamic barrier to ADP release. If this second substep corresponds to the 32° rotation of the lever arm seen in cryo-EM reconstructions in the presence and absence of ADP (Jontes, Wilson-Kubalek & Milligan 1995, Whittaker et al. 1995), we calculate the effective lever arm length of myo1b^b to be $6.0 + 0.63$ nm. If the lever arm were rigid, a similar number of IQ motifs would be predicted to have a 20 nm lever arm length (Warshaw et al. 2000a). At present, we do not have an explanation for the inconsistency of our measurement with the displacement predicted by rotation shown in the cryo-EM studies. It is possible that our measurements are an underestimate due to compliance between the bead and actin filaments, although we

do not consider this to be a significant source of error as the bead-actin connection stiffness is estimated to be an order of magnitude greater than the myosin stiffness. Alternatively, the 32° rotation may not indicate the actual structural states of a myo1b molecule undergoing force production. Another possibility is that the LCBD of myo1b may not fold into a fully extended, linear alpha-helix.

4.3 Myosin-Ib is a high duty-ratio motor under load

The first specific aim of this thesis was to characterize the response of myo1b to an external load resisting the motion of the power stroke. Using the three-bead assay geometry, we examined the lifetimes of actomyo1b attachment as a function of force and discovered that myo1b is an extraordinarily strain sensitive motor at small forces. Furthermore, we biochemically characterized the structural states responsible for the substeps visualized via ensemble averaging and determined that the sensitivity of ATP binding to force could not account for the tension sensitivity of myo1b. Based on this work, we show that myo1b can potentially function as a tension sensor *in vivo*.

4.3.1 Myosin-Ib is extremely sensitive to low physiological forces

The force dependence of myo1b is easily recognizable in the raw data traces (figure 3.5) and the plot of attachment duration versus average interaction force (figure 3.6). The average attachment lifetimes of actomyo1b interactions at

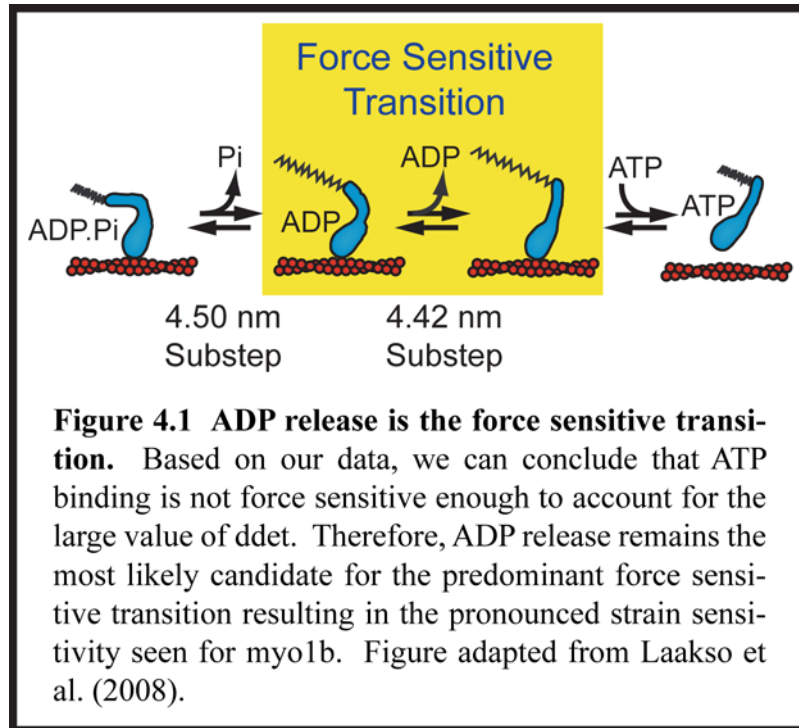
saturating ATP concentration transition from less than one second to > 50 seconds at forces greater than 1.5 pN. The effect is most clearly illustrated in a plot of k_{det} vs. force (figure 3.7), where it can be seen that k_{det} decreases > 75 fold with ~ 1.5 pN of resisting force. At the low forces experienced by myo1b in the absence of the isometric clamp, a 1.5 fold decrease in k_{det} is predicted over the unloaded rate (k_{g0}) due to the force imposed on the myosin molecule strictly from the stiffness of the optical trap. This reduction is consistent with the values of k_{start} measured from the start time averages (figure 3.2). As myo1b experiences higher resisting forces the lifetime of attachment to the actin filament increases until reaching a plateau with a rate of detachment of 0.021 s^{-1} . Consequently, myo1b transitions from a low duty motor to a high duty ratio motor at increasing forces resisting the power stroke in the presence of high local actin concentration.

An estimate of relative tension sensitivity is given by the distance parameter, d_{det} , which is ~ 14 nm for myo1b^b. This distance parameter is larger than that measured for nearly any other myosin to date, including molecular motors whose tension-sensitivity is necessary for processive movement along the actin filament (Veigel et al. 2005), highlighting the potential importance of tension-sensing in myo1b function. Strikingly, myo1b is highly force dependent over relatively weak forces (< 2 pN) in contrast to other strongly strain-sensitive proteins such as myosin-VI, which is extremely force sensitive at this range only at higher ADP concentrations (Altman, Sweeney & Spudich 2004). It is possible, based on these results, for a single myo1b to produce enough force to stall itself if it were coupled

to a sufficiently rigid element that resisted the motion of the power stroke. A small cluster of myo1b molecules would be expected to be essentially irreversibly attached to the actin filament and immobile under the same conditions. This phenomenon would be similar to the proposed load-induced anchoring model for myosin VI (Altman, Sweeney & Spudich 2004).

4.3.2 ADP release is the force sensitive transition

While the measured end-time averages for myo1b detachment as a function of force show some sensitivity to force as measured in our experiments (figure 3.8), d_{end} is not nearly large enough to correspond to the predominant force sensitive transition responsible for the ~ 14 nm value for d_{det} . Since the end-time averages show the rate of ATP binding, we conclude that ADP release corresponds to the predominant force-sensitive transition for myo1b, according to the model in figure 4.1. This conclusion agrees with other investigations of myosin at the single molecule level that identified



ADP release as a strain sensing transition (Veigel et al. 2002, Veigel et al. 2005, Veigel et al. 2003), however it remains possible that other biochemical steps such as phosphate release are strain dependent to different degrees for different myosins (Takagi et al. 2006a). Our own data shows some strain dependence for ATP binding (figure 3.8), even if it is relatively modest in comparison with ADP release for myo1b. Our time resolution at the feedback gain settings used in the experiments described in the results section of this thesis does not at the moment permit us to observe myo1b in the ADP·Pi state due to the increased amount of reversal events (see methods and figure 2.8), even though phosphate release is rate limiting under solution kinetics conditions for myo1b at 0.58 s^{-1} at 37°C . Strain dependence in myosins, therefore, could represent a tunable property that differs

among members of the myosin superfamily to optimize their diverse molecular functions inside a cell. This property is demonstrated in muscle as the Fenn effect, which may be the result of multiple strain dependent states (Takagi et al. 2006a).

4.3.3 The force sensitive state is not reversible by excess phosphate

Sleep and Hutton proposed in 1980 that there were two AM·ADP states, one of which could rebind phosphate in solution (Sleep, Hutton 1980). In the general myosin kinetic scheme (figure 1.10), AM·ADP·Pi is a weakly bound state, predominantly detached from the actin filament during the biochemical cycle. Since the AM·ADP state is the likely long lived force sensitive state observed in our isometric force clamp experiments, it is possible that phosphate could reassociate with an AM·ADP state that is energetically different from the strongly bound state observed in solution kinetics studies. This reassociation may represent a Pi-exchangeable state observed by Sleep and Hutton. In the case of myosin-II, reversal of the power stroke to a weakly-bound state was observed upon photoactivation of caged phosphate in glycerinated muscle fibers (Dantzig et al. 1992). We therefore repeated our isometric force clamp measurements in the presence of 10 mM free phosphate in an attempt to induce a weakly bound AM·ADP·Pi state.

In the presence of 10 mM free phosphate, we do not observe a redistribution of forces or attachment durations when compared with low phosphate conditions (figure 3.11). This suggests that the application of force favors an AM·ADP state that is unable to rebind phosphate and induce a weakly-bound conformation. Based

on our preliminary filtered data showing the transition between two states directly (figure 3.15), it is possible that force causes myo1b to transition to a conformation that is unable to release ADP and is also inaccessible to free phosphate. It should be noted that our results do not distinguish between the inability to rebind phosphate versus the generation of a strongly bound AM·ADP·Pi pre-powerstroke state, the existence of which has been proposed based on spectroscopic studies of myosin-II (Sun et al. 2008). As our results in figure (3.10) show, the kinetics of the actomyo1b attachment as a function of force, as estimated by the distance parameter, is not significantly different between the experiments in the presence or absence of 10 mM free phosphate. Therefore, phosphate rebinding does not appear to be a likely candidate for modification of myo1b attachment duration under load.

4.3.4 Alternative splicing tunes the force sensitivity of myo1b

The effect of alternative splicing along the LCBD is clearly illustrated in the data generated from measuring the attachment lifetime of myo1b to actin as a function of force. Based on the global fit of our data to the model described in equation 10, we can derive the kinetic parameters shown in table 3.1. Values for k_{g0} and d_{det} agree with our earlier measurements for myo1b^b (Laakso et al. 2008), however the global fit arrives at a twofold smaller value for k_i than was reported in our measurement without stage feedback (0.01 s^{-1} versus 0.02 s^{-1}). This is perhaps expected when one considers the reduction in force fluctuations due to precise control of stage position with the stage feedback loop (figure 3.16). The ensemble

averages of our data collected with force feedback but without stage feedback all show transient decreases in force immediately prior to detachment (figure 3.9), which may represent force fluctuations due to noise in our measurement. If mechanical noise causes the myosin to transiently experience a lower resisting force, it may be able to rotate the lever arm and release ADP before the feedback loop responds. We therefore believe that the measurement made in the presence of stage feedback represents the more accurate description of k_i

The distance parameters generated from the global fit to the data show force sensitivity, yet the degree to which each construct is force sensitive appears to depend on the number of IQ motifs in a linear fashion (figure 3.19 and table 3.1). The immediate conclusion from this data is that alternative splicing of *myo1b* generates proteins with varying tension sensitivities at extremely low ($< 2\text{pN}$) forces. The native constructs, consistent with our previous measurement of the 5-IQ motif construct, are all extremely tension-sensitive relative to other motor proteins and confirm that tension sensing is potentially an important functional property of *myo1b*. Apart from functionality, the different constructs offer a way to probe the mechanical nature of the distance parameter as a measurement of force sensitivity. A plot of distance parameter vs. 2nd step size is shown in figure 3.19, illustrating the linear relationship between the size of the second substep and the force sensitivity of the construct. However the linear nature of the distance parameter as a function of second step size is likely due to the linear nature of the second substep as a function of IQ motifs, given that with a longer lever arm, the force produced by

conformational changes in the motor domain combined with the thermodynamic energy of the environment, must overcome more distance with a longer lever arm before reaching the force sensitive transition state. Since we consider in our earlier work (Laakso et al. 2008) that ADP release is the force sensitive transition that is associated with a second substep, the linear nature of the distance parameter versus second step size makes sense. A further point to be made is that the distance parameter is much larger than the second substep for all isoforms. If the distance parameter is an accurate indication of the distance to the force sensitive transition, or the distance over which the force acts, the nature of the difference in size between d_{det} and the second substep, and consequently the structural rearrangements of myo1b under force are faithfully communicated among the different isoforms, suggesting that the effect of alternative splicing is not to modulate the compliance of the lever arm.

In the absence of any detailed knowledge of the cellular functions of myo1b, we can only speculate as to the functional relevance of the altered tension-sensing properties of myo1b due to alternative splicing in vivo. Alternative splicing is not a novel method of regulating myosin function, recent evidence has shown that alternative splicing can modulate association with other proteins (Roland, Lapierre & Goldenring 2009, Wagner et al. 2006, Hodi et al. 2006) and control regulatory properties such as phosphorylation (Jana et al. 2009), however the demonstration that alternative splicing can modulate force sensitivity appears to be a new regulatory property. The widespread distribution of myo1b as a whole, and also the

widespread distribution of the splice isoforms in rodents (Ruppert, Kroschewski & Bahler 1993) may be so that a variety of cell types can dynamically regulate and rapidly modify their tension-sensing machinery in response to extracellular cues. The fact that there is a transition from a distance parameter of ~ 10 nm for myo1b^c to ~ 18 for myo1b^a shows that there is a dynamic range of force sensitivity for myo1b, providing further evidence that this protein, and other closely related myosins, could indeed be part of a mechanochemical tension-sensing apparatus inside a cell.

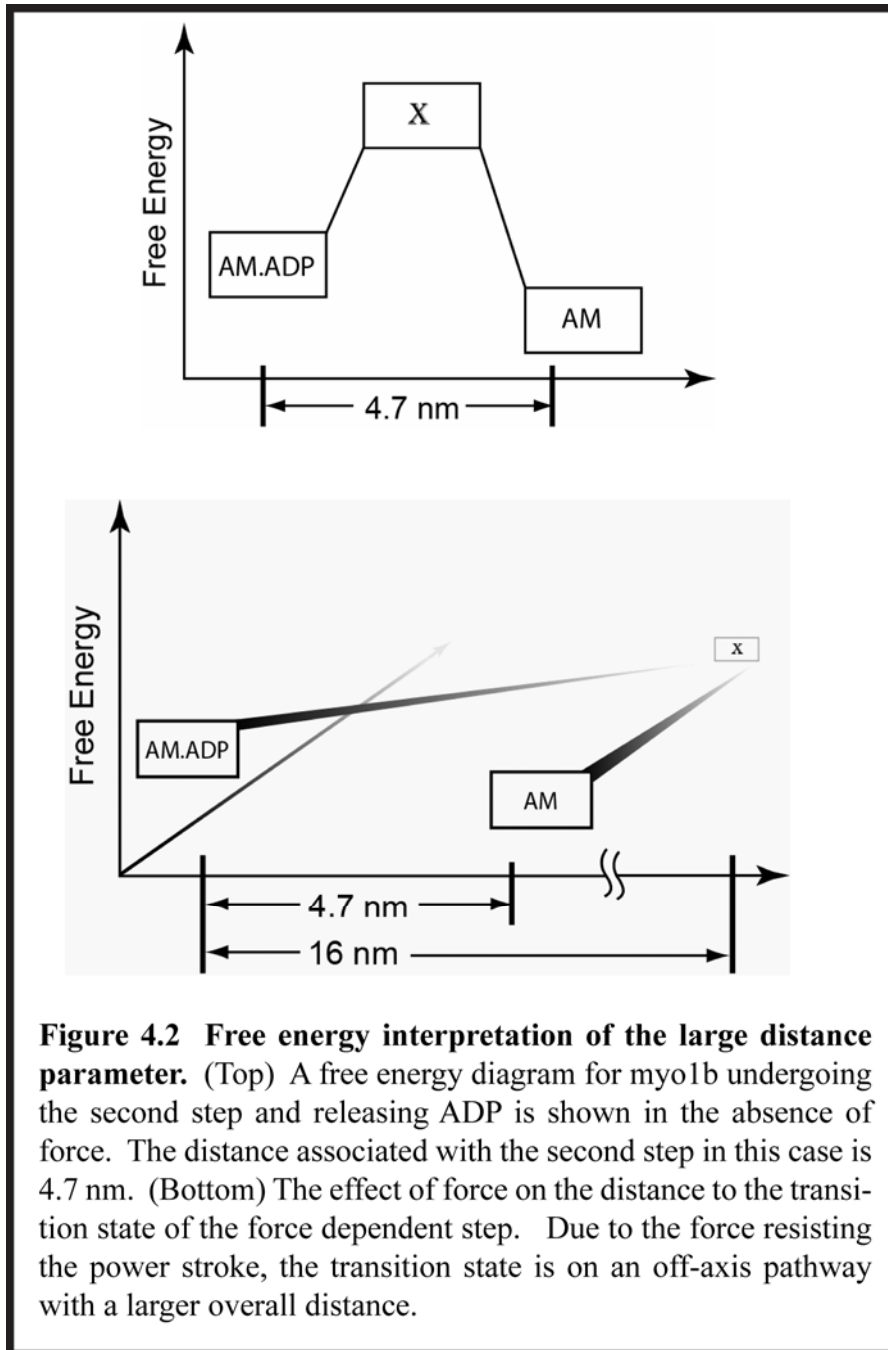
4.4 The origin of the large distance parameter

4.4.1 Motions of the lever arm under load

Considering that the distance parameter (d_{det}) represents the distance over which the force acts in the strain sensitive transition, one might expect close agreement between ADP-release substep size and distance parameter. In the case of smooth muscle myosin-II and myosin-V for example, the size of the second substep (2 nm and 5 nm respectively) is in good agreement with the distance parameter (2.7 nm and 4.3 nm respectively) (Veigel et al. 2003). If the displacement generated by the substep associated with ADP release is ~ 4.4 nm for myo1b^b, and ADP release corresponds to the force sensitive transition responsible for the tension sensitivity seen in the single molecule recordings, it is interesting that there is such a large difference in distance between d_{det} and the second substep. One possible

explanation for this observation is that effect of force is to structurally reverse the power stroke while maintaining the strong binding biochemical state, forcing the myosin to overcome a larger distance before entering a conformation capable of more readily releasing ADP. The distance parameter would then be expected to be a reflection of the motion of the total step size, which would be in agreement within error from our measurements. Another explanation is that the force sensitive transition is on a coordinate that is in line with a rigid lever arm motion, but that this transition state is further along the axis of the power stroke than the rigor conformation (figure 4.2) (Tsygankov, Fisher 2007).

The complicated histogram of myo1b^a step sizes in the absence of calcium in figure 3.20 has multiple distributions, which may reflect multiple calmodulin binding states or an unstructured region in the LCBD. In all of our stiffness measurements, the stage



movement was controlled to be on average roughly the length of the step size. If there were a region of very low stiffness (relative to the rest of the lever arm), or an unstructured element, the phase plot would be flattened over the portion of the

oscillation where the low-stiffness element existed, showing a lower stiffness value over forces in which the compliant element was slack. The lack of nonlinearity in our phase plots (figure 3.22) provides further evidence that the LCBD serves as a rigid lever arm.

4.4.2 Loop-1 of myo1b

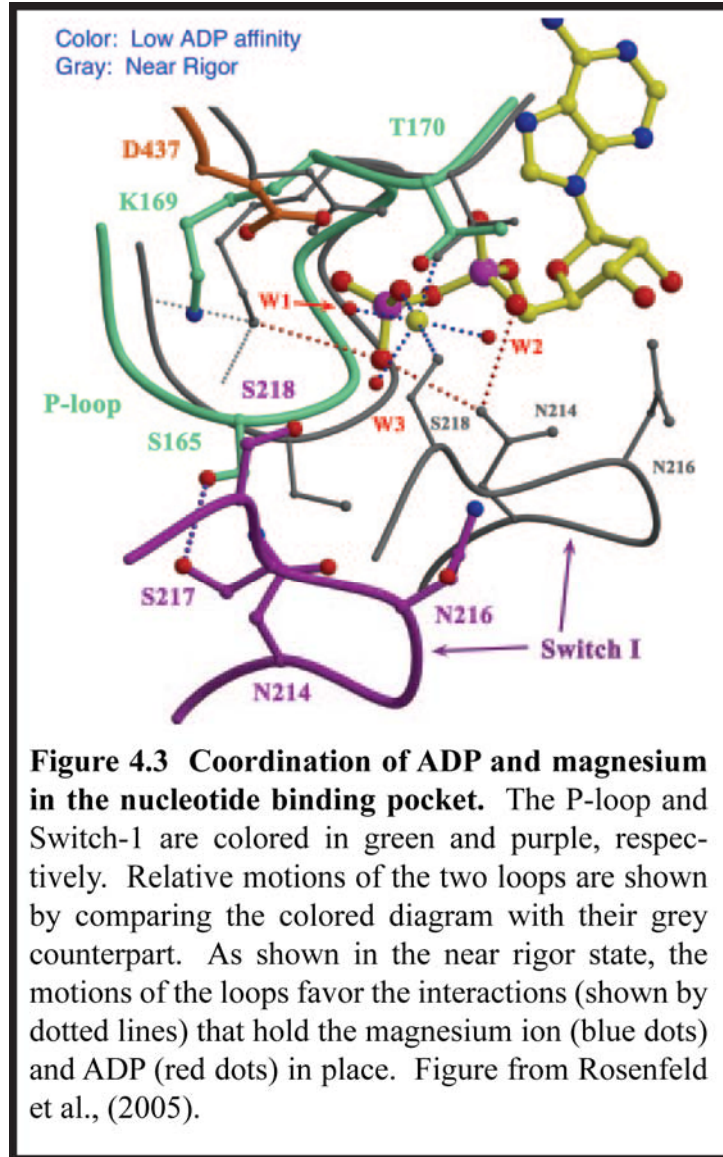
Another question that applies to all myosins is what conformational changes in the nucleotide binding pocket of the motor domain result in the inhibition or acceleration of product release in response to load. In the introduction to this thesis, the atomic structure of the myosin-II motor domain was discussed as a general example of the structure of a myosin. Although the motor sequences are highly conserved among all members of the myosin superfamily, there is a particular loop (called loop 1) that connects two important elements in the nucleotide binding pocket, the P-loop and the switch-1 helix. A number of studies implicate this loop as an important regulatory component of the ATPases of different myosins, specifically to the control of the rates of product release, suggesting it may act as a regulator of nucleotide access (Kurzawa-Goertz et al. 1998, Clark et al. 2005, Sweeney et al. 1998b). This regulation of nucleotide access is coupled to the structural changes that alter actin binding by the myosin head as well.

Consistent with this proposed role in tuning the kinetics of different myosin isoforms, loop 1 is considered a variable region of the myosin head (Uyeda, Ruppel & Spudich 1994). Loop 1 is somewhat unique for myo1b in that it is very short,

consisting of only 6 amino acids. Therefore it is expected to be less flexible and favor the ADP-bound state of the protein. Studies of myo1b with altered loop-1 primary sequence showed altered kinetic effects, suggesting that this loop should be taken into consideration in light of our tension-sensitivity results (Clark et al. 2005). It is possible that under force, the position of loop 1 and therefore switch-1 changes and the nucleotide binding pocket rearranges to result in a structural state which increases ADP affinity, possibly through altered coordination of ADP and magnesium.

4.4.3 Magnesium release as a gate for ADP release

When ATP binds to the nucleotide binding pocket at the beginning of the myosin ATPase cycle, it does so with a magnesium ion as a cofactor that coordinates that ATP in the pocket for hydrolysis. After hydrolyzing ATP and releasing phosphate, the release of ADP is biphasic with a strong binding phase that depends on the concentration of free magnesium in solution as well as a weak binding phase which is magnesium independent. It has therefore been proposed that the magnesium ion coordinates the ADP so that it binds more tightly to the myosin. Coordination of magnesium in kinesin has been similarly proposed to gate release of ADP, and a mutant of a kinesin-2 motor that prevents ADP release by stabilizing the coordination of the magnesium ion has been developed (Hoeng et al. 2008). Actin binding induces changes that favor the release of magnesium and then ADP, such that under steady state cycling conditions in the absence of load and physiological



magnesium concentrations the majority of actomyosin populates the AM·Mg·ADP state that has magnesium and ADP weakly bound, allowing virtually unrestrained release of ADP at rates similar to solution kinetics conditions (Hannemann et al. 2005, Rosenfeld, Houdusse & Sweeney 2005).

Structurally, the positions of switch 1 and the P-loop are placed in critical areas around the nucleotide binding pocket and interact extensively with both the ADP and the magnesium ion depending on the conformation of the myosin (figure 4.3). Not shown in the figure is loop 1, which connects switch 1 and the P loop. A large difference in the conformation of switch 1 is seen in the predicted weak and strong ADP binding states, with the loss of magnesium coordination resulting in changes in switch 1 that render it less tightly coordinated to ADP, although there are also predicted changes in P-loop structure (Holmes et al. 2004). The generality of a potential strain dependent magnesium release mechanism for strain-sensing is also supported by results from the class-I family of myosin motors. Work by Fujita-Becker et al., showed a reduction in actin sliding velocity by myo1d in the presence of increasing amounts of free magnesium over a physiological range of concentrations, and that this effect was due to a reduced rate of ADP release (Fujita-Becker et al. 2005).

4.5 Crossbridge stiffness and the lever arm of myo1b.

4.5.1 The actomyo1b crossbridge does not behave as an elastic cantilever

The third specific aim of this thesis was to characterize the stiffness of the actomyo1b crossbridge. The presence of an elastic element in skeletal muscle was shown in experiments by Huxley and Simmons examining small length changes in muscle (Huxley, Simmons 1971). The identity of a springlike component in the

actomyosin crossbridge then could be the lever arm, or another element within the motor domain. If the stiffness of the crossbridge is a cantilevered beam with some elasticity κ , the stiffness can be modeled as a function of the length of that beam according to:

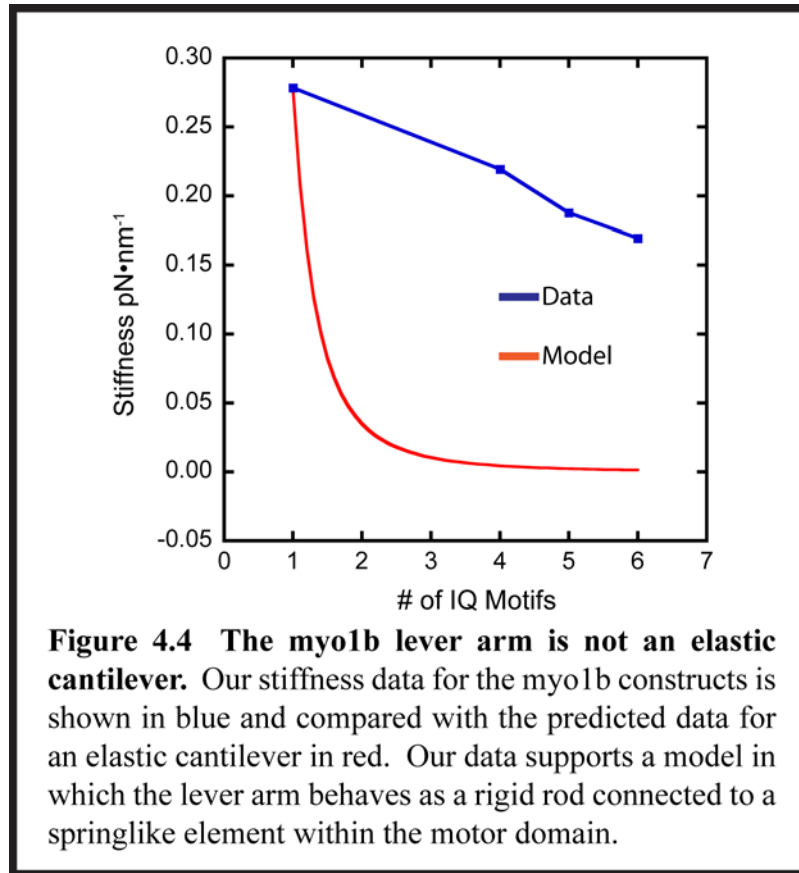
Equation 13

$$\kappa = \frac{3EI}{L^3} = \frac{3kTL_p}{L^3}$$

Where, EI/kT is the persistence length, k is the Boltzmann constant, and T is temperature. Since we show in figure (3.14) that the force (and therefore displacement) produced by the different myo1b constructs is approximately linear with the number of IQ motifs along the LCBD, we can conclude that the length of the lever arm is approximately linear with the number of IQ motifs. Therefore, we can test whether the lever arm behaves as an elastic cantilever for myo1b by measuring the stiffness of the myo1b constructs as a function of lever arm length (Uyeda, Abramson & Spudich 1996b).

By oscillating the stage by small amounts (~10 - 15 nm for native myo1b constructs) while simultaneously measuring the force produced during stretching, we were able to create a running window of the stiffness of the actomyo1b crossbridge during attachment events. As we show in figure 3.24, the stiffness appears to vary linearly with the length of the lever arm, rather than as $1/L^3$. A comparison between our data and the predicted stiffness of an elastic cantilever is shown in figure 4.4, assuming the same stiffness values for the 1 IQ motif construct. Our range of stiffness measurements for the experimental constructs used in this

thesis ($0.17 \text{ pN}\cdot\text{nm}^{-1} - 0.28 \text{ pN}\cdot\text{nm}^{-1}$) are in good agreement with other measurements of crossbridge stiffness. Veigel et al., measured the crossbridge stiffness for myosin-V and smooth muscle myosin-II at the single molecule level and found them to be ~ 0.2 and $\sim 0.45 \text{ pN}\cdot\text{nm}^{-1}$ respectively (Veigel et al. 2005). Skeletal muscle myosin-II was found to be $0.7 \text{ pN}\cdot\text{nm}^{-1}$ (Veigel et al. 1998).



The linear relationship of stiffness to lever arm length would support a model in which the lever arm were sufficiently rigid and coupled to an elastic spring within the motor domain itself (Warshaw et al. 2000c). We are limited somewhat in our measurement as shown by the large distributions associated with the stiffness values, but we can roughly conclude that a linear fit is a better representation of the

data than $1/L^3$. Increasing the resolution of our measurement could be accomplished by installing feedback loops to control the y and z axes of the stage, which may exhibit the same force fluctuations we correct for on the x-axis. Additionally, although the stiffness of the biotin-streptavidin linkage is predicted to be very high, it remains necessary to test the compliance of our biotin-streptavidin anchor linkage. This could be accomplished using biotinylated actin at a very low molar ratio to unlabeled actin.

4.6 Calcium regulation of force sensitivity

4.6.1 Calcium reduces the force sensitivity of myo1b

Based on the force sensitivity of the myo1b, it is likely that a cluster of myo1b molecules inside a cell could exist as a static tether, linking a membrane bound compartment to the cortical actin cytoskeleton to immobilize it. In this case, a regulatory mechanism could exist to initiate cycling of myo1b either by relaxing the tension along the myo1b lever arm while it is still attached to the actin filament, or by inducing a biochemical or structural state of myo1b that is weakly bound to the actin filament. Calcium has been shown previously to be an important regulator of myosin function. In the case of myosin-II in skeletal muscle, the effect of calcium is indirect, acting through calcium sensitive regulatory proteins bound to the thin filament (Gordon, Homsher & Regnier 2000). In the absence of calcium, tropomyosin blocks the binding sites on the actin filament for myosin, but is

induced to move by binding of calcium to the associated regulatory protein troponin C. In the case of smooth muscle myosin-II, calcium acts to activate the muscle by activating myosin light chain kinase, which then activates smooth muscle myosin-II by phosphorylation of the regulatory light chain of myosin (Kamm, Stull 1985).

A more direct effect of calcium binding is observed for myosin-Va, which exists in the absence of calcium or bound cargo in a compact, folded, enzymatically inactive state (Sellers et al. 2008, Thirumurugan et al. 2006, Liu et al. 2006). In the presence of calcium, or induced by cargo binding, the MgATPase of myosin-V is activated and the protein becomes more elongated (Sellers et al. 2008, Li et al. 2004). In contrast to this activation, calcium also causes dissociation of one or more light chains along the lever arm of myosin-V, reducing its ability to move processively along the actin filament. It is therefore likely that cargo binding is the physiological activator of myosin-V function, although the calcium binding properties may be important for regulation as well (Lu, Kremontsova & Trybus 2006, Trybus et al. 2007, Li, Ikebe & Ikebe 2005).

In the case of myosin-I, calcium binding to light chains is also known to cause dissociation of at least one calmodulin from the lever arm of myo1c, which is likely responsible for the alterations in kinetic and motility properties observed in vitro (Gillespie, Cyr 2002)(Manceva et al. 2007). Adamek et al., used transient kinetics techniques to demonstrate that although the steady state ATPase activity of myo1c is similar +/- calcium, there are a number of effects on the individual rate constants of the myo1c ATPase. In particular, the rate constant for ATP hydrolysis

is inhibited, while the rate constant for ADP dissociation is accelerated > 10-fold in the presence of calcium (Adamek, Coluccio & Geeves 2008). Alternatively, for the case of myo1b, calcium increases the rate of ADP release roughly twofold, and increases the rate of phosphate release roughly threefold. Therefore calcium could have an effect on the tension-sensitive properties of myo1b, both through alterations in calmodulin binding on IQ1 to relax the tension in the lever arm, and through simultaneous acceleration of ADP release.

Our investigations of the effect of calcium on the tension-sensing properties of myo1b show that calcium can reduce the force sensitivity of myosin-Ib at the single molecule level. The mechanism of this reduction in tension-sensitivity is currently unknown, although the step size of myo1b^a is greatly reduced in increasing amounts of free calcium in solution. This suggests that the LCBD is uncoupled from the structural changes in the motor domain which are normally amplified by the lever arm. The possibility that calcium binding to calmodulins along the lever arm of myo1b serves to increase compliance and cause the myo1b lever arm to become flaccid will be investigated in the next section of this discussion.

4.6.2 How does calcium binding affect the force sensitivity

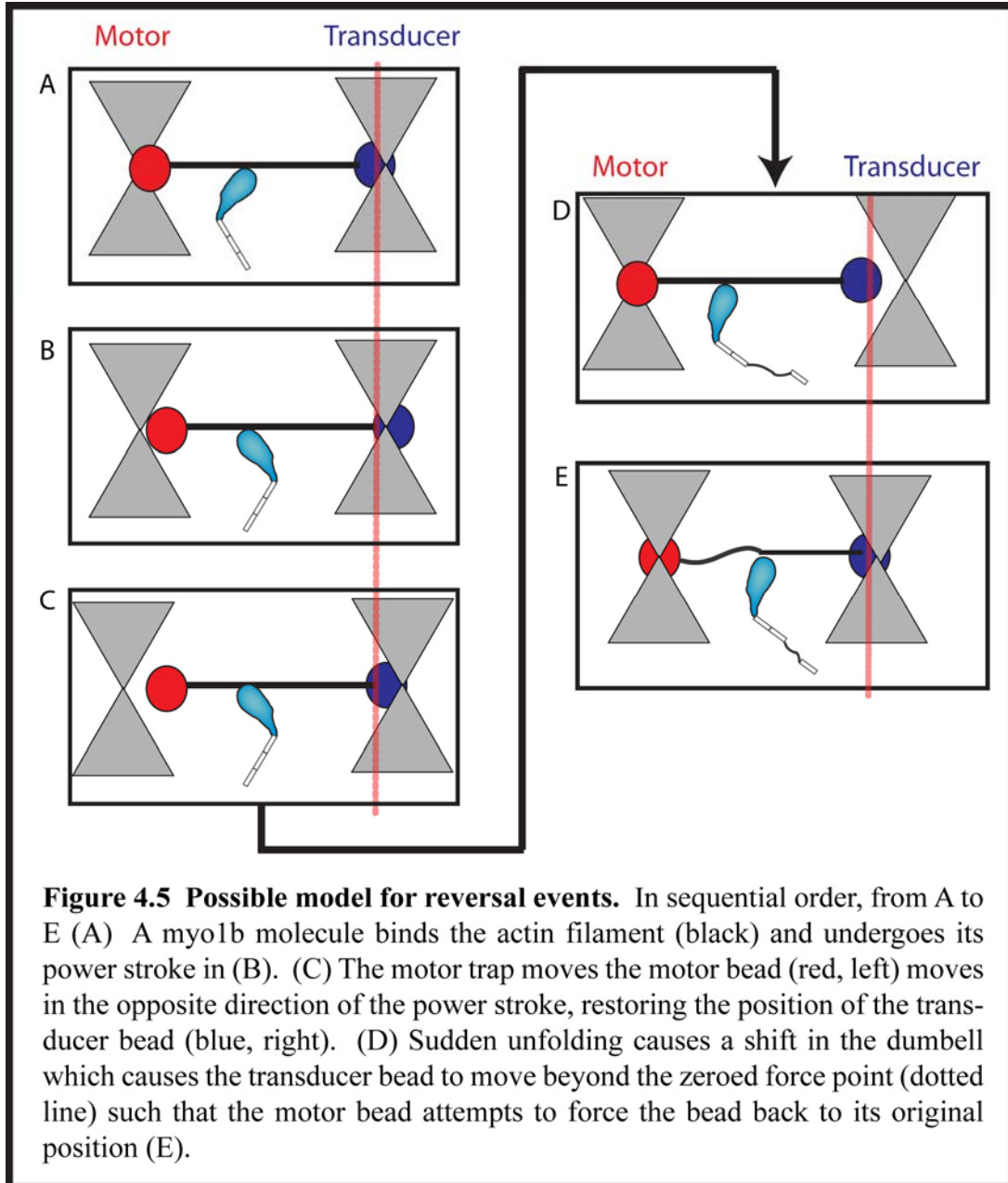
As discussed earlier, the effect of calcium on force sensitivity could be brought about by two factors, a decrease in the step size of the motor and an increase in the rate of ADP release. This effect probably is due to modulation of calmodulin binding along the other IQ motifs of the LCBD. In that regard, it is

interesting that we observe such a mild reduction in stiffness for our stiffness experiments in the presence of 9 μM free calcium. We conducted our experiments in the presence of 20 μM calmodulin to ensure that all the IQ motifs have bound calmodulin, so the effect of calcium in this case is likely due to altered binding of calmodulins along the LCBD rather than dissociation of any individual calmodulins (Lin, Tang & Ostap 2005).

IQ1, being the closest IQ motif to the motor domain, may have a more direct interaction with the motor domain of the protein than the other IQ motifs. If the effect of calcium, through modification of the IQ1-calmodulin interaction, serves to decouple the force sensitivity of the motor by abolishing specific contacts between IQ1 and the motor domain, then perhaps a complete reduction in stiffness of the lever arm of myo1b is not necessary to uncouple the changes in the motor domain from the production of force. By analogy to myosin-II, the light chain bound to the IQ motif closest to the motor domain, the essential light chain, is involved in a number of contacts with the motor domain that modulate the ATPase, with mutations in about this domain having consequences in familial hypertrophic cardiomyopathy (Houdusse and Cohen 1996, Ushakov, 2008).

4.7 The observation of high-gain “reversals”

During our experiments in which we measured the stiffness of individual myo1b crossbridges, it was necessary to decrease the response time of the feedback



loop to levels approaching those used in the experiments of Takagi et al., (2006).

The decreased response time ensured that during stage oscillation, the compliance of the bead-actin-bead dumbbell would be restored rapidly enough such that the force

due to stretching the myosin molecule would not be transmitted to the transducer bead, ensuring that the force measurement on the motor bead was an accurate representation of the force due to stretching (see figure 2.9). By increasing the gain, we observed a greater proportion of “reversals” immediately following attachment and generation of force (figure 2.8 and 3.23). These reversals are very similar to the published bipolar force events observed by Takagi et al. The character of these reversals, therefore, is quite interesting even though we only have a qualitative understanding of them at the moment.

A description of the sort of unfolding event that could result in a reversal is modeled in figure 4.5. If this shift is greater than the pretension force on the actin filament, the transducer bead would cross the zero point of the force level and the motor bead would attempt to “push” the transducer bead in the direction of the power stroke. Due to the stiffness of the myosin crossbridge, it would be unable to do so and the actin filament would go slack. Since our pretension force is on the order of ~2-3 pN, and a myo1b molecule working in our optical trap can produce such a force this much force when working against a load, a rapid structural reversal, or forced unfolding, could account for the reversal traces. Figure 2.8 is a typical example of this kind of event, where it can be seen that the myosin dissociates from the actin filament shortly after undergoing the reversal. Alternatively, during stiffness oscillations, we occasionally observe events that undergo a reversal and then switch back to non-reversal force production while still bound to the actin filament (figure 3.25).

We consider three possible reasons for the rapid reversals in force seen in figures 2.8 and 3.25. (1.) An unfolding event, or loss of calmodulin causes a rapid relaxation along the lever arm of myo1b during an event. This causes the transducer bead to rapidly cross the zero force point and the motor bead will then attempt to push the transducer back in place. (2.) The myosin rapidly reverses the power stroke during a near-isometric event and pulls the transducer bead past the zero force point, and the portion of the actin filament between the motor bead and the myosin goes slack. (3) Consistent with the observation made by Takagi et al., the myosin molecule “slips” along the actin filament until it reaches another target binding site. This slippage occurs quickly enough that the time the myosin spends traveling along the actin filament is faster than the response time of the feedback loop, and when it rebinds it changes the average force on the beads and pulls the transducer past the zero force point. At this point we cannot distinguish between any of these three mechanisms, although we consider the third possibility (slipping along the actin filament) to be less likely for myosin-Ib due to the fact that reversals can be returned to the pre-reversal force levels by the oscillation of the stage during stiffness measurements.

4.8 Cellular implications

Based on the predicted change in duty ratio as a function of force, in this thesis we propose a potential model for the molecular function of myosin-I (figure

4.6). When attached to a specific cargo or membrane, myosin-I interacts with actin and generates a displacement that stretches a cellular “spring”. This spring may be the deformation of membranes during endocytosis, the deformation of stiff actin networks during the transport of membranes or vesicles, or the tensioning of mechano-sensitive ion channels in the adaptation response of sensory hair cells. Tension on myosin-I results in a dramatically reduced rate of ADP release, and the myosin acts as an anchoring protein with attachment lifetimes > 45 s. When strain on the spring is relaxed via membrane or protein movements, ADP is released, and active ATP cycling and motility of the motor complex resume.

A more detailed functional characterization of various myosin-I_s, including myo1b, is necessary to test our proposed model. Emerging evidence suggests that the generation of membrane tension by linking the plasma membrane to the underlying actin cytoskeleton, such as the structural maintenance of intestinal brush border microvilli by myo1a, is a general property of class-I myosins *in vivo* (Nambiar, McConnell & Tyska 2009, Tyska et al. 2005a). Intracellular localization of myo1b is consistent with this general functional role (Ruppert et al. 1995), and the elongated structure of myo1b in solution could be optimal for crosslinking the plasma membrane with cortical actin filaments (Stafford et al. 2005). Myo1c is an excellent example of a closely related myosin with a well characterized role as the adaptation motor in hair cell stereocillia of the inner ear (Batters et al. 2004c, Gillespie, Cyr 2004, Holt et al. 2002, Batters et al. 2004a). For myo1c, a strain sensing mechanism was proposed to regulate the open/closed probability and

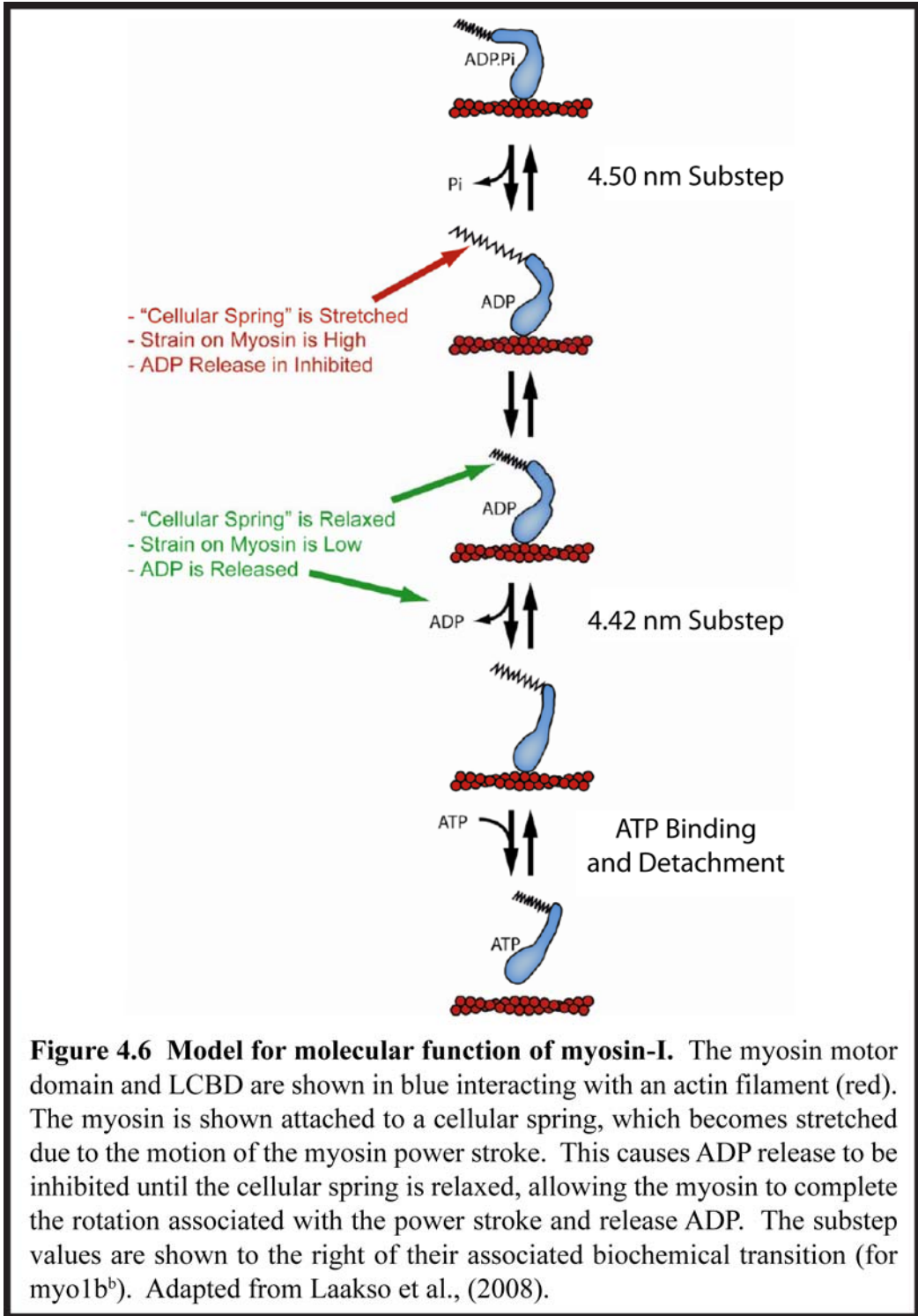


Figure 4.6 Model for molecular function of myosin-I. The myosin motor domain and LCBD are shown in blue interacting with an actin filament (red). The myosin is shown attached to a cellular spring, which becomes stretched due to the motion of the myosin power stroke. This causes ADP release to be inhibited until the cellular spring is relaxed, allowing the myosin to complete the rotation associated with the power stroke and release ADP. The substep values are shown to the right of their associated biochemical transition (for myo1b^b). Adapted from Laakso et al., (2008).

positioning of mechanosensitive ion channels, incorporating a strain-dependent ADP release step. Our results support this and similar functional models for myosin-I, where myosin-Is function to generate and sustain tension, rather than rapidly transport cargoes. This new understanding of myosin-I mechanics allows a more rigorous assignment of this motor's molecular roles in controlling organelle morphology (Salas-Cortes et al. 2005) and dynamics (Bose et al. 2002) in the wide variety of cell types in which it is expressed.

4.9 Conclusions

The experiments presented in this thesis demonstrate a number of interesting properties of myo1b and how they might be regulated. By characterizing the response of myo1b to an external force, we showed that myo1b is extraordinarily strain sensitive, and that ADP release represents the likely force-sensitive transition in the myo1b biochemical cycle. We further characterized the biochemistry of the force-sensitive state by showing that phosphate does not rebind and induce a weakly-bound conformation. We then examined the regulation of this tension sensitivity by alternative splicing and calcium binding. These results showed that alternative splicing can create a dynamic range of tension sensitivities for myo1b and that calcium binding can uncouple the force sensing properties of myo1b from the structural changes in the motor domain during the power stroke. Finally, we examined the stiffness of the actomyo1b crossbridge as a function of lever arm

length and showed that stiffness of the actomyo1b crossbridge is largely insensitive to lever arm length, although there does appear to be a slight linear dependence. Accomplishing these goals, as outlined in specific aims, provides evidence to support models in which myosin-Is generally serve to generate and maintain membrane tension.

References

- Adamek, N., Coluccio, L.M. & Geeves, M.A. 2008, "Calcium sensitivity of the cross-bridge cycle of Myo1c, the adaptation motor in the inner ear", *Proceedings of the National Academy of Sciences of the United States of America*, vol. 105, no. 15, pp. 5710-5715.
- Adams, R.J. & Pollard, T.D. 1989, "Binding of myosin I to membrane lipids", *Nature*, vol. 340, no. 6234, pp. 565-568.
- Altman, D., Sweeney, H.L. & Spudich, J.A. 2004, "The mechanism of myosin VI translocation and its load-induced anchoring", *Cell*, vol. 116, no. 5, pp. 737-749.
- Anson, M., Geeves, M.A., Kurzawa, S.E. & Manstein, D.J. 1996, "Myosin motors with artificial lever arms", *The EMBO journal*, vol. 15, no. 22, pp. 6069-6074.
- Ashkin, A. 1997, "Optical trapping and manipulation of neutral particles using lasers", *Proceedings of the National Academy of Sciences of the United States of America*, vol. 94, no. 10, pp. 4853-4860.
- Ashkin, A. & Dziedzic, J.M. 1989, "Internal cell manipulation using infrared laser traps", *Proceedings of the National Academy of Sciences of the United States of America*, vol. 86, no. 20, pp. 7914-7918.
- Ashkin, A. & Dziedzic, J.M. 1987, "Optical trapping and manipulation of viruses and bacteria", *Science (New York, N.Y.)*, vol. 235, no. 4795, pp. 1517-1520.
- Ashkin, A. & Dziedzic, J.M. 1975, "Optical Levitation of Liquid Drops by Radiation Pressure", *Science (New York, N.Y.)*, vol. 187, no. 4181, pp. 1073-1075.
- Ashkin, A., Dziedzic, J.M. & Yamane, T. 1987, "Optical trapping and manipulation of single cells using infrared laser beams", *Nature*, vol. 330, no. 6150, pp. 769-771.
- Bahler, M. & Rhoads, A. 2002, "Calmodulin signaling via the IQ motif", *FEBS letters*, vol. 513, no. 1, pp. 107-113.
- Batters, C., Arthur, C.P., Lin, A., Porter, J., Geeves, M.A., Milligan, R.A., Molloy, J.E. & Coluccio, L.M. 2004a, "Myo1c is designed for the adaptation response in the inner ear", *The EMBO journal*, vol. 23, no. 7, pp. 1433-1440.

- Batters, C., Arthur, C.P., Lin, A., Porter, J., Geeves, M.A., Milligan, R.A., Molloy, J.E. & Coluccio, L.M. 2004b, "Myo1c is designed for the adaptation response in the inner ear", *The EMBO journal*, vol. 23, no. 7, pp. 1433-1440.
- Batters, C., Wallace, M.I., Coluccio, L.M. & Molloy, J.E. 2004c, "A model of stereocilia adaptation based on single molecule mechanical studies of myosin I", *Philosophical transactions of the Royal Society of London. Series B, Biological sciences*, vol. 359, no. 1452, pp. 1895-1905.
- Berg, J.S., Powell, B.C. & Cheney, R.E. 2001, "A millennial myosin census", *Molecular biology of the cell*, vol. 12, no. 4, pp. 780-794.
- Bose, A., Guilherme, A., Robida, S.I., Nicoloso, S.M., Zhou, Q.L., Jiang, Z.Y., Pomerleau, D.P. & Czech, M.P. 2002, "Glucose transporter recycling in response to insulin is facilitated by myosin Myo1c", *Nature*, vol. 420, no. 6917, pp. 821-824.
- Brune, M., Hunter, J.L., Corrie, J.E. & Webb, M.R. 1994, "Direct, real-time measurement of rapid inorganic phosphate release using a novel fluorescent probe and its application to actomyosin subfragment 1 ATPase", *Biochemistry*, vol. 33, no. 27, pp. 8262-8271.
- Cheney, R.E. & Mooseker, M.S. 1992, "Unconventional myosins", *Current opinion in cell biology*, vol. 4, no. 1, pp. 27-35.
- Cheney, R.E., O'Shea, M.K., Heuser, J.E., Coelho, M.V., Wolenski, J.S., Espreafico, E.M., Forscher, P., Larson, R.E. & Mooseker, M.S. 1993, "Brain myosin-V is a two-headed unconventional myosin with motor activity", *Cell*, vol. 75, no. 1, pp. 13-23.
- Chu, S., Bjorkholm, J.E., Ashkin, A. & Cable, A. 1986, "Experimental observation of optically trapped atoms", *Physical Review Letters*, vol. 57, no. 3, pp. 314-317.
- Chu, S., Hollberg, L., Bjorkholm, J.E., Cable, A. & Ashkin, A. 1985, "Three-dimensional viscous confinement and cooling of atoms by resonance radiation pressure", *Physical Review Letters*, vol. 55, no. 1, pp. 48-51.
- Clark, R., Ansari, M.A., Dash, S., Geeves, M.A. & Coluccio, L.M. 2005, "Loop 1 of transducer region in mammalian class I myosin, Myo1b, modulates actin affinity, ATPase activity, and nucleotide access", *The Journal of biological chemistry*, vol. 280, no. 35, pp. 30935-30942.

- Coluccio, L.M. 1997, "Myosin I", *The American Journal of Physiology*, vol. 273, no. 2 Pt 1, pp. C347-59.
- Coluccio, L.M. & Geeves, M.A. 1999, "Transient kinetic analysis of the 130-kDa myosin I (MYR-1 gene product) from rat liver. A myosin I designed for maintenance of tension?", *The Journal of biological chemistry*, vol. 274, no. 31, pp. 21575-21580.
- Cote, G.P., Albanesi, J.P., Ueno, T., Hammer, J.A., 3rd & Korn, E.D. 1985, "Purification from *Dictyostelium discoideum* of a low-molecular-weight myosin that resembles myosin I from *Acanthamoeba castellanii*", *The Journal of biological chemistry*, vol. 260, no. 8, pp. 4543-4546.
- Cox, D., Berg, J.S., Cammer, M., Chingwundoh, J.O., Dale, B.M., Cheney, R.E. & Greenberg, S. 2002, "Myosin X is a downstream effector of PI(3)K during phagocytosis", *Nature cell biology*, vol. 4, no. 7, pp. 469-477.
- Dai, J., Ting-Beall, H.P., Hochmuth, R.M., Sheetz, M.P. & Titus, M.A. 1999, "Myosin I contributes to the generation of resting cortical tension", *Biophysical journal*, vol. 77, no. 2, pp. 1168-1176.
- Dantzig, J.A., Goldman, Y.E., Millar, N.C., Lactis, J. & Homsher, E. 1992, "Reversal of the cross-bridge force-generating transition by photogeneration of phosphate in rabbit psoas muscle fibres", *The Journal of physiology*, vol. 451, pp. 247-278.
- Dantzig, J.A., Liu, T.Y. & Goldman, Y.E. 2006, "Functional studies of individual myosin molecules", *Annals of the New York Academy of Sciences*, vol. 1080, pp. 1-18.
- De La Cruz, E.M. & Ostap, E.M. 2004, "Relating biochemistry and function in the myosin superfamily", *Current opinion in cell biology*, vol. 16, no. 1, pp. 61-67.
- De La Cruz, E.M., Sweeney, H.L. & Ostap, E.M. 2000, "ADP inhibition of myosin V ATPase activity", *Biophysical journal*, vol. 79, no. 3, pp. 1524-1529.
- Dominguez, R., Freyzon, Y., Trybus, K.M. & Cohen, C. 1998, "Crystal structure of a vertebrate smooth muscle myosin motor domain and its complex with the essential light chain: visualization of the pre-power stroke state", *Cell*, vol. 94, no. 5, pp. 559-571.
- Dreizen, P., Gershman, L.C., Trotta, P.P. & Stracher, A. 1967, "Subunits and their interactions", *The Journal of general physiology*, vol. 50, no. 6, pp. Suppl:85-118.

- Eisenberg, E., Zobel, C.R. & Moos, C. 1968, "Subfragment 1 of myosin: adenosine triphosphatase activation by actin", *Biochemistry*, vol. 7, no. 9, pp. 3186-3194.
- El Mezgueldi, M., Tang, N., Rosenfeld, S.S. & Ostap, E.M. 2002, "The kinetic mechanism of Myo1e (human myosin-IC)", *The Journal of biological chemistry*, vol. 277, no. 24, pp. 21514-21521.
- Evangelista, M., Klebl, B.M., Tong, A.H., Webb, B.A., Leeuw, T., Leberer, E., Whiteway, M., Thomas, D.Y. & Boone, C. 2000, "A role for myosin-I in actin assembly through interactions with Vrp1p, Bee1p, and the Arp2/3 complex", *The Journal of cell biology*, vol. 148, no. 2, pp. 353-362.
- Fenn, W.O. 1923, "A quantitative comparison between the energy liberated and the work performed by the isolated sartorius muscle of the frog", *The Journal of physiology*, vol. 58, no. 2-3, pp. 175-203.
- Finer, J.T., Simmons, R.M. & Spudich, J.A. 1994, "Single myosin molecule mechanics: piconewton forces and nanometre steps", *Nature*, vol. 368, no. 6467, pp. 113-119.
- Foth, B.J., Goedecke, M.C. & Soldati, D. 2006, "New insights into myosin evolution and classification", *Proceedings of the National Academy of Sciences of the United States of America*, vol. 103, no. 10, pp. 3681-3686.
- Frankel, F.R. 1976, "Organization and energy-dependent growth of microtubules in cells", *Proceedings of the National Academy of Sciences of the United States of America*, vol. 73, no. 8, pp. 2798-2802.
- Frederiksen, D.W. & Holtzer, A. 1968, "The substructure of the myosin molecule. Production and properties of the alkali subunits", *Biochemistry*, vol. 7, no. 11, pp. 3935-3950.
- Fujita-Becker, S., Durrwang, U., Erent, M., Clark, R.J., Geeves, M.A. & Manstein, D.J. 2005, "Changes in Mg²⁺ ion concentration and heavy chain phosphorylation regulate the motor activity of a class I myosin", *The Journal of biological chemistry*, vol. 280, no. 7, pp. 6064-6071.
- Furch, M., Geeves, M.A. & Manstein, D.J. 1998, "Modulation of actin affinity and actomyosin adenosine triphosphatase by charge changes in the myosin motor domain", *Biochemistry*, vol. 37, no. 18, pp. 6317-6326.
- Geeves, M.A., Perreault-Micale, C. & Coluccio, L.M. 2000, "Kinetic analyses of a truncated mammalian myosin I suggest a novel isomerization event preceding

- nucleotide binding", *The Journal of biological chemistry*, vol. 275, no. 28, pp. 21624-21630.
- Geli, M.I., Lombardi, R., Schmelzl, B. & Riezman, H. 2000, "An intact SH3 domain is required for myosin I-induced actin polymerization", *The EMBO journal*, vol. 19, no. 16, pp. 4281-4291.
- GERGELY, J. 1953, "Studies on myosin-adenosinetriphosphatase", *The Journal of biological chemistry*, vol. 200, no. 2, pp. 543-550.
- Gershman, L.C., Stracher, A. & Dreizen, P. 1969, "Subunit structure of myosin. 3. A proposed model for rabbit skeletal myosin", *The Journal of biological chemistry*, vol. 244, no. 10, pp. 2726-2736.
- Gillespie, P.G. & Cyr, J.L. 2004, "Myosin-1c, the hair cell's adaptation motor", *Annual Review of Physiology*, vol. 66, pp. 521-545.
- Gillespie, P.G. & Cyr, J.L. 2002, "Calmodulin binding to recombinant myosin-1c and myosin-1c IQ peptides", *BMC biochemistry*, vol. 3, pp. 31.
- Gordon, A.M., Homsher, E. & Regnier, M. 2000, "Regulation of contraction in striated muscle", *Physiological Reviews*, vol. 80, no. 2, pp. 853-924.
- Grabarek, Z. 2006, "Structural basis for diversity of the EF-hand calcium-binding proteins", *Journal of Molecular Biology*, vol. 359, no. 3, pp. 509-525.
- Gyoeva, F.K. & Gelfand, V.I. 1991, "Coalignment of vimentin intermediate filaments with microtubules depends on kinesin", *Nature*, vol. 353, no. 6343, pp. 445-448.
- Hammer, J.A., 3rd, Jung, G. & Korn, E.D. 1986, "Genetic evidence that *Acanthamoeba* myosin I is a true myosin", *Proceedings of the National Academy of Sciences of the United States of America*, vol. 83, no. 13, pp. 4655-4659.
- Hannemann, D.E., Cao, W., Olivares, A.O., Robblee, J.P. & De La Cruz, E.M. 2005, "Magnesium, ADP, and actin binding linkage of myosin V: evidence for multiple myosin V-ADP and actomyosin V-ADP states", *Biochemistry*, vol. 44, no. 24, pp. 8826-8840.
- Hayden, S.M., Wolenski, J.S. & Mooseker, M.S. 1990, "Binding of brush border myosin I to phospholipid vesicles", *The Journal of cell biology*, vol. 111, no. 2, pp. 443-451.

- Helfand, B.T., Chang, L. & Goldman, R.D. 2004, "Intermediate filaments are dynamic and motile elements of cellular architecture", *Journal of cell science*, vol. 117, no. Pt 2, pp. 133-141.
- Helfand, B.T., Mikami, A., Vallee, R.B. & Goldman, R.D. 2002, "A requirement for cytoplasmic dynein and dynactin in intermediate filament network assembly and organization", *The Journal of cell biology*, vol. 157, no. 5, pp. 795-806.
- Hibberd, M.G., Dantzig, J.A., Trentham, D.R. & Goldman, Y.E. 1985, "Phosphate release and force generation in skeletal muscle fibers", *Science (New York, N.Y.)*, vol. 228, no. 4705, pp. 1317-1319.
- Hodi, Z., Nemeth, A.L., Radnai, L., Hetenyi, C., Schlett, K., Bodor, A., Perczel, A. & Nyitrai, L. 2006, "Alternatively spliced exon B of myosin Va is essential for binding the tail-associated light chain shared by dynein", *Biochemistry*, vol. 45, no. 41, pp. 12582-12595.
- Hoeng, J.C., Dawson, S.C., House, S.A., Sagolla, M.S., Pham, J.K., Mancuso, J.J., Lowe, J. & Cande, W.Z. 2008, "High-resolution crystal structure and in vivo function of a kinesin-2 homologue in *Giardia intestinalis*", *Molecular biology of the cell*, vol. 19, no. 7, pp. 3124-3137.
- Hokanson, D.E., Laakso, J.M., Lin, T., Sept, D. & Ostap, E.M. 2006, "Myo1c binds phosphoinositides through a putative pleckstrin homology domain", *Molecular biology of the cell*, vol. 17, no. 11, pp. 4856-4865.
- Hokanson, D.E. & Ostap, E.M. 2006, "Myo1c binds tightly and specifically to phosphatidylinositol 4,5-bisphosphate and inositol 1,4,5-trisphosphate", *Proceedings of the National Academy of Sciences of the United States of America*, vol. 103, no. 9, pp. 3118-3123.
- Holmes, K.C., Schroder, R.R., Sweeney, H.L. & Houdusse, A. 2004, "The structure of the rigor complex and its implications for the power stroke", *Philosophical transactions of the Royal Society of London. Series B, Biological sciences*, vol. 359, no. 1452, pp. 1819-1828.
- Holt, J.R., Gillespie, S.K., Provance, D.W., Shah, K., Shokat, K.M., Corey, D.P., Mercer, J.A. & Gillespie, P.G. 2002, "A chemical-genetic strategy implicates myosin-1c in adaptation by hair cells", *Cell*, vol. 108, no. 3, pp. 371-381.
- Houdusse, A., Gaucher, J.F., Kremontsova, E., Mui, S., Trybus, K.M. & Cohen, C. 2006, "Crystal structure of apo-calmodulin bound to the first two IQ motifs of myosin V reveals essential recognition features", *Proceedings of the National*

Academy of Sciences of the United States of America, vol. 103, no. 51, pp. 19326-19331.

- HUXLEY, A.F. 1957, "Muscle structure and theories of contraction", *Progress in biophysics and biophysical chemistry*, vol. 7, pp. 255-318.
- HUXLEY, A.F. & NIEDERGERKE, R. 1954, "Structural changes in muscle during contraction; interference microscopy of living muscle fibres", *Nature*, vol. 173, no. 4412, pp. 971-973.
- Huxley, A.F. & Simmons, R.M. 1971, "Proposed mechanism of force generation in striated muscle", *Nature*, vol. 233, no. 5321, pp. 533-538.
- Huxley, H.E. 1969, "The mechanism of muscular contraction", *Science (New York, N.Y.)*, vol. 164, no. 886, pp. 1356-1365.
- HUXLEY, H.E. 1963, "Electron Microscope Studies on the Structure of Natural and Synthetic Protein Filaments from Striated Muscle", *Journal of Molecular Biology*, vol. 7, pp. 281-308.
- HUXLEY, H.E. 1957, "The double array of filaments in cross-striated muscle", *The Journal of biophysical and biochemical cytology*, vol. 3, no. 5, pp. 631-648.
- Huxley, H.E. & Brown, W. 1967, "The low-angle x-ray diagram of vertebrate striated muscle and its behaviour during contraction and rigor", *Journal of Molecular Biology*, vol. 30, no. 2, pp. 383-434.
- Huxley, H.E., Brown, W. & Holmes, K.C. 1965, "Constancy of axial spacings in frog sartorius muscle during contraction", *Nature*, vol. 206, no. 991, pp. 1358.
- Huxley, H.E., Simmons, R.M., Faruqi, A.R., Kress, M., Bordas, J. & Koch, M.H. 1983, "Changes in the X-ray reflections from contracting muscle during rapid mechanical transients and their structural implications", *Journal of Molecular Biology*, vol. 169, no. 2, pp. 469-506.
- Ikura, M., Clore, G.M., Gronenborn, A.M., Zhu, G., Klee, C.B. & Bax, A. 1992, "Solution structure of a calmodulin-target peptide complex by multidimensional NMR", *Science (New York, N.Y.)*, vol. 256, no. 5057, pp. 632-638.
- Jana, S.S., Kim, K.Y., Mao, J., Kawamoto, S., Sellers, J.R. & Adelstein, R.S. 2009, "An alternatively spliced isoform of non-muscle myosin II-C is not regulated by myosin light chain phosphorylation", *The Journal of biological chemistry*, vol. 284, no. 17, pp. 11563-11571.

- Jontes, J.D., Wilson-Kubalek, E.M. & Milligan, R.A. 1995, "A 32 degree tail swing in brush border myosin I on ADP release", *Nature*, vol. 378, no. 6558, pp. 751-753.
- Jung, G., Remmert, K., Wu, X., Volosky, J.M. & Hammer, J.A.,3rd 2001, "The Dictyostelium CARMIL protein links capping protein and the Arp2/3 complex to type I myosins through their SH3 domains", *The Journal of cell biology*, vol. 153, no. 7, pp. 1479-1497.
- Jung, G., Wu, X. & Hammer, J.A.,3rd 1996, "Dictyostelium mutants lacking multiple classic myosin I isoforms reveal combinations of shared and distinct functions", *The Journal of cell biology*, vol. 133, no. 2, pp. 305-323.
- Kamm, K.E. & Stull, J.T. 1985, "The function of myosin and myosin light chain kinase phosphorylation in smooth muscle", *Annual Review of Pharmacology and Toxicology*, vol. 25, pp. 593-620.
- Kim, S.V. & Flavell, R.A. 2008, "Myosin I: from yeast to human", *Cellular and molecular life sciences : CMLS*, vol. 65, no. 14, pp. 2128-2137.
- Knight, A.E., Mashanov, G. & Molloy, J.E. 2005, "Single molecule measurements and biological motors", *European biophysics journal : EBJ*, vol. 35, no. 1, pp. 89.
- Kron, S.J. & Spudich, J.A. 1986, "Fluorescent actin filaments move on myosin fixed to a glass surface", *Proceedings of the National Academy of Sciences of the United States of America*, vol. 83, no. 17, pp. 6272-6276.
- Kurzawa-Goertz, S.E., Perreault-Micale, C.L., Trybus, K.M., Szent-Gyorgyi, A.G. & Geeves, M.A. 1998, "Loop I can modulate ADP affinity, ATPase activity, and motility of different scallop myosins. Transient kinetic analysis of S1 isoforms", *Biochemistry*, vol. 37, no. 20, pp. 7517-7525.
- Laakso, J.M., Lewis, J.H., Shuman, H. & Ostap, E.M. 2008, "Myosin I can act as a molecular force sensor", *Science (New York, N.Y.)*, vol. 321, no. 5885, pp. 133-136.
- Lechler, T., Shevchenko, A. & Li, R. 2000, "Direct involvement of yeast type I myosins in Cdc42-dependent actin polymerization", *The Journal of cell biology*, vol. 148, no. 2, pp. 363-373.
- Lee, W.L., Bezanilla, M. & Pollard, T.D. 2000, "Fission yeast myosin-I, Myo1p, stimulates actin assembly by Arp2/3 complex and shares functions with WASp", *The Journal of cell biology*, vol. 151, no. 4, pp. 789-800.

- Lewis, J.H., Lin, T., Hokanson, D.E. & Ostap, E.M. 2006, "Temperature dependence of nucleotide association and kinetic characterization of myo1b", *Biochemistry*, vol. 45, no. 38, pp. 11589-11597.
- Li, X.D., Ikebe, R. & Ikebe, M. 2005, "Activation of myosin Va function by melanophilin, a specific docking partner of myosin Va", *The Journal of biological chemistry*, vol. 280, no. 18, pp. 17815-17822.
- Li, X.D., Mabuchi, K., Ikebe, R. & Ikebe, M. 2004, "Ca²⁺-induced activation of ATPase activity of myosin Va is accompanied with a large conformational change", *Biochemical and biophysical research communications*, vol. 315, no. 3, pp. 538-545.
- Lin, T., Tang, N. & Ostap, E.M. 2005, "Biochemical and motile properties of Myo1b splice isoforms", *The Journal of biological chemistry*, vol. 280, no. 50, pp. 41562-41567.
- Lindberg, U., Hoglund, A.S. & Karlsson, R. 1981, "On the ultrastructural organization of the microfilament system and the possible role of profilactin", *Biochimie*, vol. 63, no. 4, pp. 307-323.
- Lionne, C., Brune, M., Webb, M.R., Travers, F. & Barman, T. 1995, "Time resolved measurements show that phosphate release is the rate limiting step on myofibrillar ATPases", *FEBS letters*, vol. 364, no. 1, pp. 59-62.
- Lionne, C., Iorga, B., Candau, R., Piroddi, N., Webb, M.R., Belus, A., Travers, F. & Barman, T. 2002, "Evidence that phosphate release is the rate-limiting step on the overall ATPase of psoas myofibrils prevented from shortening by chemical cross-linking", *Biochemistry*, vol. 41, no. 44, pp. 13297-13308.
- Liu, J., Taylor, D.W., Kremntsova, E.B., Trybus, K.M. & Taylor, K.A. 2006, "Three-dimensional structure of the myosin V inhibited state by cryoelectron tomography", *Nature*, vol. 442, no. 7099, pp. 208-211.
- Lowey, S., Slayter, H.S., Weeds, A.G. & Baker, H. 1969, "Substructure of the myosin molecule. I. Subfragments of myosin by enzymic degradation", *Journal of Molecular Biology*, vol. 42, no. 1, pp. 1-29.
- Lu, H., Kremntsova, E.B. & Trybus, K.M. 2006, "Regulation of myosin V processivity by calcium at the single molecule level", *The Journal of biological chemistry*, vol. 281, no. 42, pp. 31987-31994.
- Lymn, R.W. & Taylor, E.W. 1971, "Mechanism of adenosine triphosphate hydrolysis by actomyosin", *Biochemistry*, vol. 10, no. 25, pp. 4617-4624.

- Lymn, R.W. & Taylor, E.W. 1970, "Transient state phosphate production in the hydrolysis of nucleoside triphosphates by myosin", *Biochemistry*, vol. 9, no. 15, pp. 2975-2983.
- Manceva, S., Lin, T., Pham, H., Lewis, J.H., Goldman, Y.E. & Ostap, E.M. 2007, "Calcium regulation of calmodulin binding to and dissociation from the myo1c regulatory domain", *Biochemistry*, vol. 46, no. 42, pp. 11718-11726.
- Margolis, R.L. & Wilson, L. 1978, "Opposite end assembly and disassembly of microtubules at steady state in vitro", *Cell*, vol. 13, no. 1, pp. 1-8.
- Maruta, H., Gadasi, H., Collins, J.H. & Korn, E.D. 1979, "Multiple forms of Acanthamoeba myosin I", *The Journal of biological chemistry*, vol. 254, no. 9, pp. 3624-3630.
- McConnell, R.E., Higginbotham, J.N., Shifrin, D.A., Jr, Tabb, D.L., Coffey, R.J. & Tyska, M.J. 2009, "The enterocyte microvillus is a vesicle-generating organelle", *The Journal of cell biology*, vol. 185, no. 7, pp. 1285-1298.
- Mehta, A.D., Rock, R.S., Rief, M., Spudich, J.A., Mooseker, M.S. & Cheney, R.E. 1999a, "Myosin-V is a processive actin-based motor", *Nature*, vol. 400, no. 6744, pp. 590-593.
- Mehta, A.D., Rock, R.S., Rief, M., Spudich, J.A., Mooseker, M.S. & Cheney, R.E. 1999b, "Myosin-V is a processive actin-based motor", *Nature*, vol. 400, no. 6744, pp. 590-593.
- MIHALYI, E. & SZENT-GYORGYI, A.G. 1953, "Trypsin digestion of muscle proteins. III. Adenosinetriphosphatase activity and actinbinding capacity of the digested myosin", *The Journal of biological chemistry*, vol. 201, no. 1, pp. 211-219.
- Mitchison, T. & Kirschner, M. 1984, "Dynamic instability of microtubule growth", *Nature*, vol. 312, no. 5991, pp. 237-242.
- Mooseker, M.S., Pollard, T.D. & Fujiwara, K. 1978, "Characterization and localization of myosin in the brush border of intestinal epithelial cells", *The Journal of cell biology*, vol. 79, no. 2 Pt 1, pp. 444-453.
- Mullins, R.D., Heuser, J.A. & Pollard, T.D. 1998, "The interaction of Arp2/3 complex with actin: nucleation, high affinity pointed end capping, and formation of branching networks of filaments", *Proceedings of the National Academy of Sciences of the United States of America*, vol. 95, no. 11, pp. 6181-6186.

- Nambiar, R., McConnell, R.E. & Tyska, M.J. 2009, "Control of cell membrane tension by myosin-I", *Proceedings of the National Academy of Sciences of the United States of America*, .
- Nyitrai, M. & Geeves, M.A. 2004, "Adenosine diphosphate and strain sensitivity in myosin motors", *Philosophical transactions of the Royal Society of London. Series B, Biological sciences*, vol. 359, no. 1452, pp. 1867-1877.
- Oguchi, Y., Mikhailenko, S.V., Ohki, T., Olivares, A.O., De La Cruz, E.M. & Ishiwata, S. 2008, "Load-dependent ADP binding to myosins V and VI: implications for subunit coordination and function", *Proceedings of the National Academy of Sciences of the United States of America*, vol. 105, no. 22, pp. 7714-7719.
- Ostap, E.M. 2008, "Tropomyosins as discriminators of myosin function", *Advances in Experimental Medicine and Biology*, vol. 644, pp. 273-282.
- Ostap, E.M., Maupin, P., Doberstein, S.K., Baines, I.C., Korn, E.D. & Pollard, T.D. 2003, "Dynamic localization of myosin-I to endocytic structures in *Acanthamoeba*", *Cell motility and the cytoskeleton*, vol. 54, no. 1, pp. 29-40.
- PAGE, S.G. & HUXLEY, H.E. 1963, "Filament Lengths in Striated Muscle", *The Journal of cell biology*, vol. 19, pp. 369-390.
- Pantaloni, D., Le Clairche, C. & Carlier, M.F. 2001, "Mechanism of actin-based motility", *Science (New York, N.Y.)*, vol. 292, no. 5521, pp. 1502-1506.
- Patterson, B., Ruppel, K.M., Wu, Y. & Spudich, J.A. 1997, "Cold-sensitive mutants G680V and G691C of Dictyostelium myosin II confer dramatically different biochemical defects", *The Journal of biological chemistry*, vol. 272, no. 44, pp. 27612-27617.
- Pollard, T.D. & Borisy, G.G. 2003, "Cellular motility driven by assembly and disassembly of actin filaments", *Cell*, vol. 112, no. 4, pp. 453-465.
- Pollard, T.D. & Korn, E.D. 1973, "Acanthamoeba myosin. I. Isolation from *Acanthamoeba castellanii* of an enzyme similar to muscle myosin", *The Journal of biological chemistry*, vol. 248, no. 13, pp. 4682-4690.
- Rall, J.A. 1982, "Sense and nonsense about the Fenn effect", *The American Journal of Physiology*, vol. 242, no. 1, pp. H1-6.
- Rayment, I., Holden, H.M., Whittaker, M., Yohn, C.B., Lorenz, M., Holmes, K.C. & Milligan, R.A. 1993a, "Structure of the actin-myosin complex and its

- implications for muscle contraction", *Science (New York, N.Y.)*, vol. 261, no. 5117, pp. 58-65.
- Rayment, I., Rypniewski, W.R., Schmidt-Base, K., Smith, R., Tomchick, D.R., Benning, M.M., Winkelmann, D.A., Wesenberg, G. & Holden, H.M. 1993b, "Three-dimensional structure of myosin subfragment-1: a molecular motor", *Science (New York, N.Y.)*, vol. 261, no. 5117, pp. 50-58.
- Reedy, M.K., Holmes, K.C. & Tregear, R.T. 1965, "Induced changes in orientation of the cross-bridges of glycerinated insect flight muscle", *Nature*, vol. 207, no. 5003, pp. 1276-1280.
- Richards, T.A. & Cavalier-Smith, T. 2005, "Myosin domain evolution and the primary divergence of eukaryotes", *Nature*, vol. 436, no. 7054, pp. 1113-1118.
- Rock, R.S., Rice, S.E., Wells, A.L., Purcell, T.J., Spudich, J.A. & Sweeney, H.L. 2001, "Myosin VI is a processive motor with a large step size", *Proceedings of the National Academy of Sciences of the United States of America*, vol. 98, no. 24, pp. 13655-13659.
- Roland, J.T., Lapierre, L.A. & Goldenring, J.R. 2009, "Alternative splicing in class V myosins determines association with Rab10", *The Journal of biological chemistry*, vol. 284, no. 2, pp. 1213-1223.
- Rosenfeld, S.S., Houdusse, A. & Sweeney, H.L. 2005, "Magnesium regulates ADP dissociation from myosin V", *The Journal of biological chemistry*, vol. 280, no. 7, pp. 6072-6079.
- Ross, J.L., Ali, M.Y. & Warshaw, D.M. 2008, "Cargo transport: molecular motors navigate a complex cytoskeleton", *Current opinion in cell biology*, vol. 20, no. 1, pp. 41-47.
- Ross, J.L., Wallace, K., Shuman, H., Goldman, Y.E. & Holzbaur, E.L. 2006, "Processive bidirectional motion of dynein-dynactin complexes in vitro", *Nature cell biology*, vol. 8, no. 6, pp. 562-570.
- Ruppert, C., Godel, J., Muller, R.T., Kroschewski, R., Reinhard, J. & Bahler, M. 1995, "Localization of the rat myosin I molecules myr 1 and myr 2 and in vivo targeting of their tail domains", *Journal of cell science*, vol. 108 (Pt 12), no. Pt 12, pp. 3775-3786.
- Ruppert, C., Kroschewski, R. & Bahler, M. 1993, "Identification, characterization and cloning of myr 1, a mammalian myosin-I", *The Journal of cell biology*, vol. 120, no. 6, pp. 1393-1403.

- Sakamoto, T., Wang, F., Schmitz, S., Xu, Y., Xu, Q., Molloy, J.E., Veigel, C. & Sellers, J.R. 2003, "Neck length and processivity of myosin V", *The Journal of biological chemistry*, vol. 278, no. 31, pp. 29201-29207.
- Salas-Cortes, L., Ye, F., Tenza, D., Wilhelm, C., Theos, A., Louvard, D., Raposo, G. & Coudrier, E. 2005, "Myosin Ib modulates the morphology and the protein transport within multi-vesicular sorting endosomes", *Journal of cell science*, vol. 118, no. Pt 20, pp. 4823-4832.
- Sellers, J.R., Thirumurugan, K., Sakamoto, T., Hammer, J.A., 3rd & Knight, P.J. 2008, "Calcium and cargoes as regulators of myosin 5a activity", *Biochemical and biophysical research communications*, vol. 369, no. 1, pp. 176-181.
- Semenova, I., Burakov, A., Berardone, N., Zaliapin, I., Slepchenko, B., Svitkina, T., Kashina, A. & Rodionov, V. 2008, "Actin dynamics is essential for myosin-based transport of membrane organelles", *Current biology : CB*, vol. 18, no. 20, pp. 1581-1586.
- Siemankowski, R.F., Wiseman, M.O. & White, H.D. 1985, "ADP dissociation from actomyosin subfragment 1 is sufficiently slow to limit the unloaded shortening velocity in vertebrate muscle", *Proceedings of the National Academy of Sciences of the United States of America*, vol. 82, no. 3, pp. 658-662.
- Simmons, R.M., Finer, J.T., Chu, S. & Spudich, J.A. 1996, "Quantitative measurements of force and displacement using an optical trap", *Biophysical journal*, vol. 70, no. 4, pp. 1813-1822.
- Sleep, J.A. & Hutton, R.L. 1980, "Exchange between inorganic phosphate and adenosine 5'-triphosphate in the medium by actomyosin subfragment 1", *Biochemistry*, vol. 19, no. 7, pp. 1276-1283.
- Small, J.V. & Sobieszek, A. 1977, "Ca-regulation of mammalian smooth muscle actomyosin via a kinase-phosphatase-dependent phosphorylation and dephosphorylation of the 20 000-Mr light chain of myosin", *European journal of biochemistry / FEBS*, vol. 76, no. 2, pp. 521-530.
- Soldati, T. 2003, "Unconventional myosins, actin dynamics and endocytosis: a menage a trois?", *Traffic (Copenhagen, Denmark)*, vol. 4, no. 6, pp. 358-366.
- Spudich, J.A. & Watt, S. 1971, "The regulation of rabbit skeletal muscle contraction. I. Biochemical studies of the interaction of the tropomyosin-troponin complex with actin and the proteolytic fragments of myosin", *The Journal of biological chemistry*, vol. 246, no. 15, pp. 4866-4871.

- Stafford, W.F., Walker, M.L., Trinick, J.A. & Coluccio, L.M. 2005, "Mammalian class I myosin, Myo1b, is monomeric and cross-links actin filaments as determined by hydrodynamic studies and electron microscopy", *Biophysical journal*, vol. 88, no. 1, pp. 384-391.
- STRAUB, F.B. & FEUER, G. 1950, "Adenosine triphosphate, the functional group of actin.", *Kiserletes orvostudomány*, vol. 2, no. 2, pp. 141-151.
- Sun, M., Rose, M.B., Ananthanarayanan, S.K., Jacobs, D.J. & Yengo, C.M. 2008, "Characterization of the pre-force-generation state in the actomyosin cross-bridge cycle", *Proceedings of the National Academy of Sciences of the United States of America*, vol. 105, no. 25, pp. 8631-8636.
- Svitkina, T.M. & Borisy, G.G. 1999, "Arp2/3 complex and actin depolymerizing factor/cofilin in dendritic organization and treadmilling of actin filament array in lamellipodia", *The Journal of cell biology*, vol. 145, no. 5, pp. 1009-1026.
- Svoboda, K. & Block, S.M. 1994, "Biological applications of optical forces", *Annual Review of Biophysics and Biomolecular Structure*, vol. 23, pp. 247-285.
- Svoboda, K., Schmidt, C.F., Schnapp, B.J. & Block, S.M. 1993, "Direct observation of kinesin stepping by optical trapping interferometry", *Nature*, vol. 365, no. 6448, pp. 721-727.
- Swanson, J.A., Johnson, M.T., Beningo, K., Post, P., Mooseker, M. & Araki, N. 1999, "A contractile activity that closes phagosomes in macrophages", *Journal of cell science*, vol. 112 (Pt 3), no. Pt 3, pp. 307-316.
- Sweeney, H.L., Rosenfeld, S.S., Brown, F., Faust, L., Smith, J., Xing, J., Stein, L.A. & Sellers, J.R. 1998a, "Kinetic tuning of myosin via a flexible loop adjacent to the nucleotide binding pocket", *The Journal of biological chemistry*, vol. 273, no. 11, pp. 6262-6270.
- Sweeney, H.L., Rosenfeld, S.S., Brown, F., Faust, L., Smith, J., Xing, J., Stein, L.A. & Sellers, J.R. 1998b, "Kinetic tuning of myosin via a flexible loop adjacent to the nucleotide binding pocket", *The Journal of biological chemistry*, vol. 273, no. 11, pp. 6262-6270.
- Szent-Gyorgyi, A. 1941, "Towards a New Biochemistry?", *Science (New York, N.Y.)*, vol. 93, no. 2426, pp. 609-611.
- Szent-Gyorgyi, A. & Banga, I. 1941, "Adenosinetriphosphatase", *Science (New York, N.Y.)*, vol. 93, no. 2407, pp. 158.

- SZENT-GYORGYI, A.G. 1953, "Meromyosins, the subunits of myosin", *Archives of Biochemistry and Biophysics*, vol. 42, no. 2, pp. 305-320.
- Takagi, Y., Homsher, E.E., Goldman, Y.E. & Shuman, H. 2006a, "Force generation in single conventional actomyosin complexes under high dynamic load", *Biophysical journal*, vol. 90, no. 4, pp. 1295-1307.
- Takagi, Y., Homsher, E.E., Goldman, Y.E. & Shuman, H. 2006b, "Force generation in single conventional actomyosin complexes under high dynamic load", *Biophysical journal*, vol. 90, no. 4, pp. 1295-1307.
- Takagi, Y., Shuman, H. & Goldman, Y.E. 2004, "Coupling between phosphate release and force generation in muscle actomyosin", *Philosophical transactions of the Royal Society of London. Series B, Biological sciences*, vol. 359, no. 1452, pp. 1913-1920.
- Tang, N., Lin, T., Yang, J., Foskett, J.K. & Ostap, E.M. 2007, "CIB1 and CaBP1 bind to the myo1c regulatory domain", *Journal of muscle research and cell motility*, vol. 28, no. 6, pp. 285-291.
- Tang, N. & Ostap, E.M. 2001, "Motor domain-dependent localization of myo1b (myr-1)", *Current biology : CB*, vol. 11, no. 14, pp. 1131-1135.
- Taylor, E.W., Lymn, R.W. & Moll, G. 1970, "Myosin-product complex and its effect on the steady-state rate of nucleoside triphosphate hydrolysis", *Biochemistry*, vol. 9, no. 15, pp. 2984-2991.
- Terrak, M., Wu, G., Stafford, W.F., Lu, R.C. & Dominguez, R. 2003, "Two distinct myosin light chain structures are induced by specific variations within the bound IQ motifs-functional implications", *The EMBO journal*, vol. 22, no. 3, pp. 362-371.
- Thirumurugan, K., Sakamoto, T., Hammer, J.A., 3rd, Sellers, J.R. & Knight, P.J. 2006, "The cargo-binding domain regulates structure and activity of myosin 5", *Nature*, vol. 442, no. 7099, pp. 212-215.
- Tilney, L.G. & Portnoy, D.A. 1989, "Actin filaments and the growth, movement, and spread of the intracellular bacterial parasite, *Listeria monocytogenes*", *The Journal of cell biology*, vol. 109, no. 4 Pt 1, pp. 1597-1608.
- Titus, M.A. 2000, "The role of unconventional myosins in Dictyostelium endocytosis", *The Journal of eukaryotic microbiology*, vol. 47, no. 3, pp. 191-196.

- Trybus, K.M., Gushchin, M.I., Lui, H., Hazelwood, L., Kremmentsova, E.B., Volkman, N. & Hanein, D. 2007, "Effect of calcium on calmodulin bound to the IQ motifs of myosin V", *The Journal of biological chemistry*, vol. 282, no. 32, pp. 23316-23325.
- Tsygankov, D. & Fisher, M.E. 2007, "Mechanoenzymes under superstall and large assisting loads reveal structural features", *Proceedings of the National Academy of Sciences of the United States of America*, vol. 104, no. 49, pp. 19321-19326.
- Tyreman, M.J. & Molloy, J.E. 2003, "Molecular motors: nature's nanomachines", *IEE proceedings.Nanobiotechnology*, vol. 150, no. 3, pp. 95-102.
- Tyska, M.J., Mackey, A.T., Huang, J.D., Copeland, N.G., Jenkins, N.A. & Mooseker, M.S. 2005a, "Myosin-1a is critical for normal brush border structure and composition", *Molecular biology of the cell*, vol. 16, no. 5, pp. 2443-2457.
- Tyska, M.J., Mackey, A.T., Huang, J.D., Copeland, N.G., Jenkins, N.A. & Mooseker, M.S. 2005b, "Myosin-1a is critical for normal brush border structure and composition", *Molecular biology of the cell*, vol. 16, no. 5, pp. 2443-2457.
- Uyeda, T.Q., Abramson, P.D. & Spudich, J.A. 1996a, "The neck region of the myosin motor domain acts as a lever arm to generate movement", *Proceedings of the National Academy of Sciences of the United States of America*, vol. 93, no. 9, pp. 4459-4464.
- Uyeda, T.Q., Abramson, P.D. & Spudich, J.A. 1996b, "The neck region of the myosin motor domain acts as a lever arm to generate movement", *Proceedings of the National Academy of Sciences of the United States of America*, vol. 93, no. 9, pp. 4459-4464.
- Uyeda, T.Q., Ruppel, K.M. & Spudich, J.A. 1994, "Enzymatic activities correlate with chimaeric substitutions at the actin-binding face of myosin", *Nature*, vol. 368, no. 6471, pp. 567-569.
- Veigel, C., Bartoo, M.L., White, D.C., Sparrow, J.C. & Molloy, J.E. 1998, "The stiffness of rabbit skeletal actomyosin cross-bridges determined with an optical tweezers transducer", *Biophysical journal*, vol. 75, no. 3, pp. 1424-1438.
- Veigel, C., Coluccio, L.M., Jontes, J.D., Sparrow, J.C., Milligan, R.A. & Molloy, J.E. 1999, "The motor protein myosin-I produces its working stroke in two steps", *Nature*, vol. 398, no. 6727, pp. 530-533.

- Veigel, C., Molloy, J.E., Schmitz, S. & Kendrick-Jones, J. 2003, "Load-dependent kinetics of force production by smooth muscle myosin measured with optical tweezers", *Nature cell biology*, vol. 5, no. 11, pp. 980-986.
- Veigel, C., Schmitz, S., Wang, F. & Sellers, J.R. 2005, "Load-dependent kinetics of myosin-V can explain its high processivity", *Nature cell biology*, vol. 7, no. 9, pp. 861-869.
- Veigel, C., Wang, F., Bartoo, M.L., Sellers, J.R. & Molloy, J.E. 2002, "The gated gait of the processive molecular motor, myosin V", *Nature cell biology*, vol. 4, no. 1, pp. 59-65.
- Wagner, W., Fodor, E., Ginsburg, A. & Hammer, J.A.,3rd 2006, "The binding of DYNLL2 to myosin Va requires alternatively spliced exon B and stabilizes a portion of the myosin's coiled-coil domain", *Biochemistry*, vol. 45, no. 38, pp. 11564-11577.
- Warshaw, D.M., Guilford, W.H., Freyzon, Y., Krementsova, E., Palmiter, K.A., Tyska, M.J., Baker, J.E. & Trybus, K.M. 2000a, "The light chain binding domain of expressed smooth muscle heavy meromyosin acts as a mechanical lever", *The Journal of biological chemistry*, vol. 275, no. 47, pp. 37167-37172.
- Warshaw, D.M., Guilford, W.H., Freyzon, Y., Krementsova, E., Palmiter, K.A., Tyska, M.J., Baker, J.E. & Trybus, K.M. 2000b, "The light chain binding domain of expressed smooth muscle heavy meromyosin acts as a mechanical lever", *The Journal of biological chemistry*, vol. 275, no. 47, pp. 37167-37172.
- Warshaw, D.M., Guilford, W.H., Freyzon, Y., Krementsova, E., Palmiter, K.A., Tyska, M.J., Baker, J.E. & Trybus, K.M. 2000c, "The light chain binding domain of expressed smooth muscle heavy meromyosin acts as a mechanical lever", *The Journal of biological chemistry*, vol. 275, no. 47, pp. 37167-37172.
- Wegner, A. 1976, "Head to tail polymerization of actin", *Journal of Molecular Biology*, vol. 108, no. 1, pp. 139-150.
- Weiss, S., Rossi, R., Pellegrino, M.A., Bottinelli, R. & Geeves, M.A. 2001, "Differing ADP release rates from myosin heavy chain isoforms define the shortening velocity of skeletal muscle fibers", *The Journal of biological chemistry*, vol. 276, no. 49, pp. 45902-45908.
- Wessels, D., Murray, J., Jung, G., Hammer, J.A.,3rd & Soll, D.R. 1991, "Myosin IB null mutants of Dictyostelium exhibit abnormalities in motility", *Cell motility and the cytoskeleton*, vol. 20, no. 4, pp. 301-315.

- Whittaker, M., Wilson-Kubalek, E.M., Smith, J.E., Faust, L., Milligan, R.A. & Sweeney, H.L. 1995, "A 35-A movement of smooth muscle myosin on ADP release", *Nature*, vol. 378, no. 6558, pp. 748-751.
- Wu, X., Bowers, B., Wei, Q., Kocher, B. & Hammer, J.A.,3rd 1997, "Myosin V associates with melanosomes in mouse melanocytes: evidence that myosin V is an organelle motor", *Journal of cell science*, vol. 110 (Pt 7), no. Pt 7, pp. 847-859.
- Wu, X.S., Rao, K., Zhang, H., Wang, F., Sellers, J.R., Matesic, L.E., Copeland, N.G., Jenkins, N.A. & Hammer, J.A.,3rd 2002, "Identification of an organelle receptor for myosin-Va", *Nature cell biology*, vol. 4, no. 4, pp. 271-278.
- Yildiz, A., Forkey, J.N., McKinney, S.A., Ha, T., Goldman, Y.E. & Selvin, P.R. 2003, "Myosin V walks hand-over-hand: single fluorophore imaging with 1.5-nm localization", *Science (New York, N.Y.)*, vol. 300, no. 5628, pp. 2061-2065.
- Yildiz, A., Tomishige, M., Gennerich, A. & Vale, R.D. 2008, "Intramolecular strain coordinates kinesin stepping behavior along microtubules", *Cell*, vol. 134, no. 6, pp. 1030-1041.
- Yildiz, A., Tomishige, M., Vale, R.D. & Selvin, P.R. 2004, "Kinesin walks hand-over-hand", *Science (New York, N.Y.)*, vol. 303, no. 5658, pp. 676-678.
- Zot, H.G., Doberstein, S.K. & Pollard, T.D. 1992, "Myosin-I moves actin filaments on a phospholipid substrate: implications for membrane targeting", *The Journal of cell biology*, vol. 116, no. 2, pp. 367-376.